CHARACTERIZATION OF IN-PHASE AND OUT-OF-PHASE VIBRATION MODES OF SECONDARY STRUCTURES ATTACHED TO A PRIMARY STRUCTURE BY EXPERIMENTATION AND FINITE ELEMENT ANALYSIS

A Dissertation by

Santhosh Kumar Nedukanjirathingal

Master of Science, Wichita State University, Wichita, Kansas, USA, 2006

Master of Technology, National Institute of Technology, Warangal, India, 2002

Bachelor of Technology, Cochin University of Science and Technology, India, 1999

Submitted to Department of Mechanical Engineering
and the faculty of the Graduate School of
Wichita State University
in partial fulfillment of
the requirements for the degree of
Doctor of Philosophy

May 2015

CHARACTERIZATION OF IN-PHASE AND OUT-OF-PHASE VIBRATION MODES OF SECONDARY STRUCTURES ATTACHED TO A PRIMARY STRUCTURE BY EXPERIMENTATION AND FINITE ELEMENT ANALYSIS

The following faculty members have examined the final copy of this dissertation for form and content, and recommend that it be accepted in partial fulfillment of the requirement for the Doctor of Philosophy with a major in Mechanical Engineering.

_____
Hamid Lankarani, Committee Chair

_____
Krishna Krishnan, Committee Member

_____
Ramazan Asmatulu, Committee Member

_____
Brian Driessen, Committee Member

_____
Rajeev Nair, Committee Member

Accepted for the College of Engineering

_____
Royce Bowden, Dean

Accepted for the Graduate School

_____
Abu S.M. Masud, Interim Dean

DEDICATION

To my wife, Aishwariya, my son, Neilai, and my parents and sister

ACKNOWLEDGEMENTS

I wish to express my deep and sincere gratitude to Dr. Hamid Lankarani, faculty member in the Department of Mechanical Engineering at Wichita State Universiy. His vast knowledge and continuous support have been of great value to me.

I extend my sincere gratitude to all of my committee members—Dr. Ramazan Asmatulu, Dr. Brian Driessen, Dr. Krishnan Krishna, and Dr. Rajeev Nair—for their valuable suggestions and comments. I am also grateful to Dr. Yimeshkar Yihun and Yi Yang Tay for providing considerable input regarding the completion of this dissertation. I thank my beloved wife, Aishwariya, for her support and understanding, for being with me for the past eight years, and for encouraging me to finish my doctoral degree. My parents also played an enormous role in providing me with a good education and guidance in my early days so that I could successfully pursue my degree.

I would like to thank Spirit Aerosystems Inc. and Cessna Aircraft Company for financially supporting my course work and dissertation. I also convey gratitude to my ex-colleagues—John Axtell, Craig Mundt, David Staples, and Javier Fuentalba—for all the knowledge they shared with me in the field of structural dynamics.

ABSTRACT

Ground vibration testing (GVT), is one of the most critical testing procedures for airplane certification. With proper GVT, analysts can determine the stiffness distribution, natural frequencies, mode shapes, and structural damping of each component, all of which are needed to perform flutter and dynamic load analyses. The problem identified in this dissertation is one that might lead to defects in the structural design of aircraft and catastrophic situations if proper attention is not given to GVT results. During this type of testing, technicians and engineers provide instrumentation for most of the primary components of the airplane, entirely avoiding secondary structures such as bungees, gears, control surfaces, etc. However, secondary surfaces might also be important for identifying in-phase and out-of-phase modes; otherwise, tuning of an airplane's stiffness might not be accurate. The primary goals of this dissertation are to re-create the above-mentioned problem of in-phase and out-of-phase modes for a small simple replicate wing gear-like structure using validated modeling procedures and to quantify the effects of secondary structures in GVT. To achieve these objectives the detailed methodologies of this work include the following:

- Simulating the modal experiments and finite element analysis (FEA) on a cantilever plate and free-free beam with and without flexible links attached to them.
- Determining the stiffness distribution of a primary structural component using GVT.
- Identifying the modal characteristics of primary and secondary structures.
- Characterizing in-phase and out-of-phase modes of a secondary structure attached to a primary structure by using signal processing.

Results from this study are incorporated in GVT on a component before performing the same on the fully assembled structure and instrumenting the secondary structures.

TABLE OF CONTENTS

TABLE OF CONTENTS (continued)

TABLE OF CONTENTS (continued)

LIST OF TABLES

LIST OF FIGURES

LIST OF FIGURES (continued)

LIST OF FIGURES (continued)

LIST OF FIGURES (continued)

LIST OF FIGURES (continued)

LIST OF FIGURES (continued)

LIST OF ABBREVIATIONS

CG	Center of Gravity
FAA	Federal Aviation Administration
FAR	Federal Aviation Regulations
FE	Finite Element
FEA	Finite Eement Analysis
FEM	Finite Element Method
FFT	Fast Fourier Transform
FRF	Frequency Response Function
GVT	Ground Vibration Testing
MAC	Modal Assurance Criterion
PRM	Phase Resonance Method
PSM	Phase Separation Method
UAV	Unmanned Aerial Vehicle
V-F	Velocity-Frequency

LIST OF SYMBOLS

M	Mass of a Dynamic System
C	Damping of a Dynamic System
K	Stiffness of a Dynamic System
x	Degree of Freedom (Displacement) in X-direction
$p(t)$	Applied Force as a function of time
λ	Eigen values
ω, f	Natural Frequency,Hz.
A	Area
L	Length
ρ	Density
I_p , J_p	Polar moment of Inertia
E	Young's modulus
G	Shear Modulus
J	Torsional Section Property
Φ	Modal Vectors
$H(j\omega)$	Transfer Function
$F(j\omega)$	Input Force
$X(j\omega)$	Response in X-Direction
m	Mass of the Test Article
ϑ	Angular Orientation
$I1, I2$	Bending Section properties

CHAPTER 1

INTRODUCTION

1.1 Ground Vibration Testing

Ground vibration testing (GVT) is important in aircraft certification, especially for Federal Aviation Regulations (FAR) for Parts 23 and 25 of airplanes. This testing involves the determination of dynamic characteristics and structural compliance. Dynamic characteristics involve natural frequencies, mode shapes, structural damping, and how the connectivity of each component affects different natural frequencies. GVT is an assessment whereby a company or a "dynamic analysis" team determines how well the stiffness and mass properties of the analytical model of the airplane are represented. The term "ground" in ground vibration testing is because this testing is performed while the airplane is grounded, i.e., not in flight.

In an airplane certification environment, dynamic characteristics play an important role in flutter and dynamic loads. For understanding and performing aeroelastic and dynamic load analyses of an aircraft, the primary input is stiffness, as well as mass and inertia properties of each component. Flutter and dynamic load analyses are dependent on the accuracy of the above-mentioned data. Hence, it is very important and necessary to perform GVT on an airplane. The necessary steps before performing this testing is to create an analytical model (structural dynamic model) of the structure, which involves identifying node lines as well as structural modes and frequencies, sensor calibration (accelerometer), equipment setup, data acquisition, and frequency response analysis. Input for the model is a set of signals (force on the shaker) at different frequencies that resonate through the structure at its natural frequencies. At those resonating frequencies, when the magnitude of vibration is maximum, accelerations and displacements are measured at different locations on the airplane at the same time to determine

the mode shape. It has been noted that the magnitude of the forcing function should not exceed a limit at which it causes any structural damage to the airplane. This is highly probable when resonance occurs. Hence, the input signal magnitude is kept very low but high enough to excite the modes.

1.2 Structural Dynamic Model of Airplane

The structural dynamic model of an airplane is important for correlating the analytical vibration and flutter with respect to testing. This is done so that the analyst can ensure that the analytical model is behaving dynamically in the same way as the real airplane. Structural dynamics analysis, also known as modal analysis, calculates the airplane's frequency modes and natural frequencies, also known as eigenvectors and eigenvalues, respectively. It is not necessary for the modal analysis to involve the full time-history response to a given input. The natural frequency of a system is dependent only on the stiffness of the structure, associated structure, and mass that is directly involved or attached to the structure.

1.2.1 Natural Frequency and Normal Modes

Using Newton's laws of motion, any dynamic model, as shown in Figure 1.1, can be mathematically represented as

$$M\frac{d^2x}{dt^2} + C\frac{dx}{dt} + Kx = p(t) \tag{1.1}$$

where *M* is the mass of the system, *C* is damping, *K* is the stiffness of the system, *x* is degrees of freedom, and *p(t)* is the force applied. For a free vibration system, *p(t)* is equal to zero.

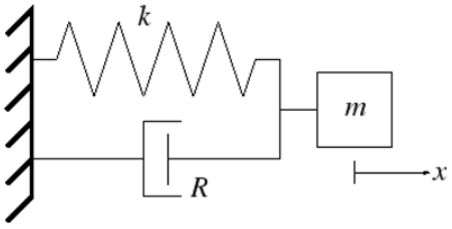

Figure 1.1. Dynamic System Showing Spring, Mass, and Damper

For a free-vibration system with zero damping, for solution convenience, equation (1.1) can be rewritten as

$$M\frac{d^2x}{dt^2} + Kx = 0 \tag{1.2}$$

$$x(t) = ae^{\lambda t} \tag{1.3}$$

$$(M\lambda^2 + K)ae^{\lambda t} = 0 \tag{1.4}$$

$$(M\lambda^2 + K) = 0 \tag{1.5}$$

$$\lambda_{1,2} = \pm\sqrt{\frac{K}{M}} \tag{1.6}$$

$$x(t) = a_1 e^{it\sqrt{\frac{K}{M}}} + a_2 e^{it\sqrt{\frac{K}{M}}} \tag{1.7}$$

$$\sqrt{\frac{K}{M}} = \omega_n \tag{1.8}$$

where ω_n is the natural frequency, and *x(t)* defines the mode shape for the respective natural frequency. For a forced vibration, assuming zero damping, equation (1.1) becomes

$$M\frac{d^2x}{dt^2} + Kx = p(t) \tag{1.9}$$

Assuming the force function is defined by

$$p(t) = Psin(\omega t) \tag{1.10}$$

and using the generalized solution

$$x(t) = Xsin(\omega t) \tag{1.11}$$

then equation (1.9) can be solved for *x(t)*, which is shown in equation (1.11) , where *X* is given by

$$X = \frac{P}{M({\omega_n}^2 - \omega^2)} \tag{1.12}$$

1.3 Finite Element Method

Accurately determining the stiffness and mass of a system is a key factor in the accuracy of natural frequencies and mode shapes of a system. One widely used approach is the finite element method (FEM). Many different software packages are used as preprocessors and postprocessors for defining the stiffness and mass matrix, and solving them for natural frequencies and modes. Some of these packages are NASTRAN, ABAQUS, and ANSYS.

Consider a uniform rod element of length L, mass density ρ, elastic modulus E, cross-sectional area A, and degrees of freedom $U(x,t)$, as shown in Figure 1.2. The stiffness matrix (K) and mass matrix (M) of the rod element are defined by equations (1.13) and (1.14), respectively.

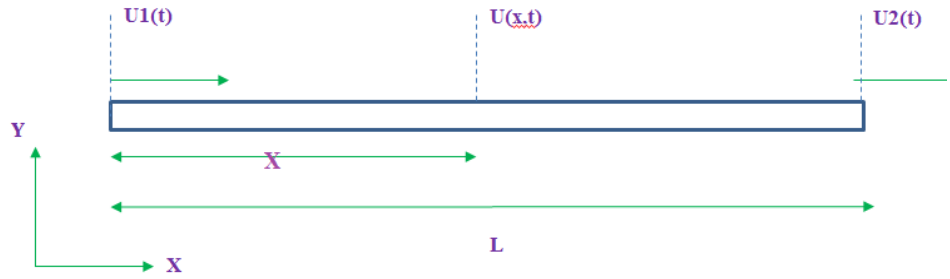

Figure 1.2. Rod Element

$$K = \frac{AE}{L}\begin{bmatrix} 1 & -1 \\ -1 & 1 \end{bmatrix} \tag{1.13}$$

$$M = \frac{\rho AL}{6}\begin{bmatrix} 2 & 1 \\ 1 & 2 \end{bmatrix} \tag{1.14}$$

Consider a uniform beam element of length L, mass density ρ, elastic modulus E, cross-sectional area A, and moment of inertia I. Let the finite element (FE) displacement coordinates for the transverse motion be the end displacements and slopes (θ), as shown in Figure 1.3. The stiffness matrix and mass matrix of the beam element are defined by equations (1.15) and (1.16), respectively.

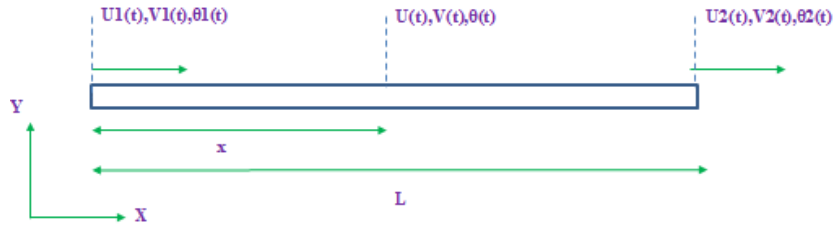

Figure 1.3. Beam Element

$$K = \frac{EI}{L}\begin{bmatrix} 12 & 6L & -12 & 6L \\ 6L & 4L^2 & -6L & 2L^2 \\ -12 & -6L & 12 & -6L \\ 6L & 2L^2 & -6L & 4L^2 \end{bmatrix} \tag{1.15}$$

$$M = \frac{\rho AL}{420}\begin{bmatrix} 156 & 22L & 54 & -13L \\ 22L & 4L^2 & 13L & -3L^2 \\ 54 & 13L & 156 & -22L \\ -13L & -3L^2 & -22L & 4L^2 \end{bmatrix} \tag{1.16}$$

Consider a torsion rod element where the local x-axis is the centroidal axis, as shown in Figure 1.4. Then the stiffness matrix (*K*) and mass matrix (*M*) of the torsion element are defined by equations (1.17) and (1.18), respectively.

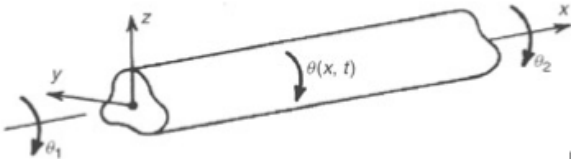

Figure 1.4. Torsion Element [53]

$$K = \frac{GJ}{L}\begin{bmatrix} 1 & -1 \\ -1 & 1 \end{bmatrix} \tag{1.17}$$

$$M = \frac{\rho I_p L}{6}\begin{bmatrix} 2 & 1 \\ 1 & 2 \end{bmatrix} \tag{1.18}$$

where I_p is the area polar moment of inertia about the centroidal axis, L is the length of the element, θ is the density, and *GJ* is the torsion stiffness.

Figure 1.5 shows a three-dimensional frame element defined by 12 degrees of freedom, indicating the local reference frame and displacement coordinates. The x-axis is located along the line of centroids of the cross sections, and the y and z axes are principal axes in the cross section.

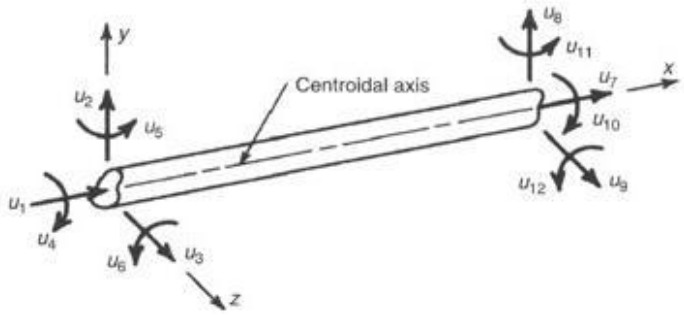

Figure 1.5. Frame Element [53]

Design and analysis scenarios in the modern-day aircraft industry have changed considerably in the past two decades. The computer "horse power" has improved multiple times, and there has been a revolutionary change in the graphical user interface and video card technology. All of this has made finite element analysis (FEA) a welcome reality in the present industry. In industry, two types of structural dynamic models are used:

- Coarse finite element model (Figure 1.6)
- Stick model or beam model (Figure 1.7)

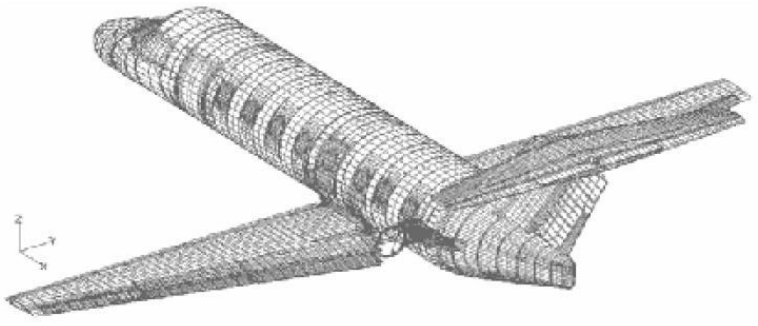

Figure 1.6. Coarse Finite Element Model of Airplane [6]

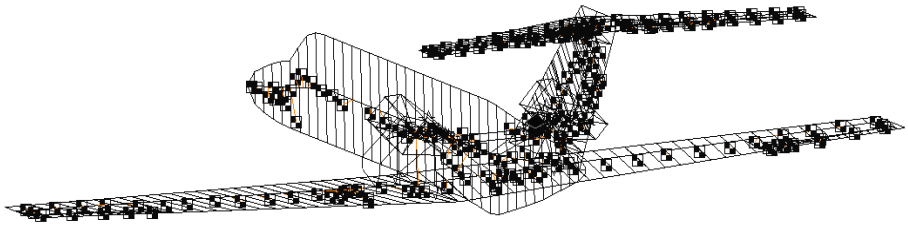

Figure 1.7. Stick Model or Beam Model of Airplane

The coarse FE model provides details of the airplane and components, with spars, shear webs, skins, stiffners, etc., modeled as plate elements, shear elements, beam elements, bar elements, etc. The stick model or beam model provides a simplified model of the coarse FE model with the same equivalent stiffness in bending and torsion. Here, each bay of an airplane component is represented by an equivalent stiffness bar or beam. The advantage of the stick model over the coarse FE model is that the stick model is very helpful for changing the stiffness properties in order to tune the analytical model to match with GVT and to do various parametric studies for flutter analysis.

According to the previous equations and matrices, it is evident that defining the stiffness and mass matrixes is the main input to a eigenvalue and eigenvector solver. In the case of a stick model, in order to define stiffness and for the solver to determine the stiffness matrix, the input data to be provided for most FEM software is the following:

- Grid points and orientation that define the location and length of beams.
- Elastic axis.
- Area of cross section of the beam or bar (A).
- Material properties *E* and *G* (Young's modulus and shear modulus).
- Area moment of inertia bending (*I1, I2*, and *J*) of each section at grid point locations.
- Connectivity and constraints of each beam.

The area moment of inertia can be determined using FEA. Load-deflection analysis is the best used tool to determine the vertical bending (*I1*), fore and aft bending (*I2*), and torsion bending (*J*). Grid points defining the elements are usually on the elastic axis. For the main components of Part 23 of an airplane, like the wing, horizontal stabilizer, and vertical fin, the elastic axis is the same as the center spar, and the grid points are defined where each rib intersects the center spar. In the case of control surfaces and tabs, the elastic axis is the same as the hinge line, which is very near the main spar. Once the model is created, as shown previously in Figure 1.7, it is employed to solve the matrix using the solver. Output from the solver will be the natural frequencies (eigenvalues) and frequency mode shapes (eigenvectors), as shown in Figure 1.8.

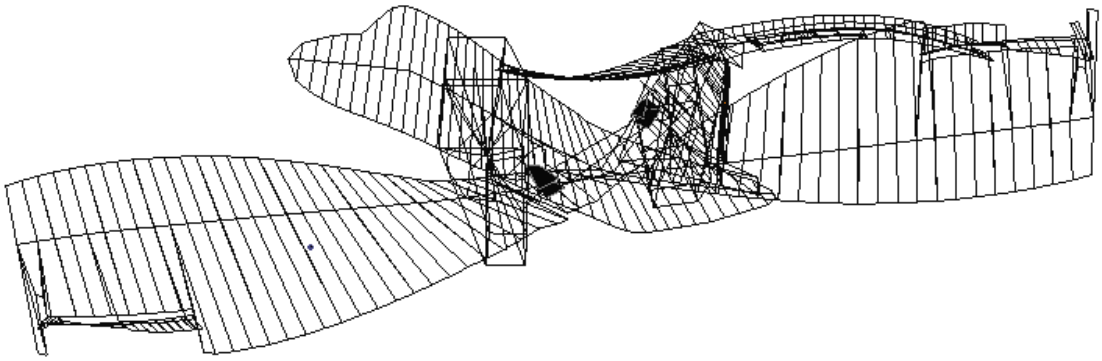

Figure 1.8. Wing Torsion Mode of Airplane

1.3.1 FEA to Determine Section Properties—*I1*, *I2*, and *J*

One of the popular ways to determine *I1, I2*, and *J* bending is by using the coarse FE model. This model, which is generally used by industry groups who test the stress of an airplane, is very detailed, meaning that it has all the dimensions and thicknesses of the skin, spar, shear web, stiffeners, spar caps, ribs, etc. Most of the elements that undergo bending are defined as "plate" elements, all the webs that undergo shear are defined and modeled as shear elements, and all the stiffeners are modeled as bar or beam elements. One such model is shown in Figure 1.9.

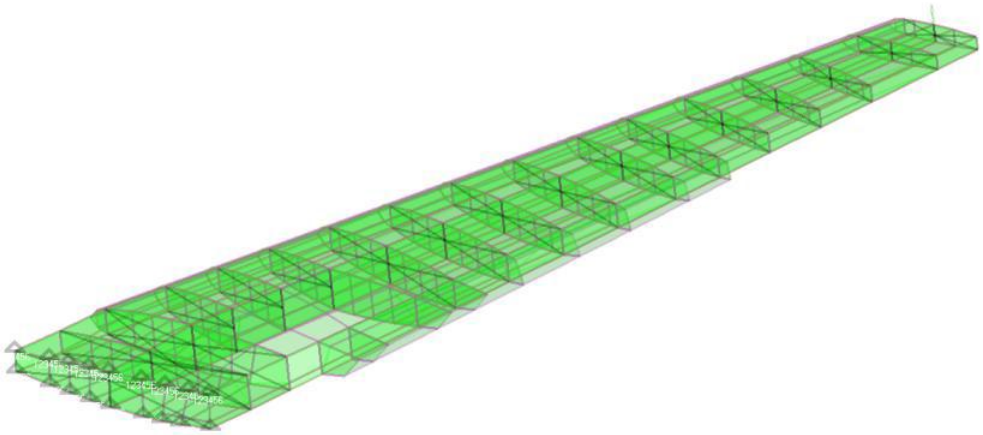

Figure 1.9. Coarse FE model of Airplane Wing

To determine *I1*, *I2* and *J* bending, a load deflection static analysis is performed on the model. In this analysis, one end of the component is constrained in all degrees of freedom. To determine I1, a moment is applied at the other end of the component. The direction of the moment is chosen appropriately with respect to the I's or J to be determined. Prior to that, grid points on each of the ribs are rigidly connected to a common point on the elastic axis of the component. For each rib, points similar to this are defined, and rotations are determined from the load deflection. The stiffness of each bay (area between ribs) is determined by calculating the difference in rotation at those ribs.

From the principles of solid mechanics,

$$\frac{M}{EI} = \frac{d\theta}{dx} \tag{1.19}$$

$$M = \frac{d\theta\ EI}{dx} \tag{1.20}$$

where M is the moment applied, E is the Young's modulus, I is the area moment of inertia, $d\Theta$ is the difference in rotation of points (which lie on the elastic axis and are rigidly connected to different points on the rib) at the end of each bay, and dx is the length of the bay. Therefore, with this information on moment, length of bay, and change in rotation at both ends of the bay, it is

possible to determine the product of Young's modulus and the area moment of inertia, or *EI*. Similarly, torsion rigidity can be determined as

$$GJ = \frac{Tdx}{d\theta} \tag{1.21}$$

1.3.2 Mass, Center of Gravity, and Inertia

In industry, usually there is a large department, or "weight group," that determines the mass, center of gravity (CG), and inertia of the respective bays so that this information can be used along with stiffness to perform the modal analysis. The CG of the mass does not necessarily have to be the same as the grid point. However, mass and inertia are determined with respect to the CG of each bay, and the inertia with respect to the grid point can be easily determined by using the basic principle of inertia, or the parallel axis theorem. The various inertia terms to be determined are *Ixx*, *Iyy*, *Izz*, *Ixy*, *Ixz*, and *Iyz*.

1.3.3 Boundary Conditions

The boundary condition is an important factor in developing the structural dynamic model and comparing it with test results. The major boundary condition for which an analyst needs to have a thorough knowledge is how the airplane rests on the ground and the way it is implemented in an analytical model. Usually the airplane rests on airbags, and the rigid body modes are determined, which have frequencies usually between 1 Hz and 3 Hz for a Part 23 airplane. It is conventional practice to model the attachment of landing gear to the ground as springs in the x-, y-, and z-directions.

1.4 Testing and Signal Processing

This section provides information about ground vibration testing as well as some prior knowledge required for the data analysis while performing ground vibration testing. The main purpose of GVT is to obtain experimental vibration data, natural frequencies, modes, mode

shapes, critical damping, etc. In the aircraft industry, GVT is usually performed either before or just after the first flight, when all surfaces and components of the airplane are unpainted. This is well in advance of performing an envelope expansion test, which is a high-risk and critical test in aircraft certification where the airplane is stretched to its limits in flight in terms of speed and altitude. GVT is performed early in the airplane's design in order to analyze flutter and dynamic load results prior to the envelope expansion test.

Usually in industry, when an airplane is in the process of design, it is advisable to perform "component" GVT before performing the "full-airplane" GVT. Component GVT is performed separately on each component of the airplane, such as the wing, horizontal stabilizer, fuselage, fin, and all control surfaces. This will provide a better understanding of the stiffness and mass of the structure. Component GVT is performed at almost the same time as component static load testing. Once the aircraft components are assembled, the "full-airplane" GVT is performed. This will provide a better understanding of the stiffness from connections rather than structural stiffness (*EI1*, *EI2*, and *GJ*) of the components. It has been said that once the "component" GVT is well correlated in the analytical model, there should be no surprises from the "full-airplane" GVT, provided that the structure-component connection stiffnesses are tuned. Tuning the connections means changing the constraints and spring constant values of connections to match the GVT frequency of a respective mode. Sometimes this spring stiffness needs to be varied slightly, depending on the frequency and mode shape shown in the "full-airplane" GVT. The fundamental concepts behind GVT are the same as that of the theory behind modal analysis. The concept of modal analysis is necessary for characterizing any deformation encountered by the structure when subjected to excitation. The number of frequencies of a

dynamic system is equal to the number of degrees of freedom of the system. While performing GVT, the following assumptions are followed:

- The dynamic system under consideration is linear
- The properties of the system do not vary with time (damping,mode and natural frequency etc.)
- An observable dynamic system.

Principle of superposition can be applied to the GVT, where the response of the structure due to a combined applied force is equal to the sum of the responses due to individual forces.. Figure 1.10 provides a representation of how GVT is performed.

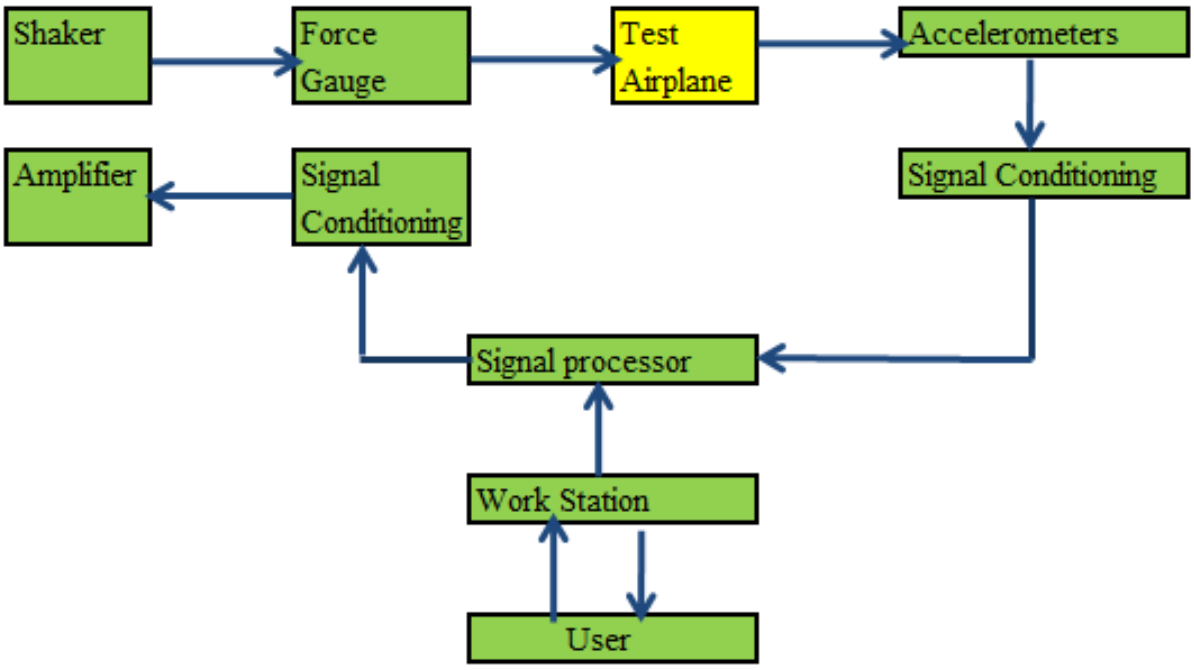

Figure 1.10. Schematic Diagram of Ground Vibration Testing

The input to the test airplane is a set of force signals from a shaker; the amplitude and sample are controlled by a computer and related software (LMS Test.Lab, which helps in providing mode shapes and natural frequencies from test signals to the user). The force signal is usually a random burst signal with a range of frequencies. The concept of this test is that when the input force's

frequency matches the natural frequencies of the airplane, it causes resonance. At resonance, the magnitude of vibration will be high enough to differentiate from the vibration of frequencies other than natural frequencies. These vibrations, with varying frequency force, are measured at different locations of the airplane using an accelerometer. Readings from the accelerometer are processed and read using the necessary software to find the airplane's mode shape and natural frequency. Most signals are processed in the frequency domain (using fast Fourier transform [FFT]), for ease of interpreting the input and output signals.

The accelerometer is chosen in such a way that its sensitivity, frequency range, and resonance matches the requirements of the test and the airplane. Care should be taken to ensure that the resonant frequency of the accelerometer is not the same as the resonant frequency of the airplane or the frequencies of interest. One of the primarily used resources for signal processing and analyzing test inputs and outputs for GVT is provided by the LMS Test.Lab. One company that specializes in providing accelerometers is PCB Piezotronics Inc., and one company that provides shakers is LDS.

During GVT, the airplane is confirmed relative to the gross weight and its structures. Usually the first GVT is done without fuel in the airplane, so that pure structural frequencies involving the primary structure can be determined. Sometimes fuel is included to determine the mode shape and frequencies that are closer to that experienced during flight. After the first GVT, the airplane is set on airbags, and the shakers and accelerometers are installed. Once all the instrumentation is installed, the airplane is ready to be tested in different configurations. For example, input is provided to the shakers as either a single input at a time from the wing, stabilizer, or fuselage etc. or as multiple input from multiple locations. Some of the technical terms and their interpretations are discussed in the following sections.

1.4.1 Phase Resonance and Phase Separation Methods

Two mainly used techniques for performing GVT are the phase resonance method and the phase separation method. Phase resonance, otherwise known as normal mode testing, is usually done by single excitation at the natural frequencies of the modes. Here, the aircraft is forced to act as a system with a single degree of freedom, and the vibration response will contain the mode of interest. Advantages of normal mode testing are as follows:

- The real modes of the corresponding structure are directly measured.
- The eigenvectors are excited at high energy levels.
- Linearity tests can be easily performed.

The main disadvantage of the phase resonance or normal mode testing is that it is time consuming. Hence, this method has recently been replaced by phase separation techniques, where modes are determined by the frequency response function (FRF), otherwise known as the random excitation technique. Excitation signals can be either a stepped sine, burst random, or swept-sine signal.

1.4.2 Frequency Response of a Structure

The frequency response (FR) otherwise called a transfer function is a ratio of output signal to the input signal in frequency domain. It can be seen that the maximum peak occurs at the point of resonance, where there is a natural frequency. Before the peak occurs on FRF, the stiffness line, is determined by the stiffness distribution of the structure and after the peak, the curvature is determined by the mass of the structure, called the mass line. When a structure excites at more than one resonant frequency, the FR is the sum of all resonant peaks and curves (stiffness line and mass line).

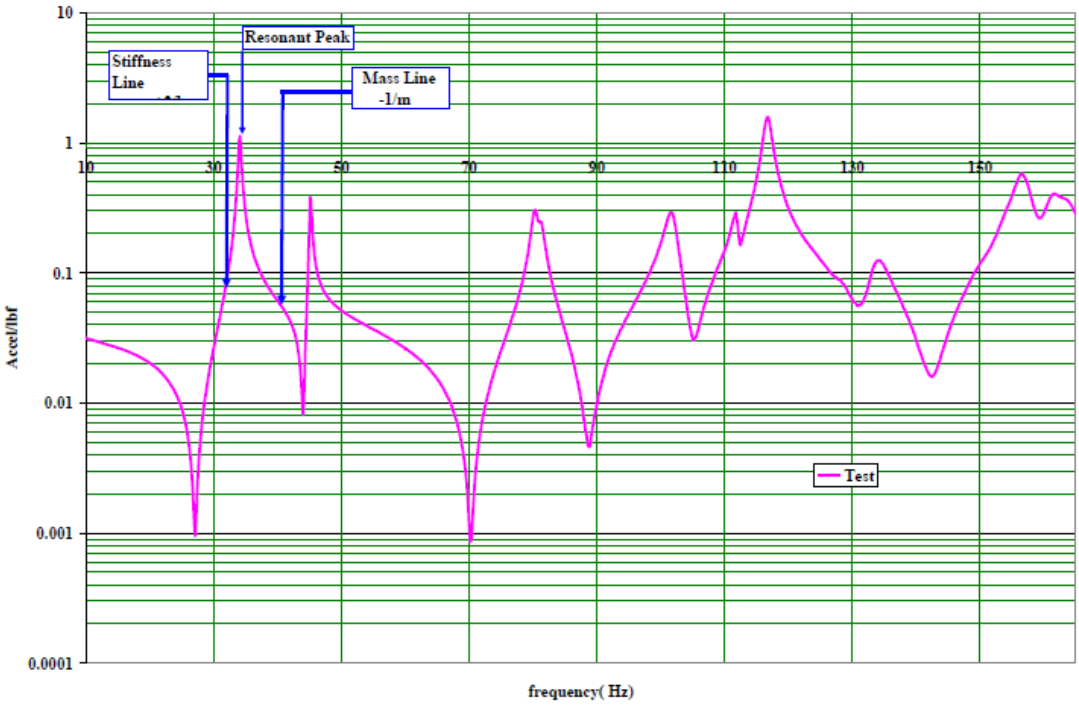

Figure 1.11. Frequency Response Function

1.4.3 Constraint of Structure and Effect of Rigid Body Mode

A free-support system is chosen as a constraint for the GVT for, it simulates the in-flight environment at zero speed. This system is chosen so that it is easy to determine low rigid-body modes that are close to that which occur in flight and much lower than structural frequencies. The free-support system is implemented by placing the airplane on airbags, i.e., landing gear is placed on top of airbags that are placed on the ground (Figure 1.12). Alternatively, small airplanes can be hung by a fixture using stiff bungee cords or springs so that all rigid body modes can be excited. Ideally, all rigid body modes are excited at zero frequency, but because there is some stiffness and friction associated with airbags or bungee cords, these cases are often excited at 1 to 2 Hz. Usually Federal Aviation Administration (FAA) regulations require all rigid body modes to occur at frequencies less than one-quarter of the first flexible mode. Other agencies suggest this to be one-tenth of the first flexible mode. Usually in Part 23 airplanes, frequencies

are excited by simply pushing the airplane in one direction and counting the cycles of oscillation. Once the time required for a certain cycle is known, then the frequency of that rigid body can be determined and, in turn, the frequency of all six rigid bodies of the airplane.

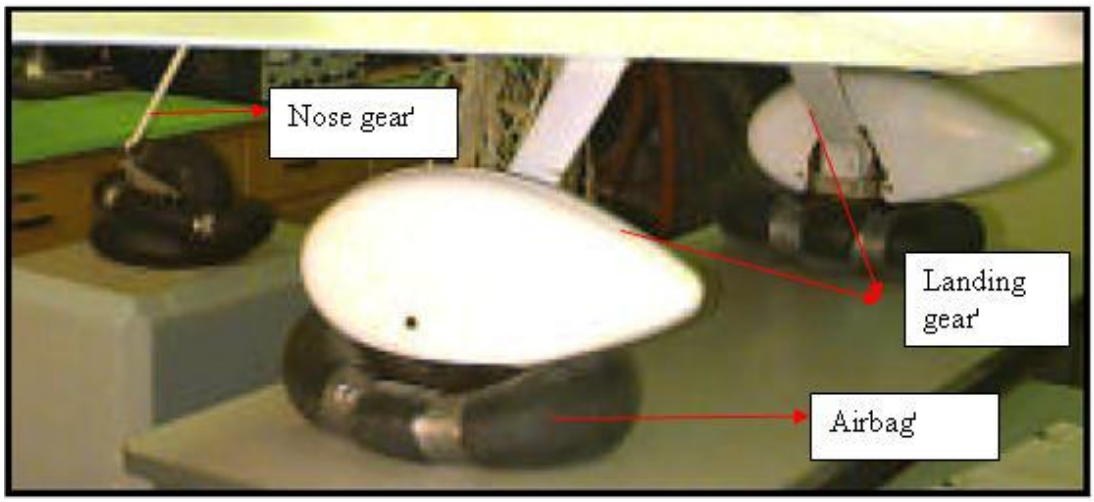

Figure 1.12. Aircraft Suspension System

1.4.4 Excitation Methods and Measurements in Modal Analysis

Excitation is the method of transferring the input force or signal to the airplane. It is assumed that the structure is linear, but in a real scenario, the structure will have some form of non-linear behavior at certain input frequencies or magnitudes. Thus, a burst random signal is the best known input signal from the shaker. The characteristics of a burst random signal are that it provide multi-frequency inputs and a good linearized model. The amplitude should be kept small. Typically, there are two types of shakers that provide these input signals: permanent magnet and electrodynamic. Inorder to transfer all input force to the airplane, it must be applied in a uni-direction, i.e., typically perpendicular to the plane where the force is applied. A stringer is used to do this, in order to transmit an axial load without forces or moments in the other direction. A shaker attached to an airplane component by way of a stringer is shown in Figure 1.13.

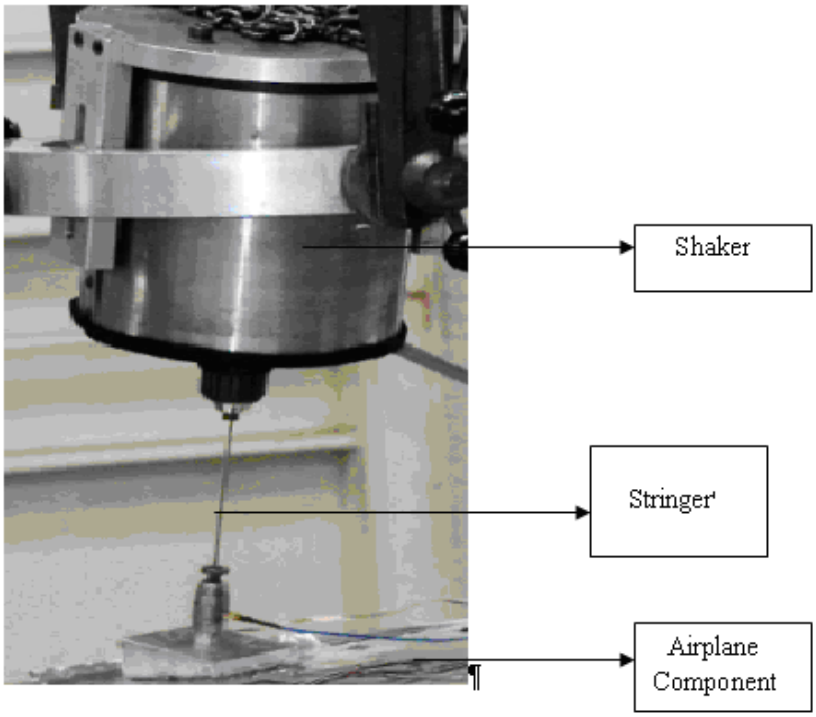

Figure 1.13. Shaker and Stringer Attachment to Airplane Component

1.4.5 Determination of Excitation Points on the Test Article

If a point on the airplane surface has zero modal deflection during vibration, then that point is known as the nodal point. Figure 1.14 shows the nodal point of a horizontal stabilizer mode, as well as the deformed and undeformed structure of the mode. If a shaker is placed at this nodal point, the mode shape corresponding to the node will have zero equivalent input. Thus, the accelerometer, which is on that nodal point, gives no output signal. Hence, care must be taken while installing the shaker and accelerometer to not place them near or on the nodal point. In order to obtain a believable modal response, it should be noted that the force input from the shaker is applied on a "hard point," for example an intersection of a spar and rib, where there is enough structure to excite the vibrations and transfer the input force.

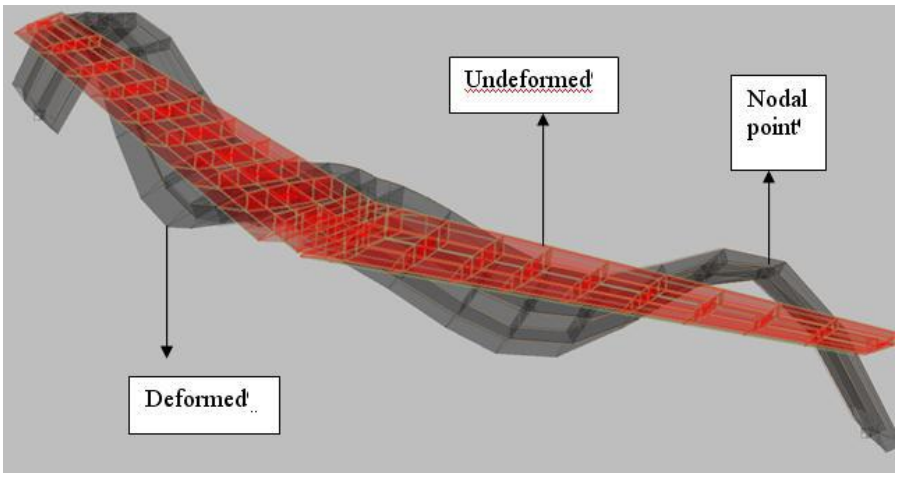

Figure 1.14. Deformed and Undeformed Structure

It is conventional practice to apply the load at an inclination to the plane of application of load, in order for it to excite both the bending modes and torsion modes. Similarly, accelerometers are also installed on structurally "hard points." If they are installed on plates or skins, they will record all the panel modes, which are of least interest in the modal analysis. The best method to find and confirm modal frequencies in a structure is to take measurements at several locations for both the shaker and accelerometer to identify each mode and the respective natural frequency. A thorough understanding of the analytical model is performed in order to understand the models and nodal points well before GVT is performed. In most airplane companies, a "full-airplane" GVT is performed to confirm the accuracy of the structural dynamic analytical model and adjust the stiffness and mass to a small amount of 10–20%, if needed. It is expensive to build the analytical model after GVT is performed. The frequency range of excitation is determined by analyzing the flutter model and determining all critical modes, that is, all low-order (first and second) bending and torsion modes of all primary components (wing, stab, fuselage, etc.) and the control surface rotation, bending, and torsion modes. It is noted that from the analytical model, the frequency range is determined in such a way that all of the above-mentioned modes and flutter critical modes are included.

1.4.6 Determination of Response Points for GVT

For Part 23 airplanes, according to modern test methods, a minimum of 150 channels or accelerometers are used to obtain all important modes seen in the analytical model. It must be noted that accelerometers should not be placed close to each other. It is always advised to choose the location using proper engineering judgment in order to extract the shape of the mode. Accelerometer locations on an airplane are shown in Figure 1.15. A test setup where an accelerometer is installed is shown in Figure 1.16.

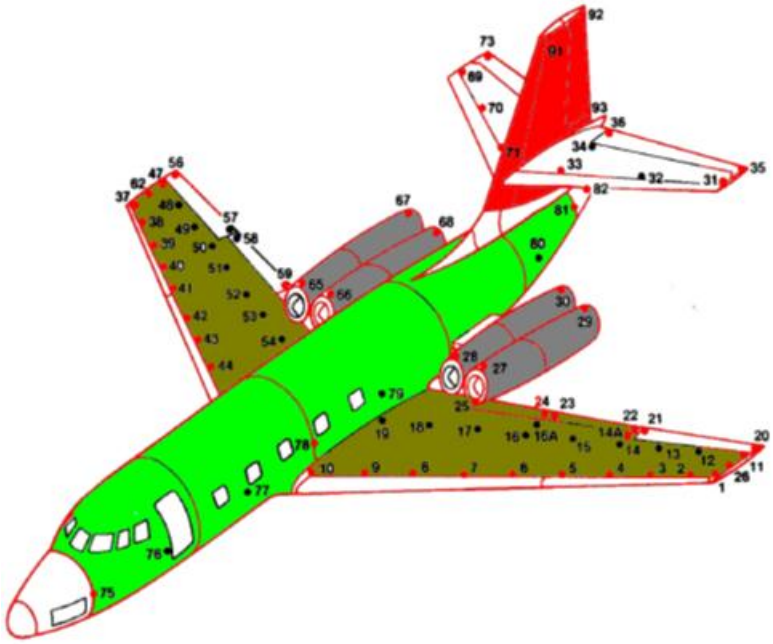

Figure 1.15. Accelerometer Locations on Airplane

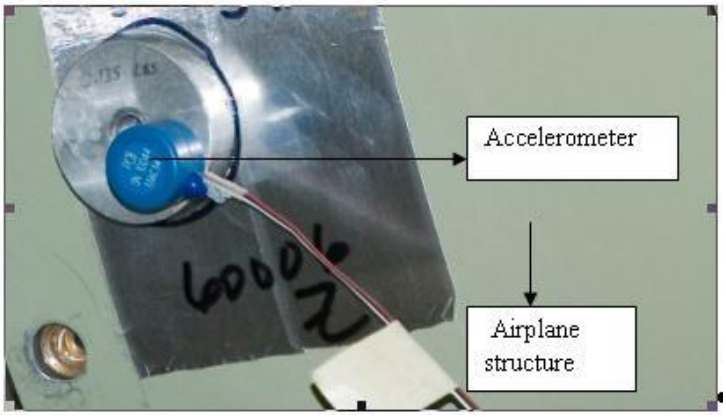

Figure 1.16. Accelerometer Installed on Airplane Structure

The increase in number of channels or accelerometers increases the cost of GVT and also time. If too few points are chosen, this may not be sufficient to interpret the mode shape. Recently performed GVT on the Airbus A380 involved 850 accelerometers, 20 exciters (shakers), and 25 persons for the test setup. It took a total of five days for the test setup, 23 days for the test performance, and one day for dismantling the setup.

1.4.7 Maxwell's Reciprocity

Maxwell's reciprocity theorem states that an excitation at point "x" and a response at point "y" are equal to the same excitation at point "y" and the response at point "x." This theorem validates the assumption of the system being linear for a GVT structure. If *Hij* is the transfer function (FRF) of input *i* and output *j*, and *Hji* is the transfer function (FRF) of input *j* and output *i*, then according to Maxwell's reciprocity theorem,

$$Hij = Hji \tag{1.22}$$

1.4.8 Signal Processing

Signal processing is very important in GVT because it involves the collection of important data, including signals with noise. Taking the airplane as a whole and considering the goal of GVT, it is very convenient if all signals are interpreted in the frequency domain rather than in the time domain. Hence, Fourier transform and fast Fourier Transform play a major role in signal processing during GVT. A property of all real signals is that they can be interpreted as the sum of a number of sine waves of varying amplitudes and frequencies. Figure 1.17 shows this concept, whereby a sine wave in the time domain is interpreted as a straight line in the frequency domain, a process using FFT. Hence, a complicated waveform in the time domain can be simplified and analyzed in a much easier way in the frequency domain.

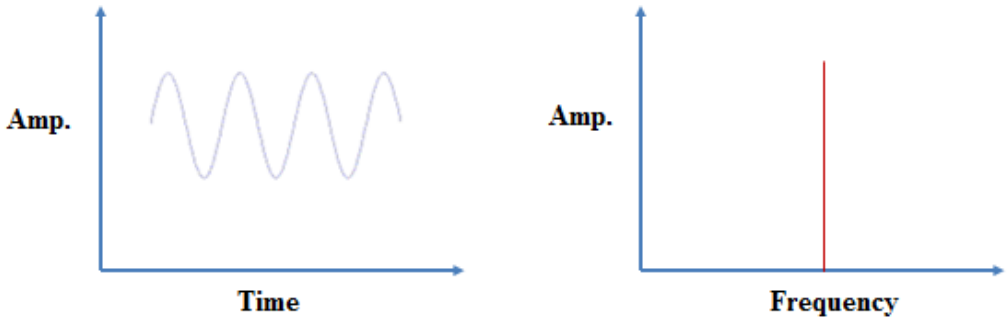

Figure 1.17. Concept of Fourier Transform

1.4.9 Coherence

Coherence, which determines the quality of the frequency response function obtained, relates the output signal to the input signal on a scale from 0 to 1. Here, a coherence of "1" represents perfect coherence, which means that all output is produced by the input and not from other sources such as noise, bad connections, etc. A coherence of "0" represents all output received from sources other than the input. In order to obtain good coherence, the signal analyzer, or location where all signals are processed and analyzed, is configured in such a way as to average the data over several responses.

1.5 Comparison of Analytical Model and Test Results

After GVT is performed, the major challenge of correlating the computer-based analytical model and the test results usually involves a considerable amount of time. If the correlation is well performed, only then can an analyst be assured of the accuracy of the analytical dynamic model. The correlation is usually performed in three stages:

- Geometric correlation.
- Correlation of modal frequencies and mode shapes.
- Determination of modal assurance criterion (MAC).

1.5.1 Geometric Correlation

The first and foremost step before analyzing the test data and comparing it with the analytical model is to correlate the geometry. Engineers and technicians performing the test must ensure that the accelerometer points are included at the same location as grid points in the finite element method. This is also applicable in locating the shaker. An appropriate coordinate system should be used to apply the input force in the FEM before comparing the transfer functions to the test result. All the above precautions will result in better correlation of the model with the test.

1.5.2 Correlation of Modal Frequencies and Mode Shapes

Once the geometric analysis is completed, usually the next step is preparing a table that includes all modal frequencies and modal descriptions. The analyst must be careful to check the strain energy of every component of the airplane in order to determine those components involved in that particular mode. The analyst must also pay attention to the node line for most of the modes. The node line provides a better relationship of the mass distribution. Once the modal table is prepared, it is made available during GVT to ensure that all modes in the analysis are excited by the shaker, especially those that are important to the flutter team. Then, the magnitude of the modal frequency values for a respective mode, say, for example, the first symmetric wing bending mode, are compared to ensure that the values differ by more than +10% or –10%. Many software packages process output signals from various accelerometers and the input signal from the shaker to display the mode shapes for each modal frequencies. Initially all modal comparisons are performed visually, including mode shapes, phasing of each component, etc., to confirm that the comparison is being made on similar modes. Table 1.1 shows one such comparison of modal frequencies from GVT and analysis. Figures 1.18 and 1.19 show the mode shape comparison from GVT and analysis, respectively, of a symmetric wing.

TABLE 1.1

COMPARISON OF GVT AND ANALYTICAL MODES

Mode	GVT Frequency (Hz)	Analytical Frequency (Hz)
Asymmetric Fin Bending	5.90	5.93
Asymmetric Fin Torsion	6.11	6.14
Symmetric Wing Bending	6.32	6.29
Symmetric Engine Pitch	10.12	10.74
Symmetric Horizontal Stabilizer	13.68	13.54

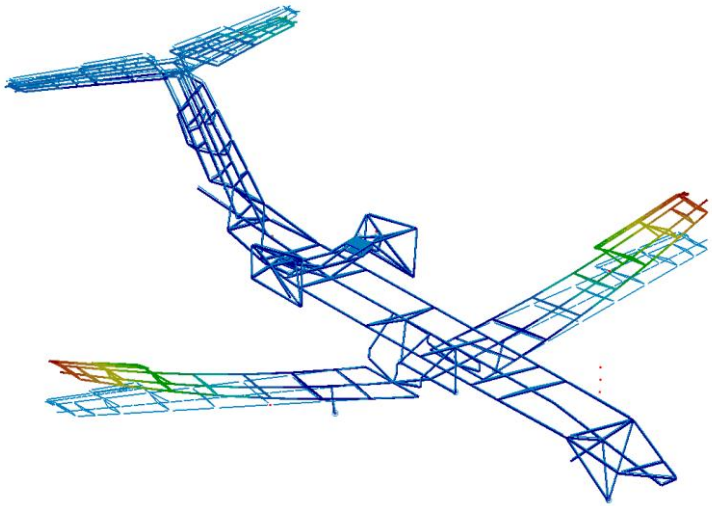

Figure 1.18. Symmetric Wing Mode from GVT

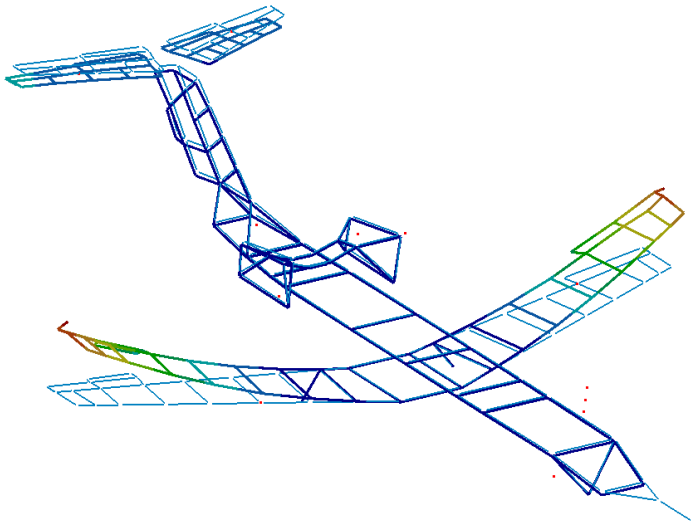

Figure 1.19. Symmetric Wing Mode from Analysis

1.5.3 Modal Assurance Criterion

The MAC expresses the degree of the relationship between a pair of vectors. These vectors can be modal vectors or response vectors, which, for instance, are from a forced response prediction. MAC values will always lie between 0 and 1. A reasonable value of MAC is above 0.9. MAC is generally plotted with one test result vs. another test result, or one test result vs. the analytical result. This criterion provides an idea of whether the frequencies and mode shapes of the two compared sets of modal results are good. MAC is determined in order to determine the linear dependence of modes. The historical development of the modal assurance criteria originated from the need for a quality assurance indicator for experimental modal vectors, which are estimated from measured frequency response functions. The standard of the late 1970s, when the modal assurance criterion was developed, was an orthogonality check. Two modes are said to be orthogonal to each other if

$$\varphi_s^T M \varphi_r = 0 \tag{1.23}$$

where φ_r and φ_s are the rth and sth modal vectors, respectively, r and s are not equal, and M is the mass matrix. Experimentally, the result of zero for the cross-orthogonality calculation can rarely be achieved, but the values up to one tenth of the magnitude of the generalized mass of each mode are considered to be acceptable.

1.6 Aeroelasticity and Flutter

Aeroelasticity and flutter involves the interaction of inertial, elastic, and aerodynamic forces. Flutter is a phenomenon whereby the amplitude of vibration modes increases to an extent that leads to structural catastrophe. A simple example is the wing of a fixed-wing airplane. Usually for a business jet (Part 23), the wing-bending mode is of low frequency (near 5 Hz), and the torsion mode is close to 40 Hz. The wing is structurally designed in such a way that both

modes are very far apart. With airspeed, the bending mode frequency has a tendency to increase, and the torsion mode frequency has a tendency to decrease. Figure 1.20 shows a typical velocity-frequency (V-F) diagram for the bending/torsion modes of an airplane. Flutter occurs when both frequencies meet at the same point on the V-F graph, that is, where there is inadequate damping, and the energy pumped into the structural component increases by an immense amount.

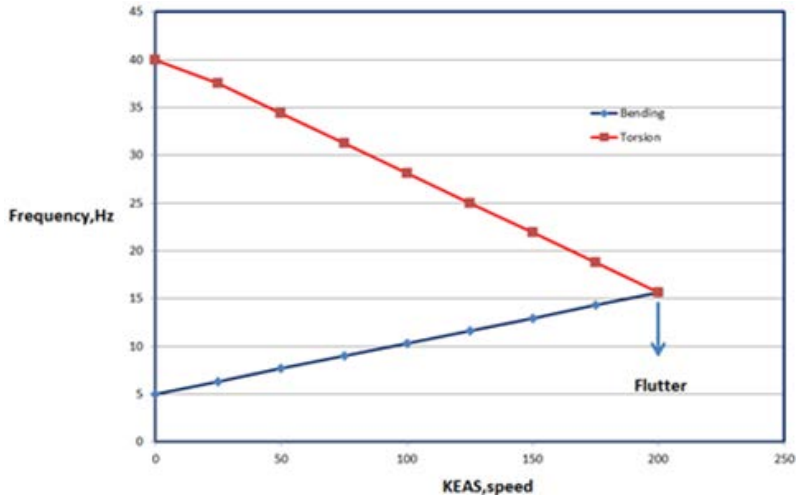

Figure 1.20. V-F Plot of Wing Flutter Analysis (KEAS-equivalent airspeed)

Figure 1.21 shows that, as the torsion frequency, i.e., torsional stiffness, is reduced, the structure will have a tendency to flutter at a lower speed. Hence, it is very important in GVT to determine the correct torsional stiffness of a structure such as the wing for the airplane's safety.

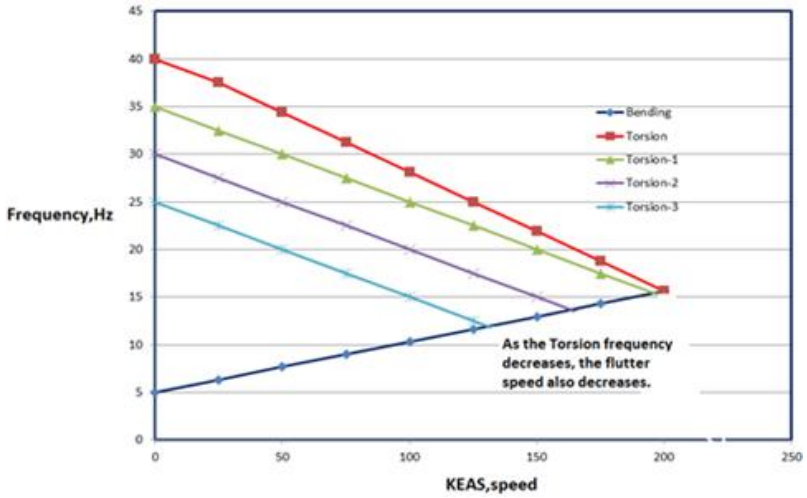

Figure 1.21 Change in Flutter Speed with Air Speed

CHAPTER 2

LITERATURE REVIEW

2.1.1 Significance of Ground Vibration Testing

An advisory circular is a set of documents that provides guidance and information to certify an aircraft by the FAA or an equivalent agency in different countries. GVT is mentioned in the advisory circular for Part 23, paragraph 23.629(a), which states [1] that "comparison of test data may be used in lieu of a totally new analysis and flutter test, in the case of dynamically similar aircraft. Comparison would usually be based upon geometry, mass and stiffness distributions, speed regime, and more importantly, upon a comparison of the measured coupled vibration modes." Ground testing normally includes the following:

- Ground vibration testing.
- Control surfaces and tab mass property determination.
- Stiffness testing of wings, stabilizers, etc.
- Free play measurement of all control surfaces and tabs.
- Rotational frequency for all control surfaces and tabs.
- Rotational stiffness for control system and tab system.

Hence, from an aircraft certification perspective and for safety concerns, it is important to perform GVT.

2.2 Ground Vibration Testing

GVT is critical for structural testing in aircraft certification [2]; hence, considerable research has gone into improving this procedure and analyzing the results. Figure 2.1 shows the steps involved in the aircraft development process [2]. According to the modern schedule-driven airplane design, Peeters et al. advises that GVT should occur shortly before the first flight.

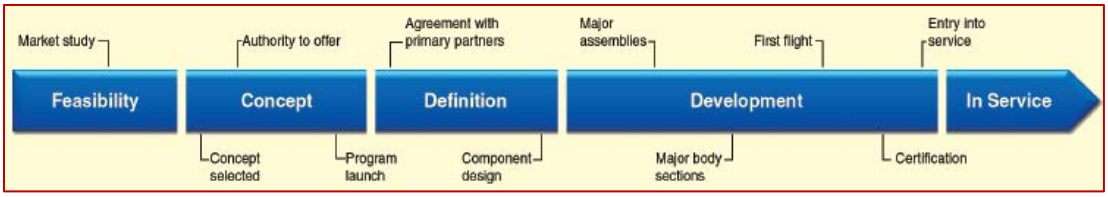

Figure 2.1. Aircraft Development Process [2]

Many companies perform GVT on the whole airplane (small and large), and some perform GVT on the airplane components. Szkudlarek et al. [3] explain the use of computer-aided engineering and testing to accelerate the airplane development process. Their research used a composite hobby aircraft and correlated GVT with the FE results, mentioning the step-by-step process involved in the correlation of testing and the FEA, as shown in Figure 2.2.

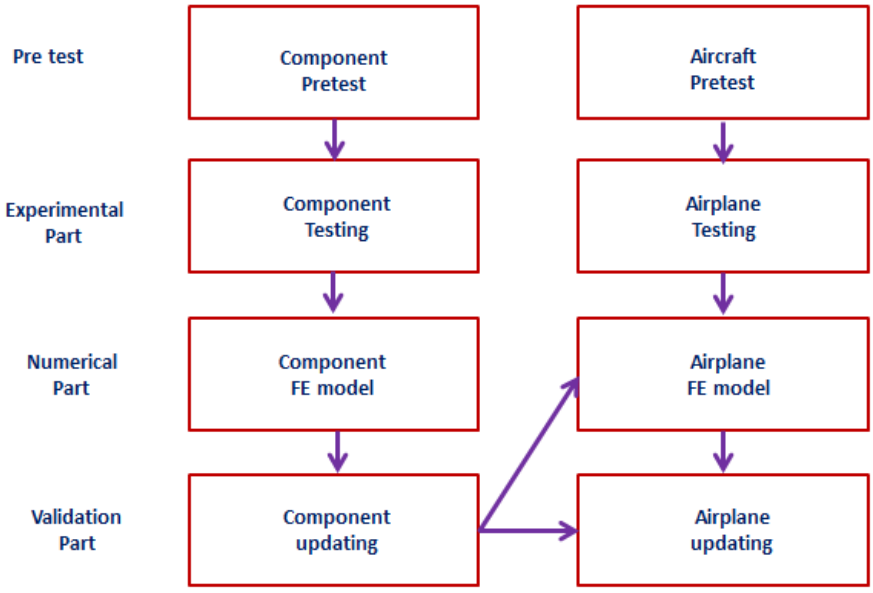

Figure 2.2. Process Involved in Correlation of GVT and FEA [3]

GVT measures the modal characteristics of a structure [4] and is used in the process of structural modifications, flutter analysis etc. Simsiriwong and Sullivan [5] state that one of the major methods to obtaining the modal characteristics of an airplane structure is by using frequency response functions, which are simply transfer functions in the frequency domain.

These transfer functions can be displacements, velocity, or accelerations, as shown in Figure 2.3. The transfer function h(jω) is the ratio of the response x(jω) to the force signal, F(jω). The discrete Fourier transform of both input and output signals from the acceleometers are determined in order to obtain f(jω) and x(jω).

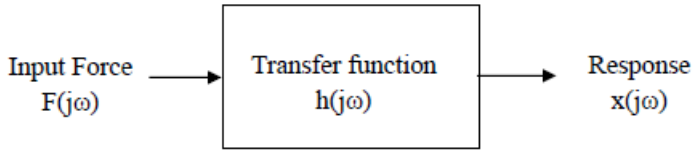

Figure 2.3. Transfer Function [5]

2.2.1 Details of Testing

Generally, electromagnetic shakers or impact hammers are used for component testing, depending on the force level and the size of the components. Impact hammers with hard tips are used to ensure a short contact time and to apply relatively lower force and high frequencies, whereas impact hammers with soft tips result in a longer contact time. Several suspension methods [3] are used during GVT of an airplane or its components, depending on the size and weight of the structure. Generally these methods involve suspension using bungee cords and suspension using an airbag system or multiple airbag systems, whereby airplane gears or those points that touch the ground are supported using airbags that are placed on the ground. The most important thing that needs to be taken into consideration with suspension systems is that all rigid-body frequencies (pitch, yaw, and roll, and the three rigid-body translations on the x, y, and z axes) should be well below the structural modal frequencies. Hence, the suspension system should be soft enough to provide the above criteria. Simsiriwong and Sullivan [5], in their testing of an ultralight unmanned aerial vehicle (UAV), mention that the modal characteristics of the UAV's fuselage are determined for a free-free configuration, which is simulated by suspending

the fuselage structure from wing attachment points by two large springs on each side, as shown in Figure 2.4. The overall bungee suspenstion test setup is shown in Figure 2.5.

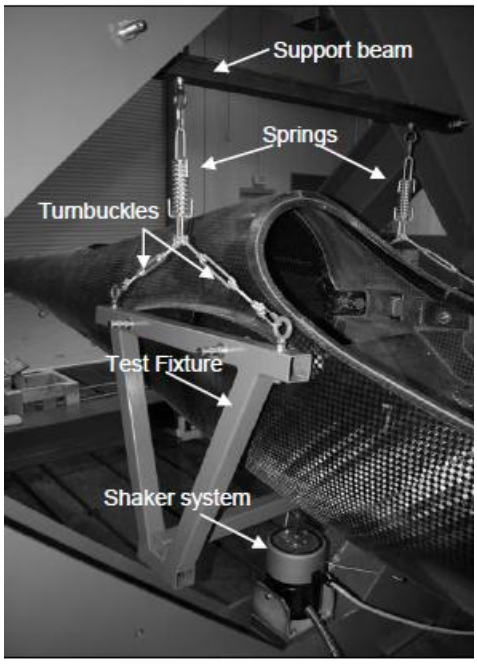

Figure 2.4. Test Fixture [5]

Figure 2.5. Bungee Suspension Setup [11]

A bungee cord [11], as shown in Figure 2.5, is widely used in testing and consists of strands of rubber that are wrapped in a woven sheath to form a cord. A bungee cord exhibits

large deflection, can stretch to approximately 150% of its undeformed length, and acts as a soft spring. To design a bungee system, the spring rate is determined by equation (2.1) as

$$K_s = m(2\pi f)^2 \tag{2.1}$$

where m is the mass of the test article, f is the natural frequency, and K_s is the total stiffness of the spring. The airbag suspension system consists of a single rubber tube enclosed by metal plates. Soft support systems are used to approximate the free-free condition by reducing frequency as much as possible. In most cases, this system includes airbags. Research performed on the Global Hawk UAV by Hensley et al. [10] involved airbags for simulating rigid body modes. The lowest fundamental flexural frequency of the airplane was on the order of 1 Hz. Figure 2.6 shows the whole GVT test setup.

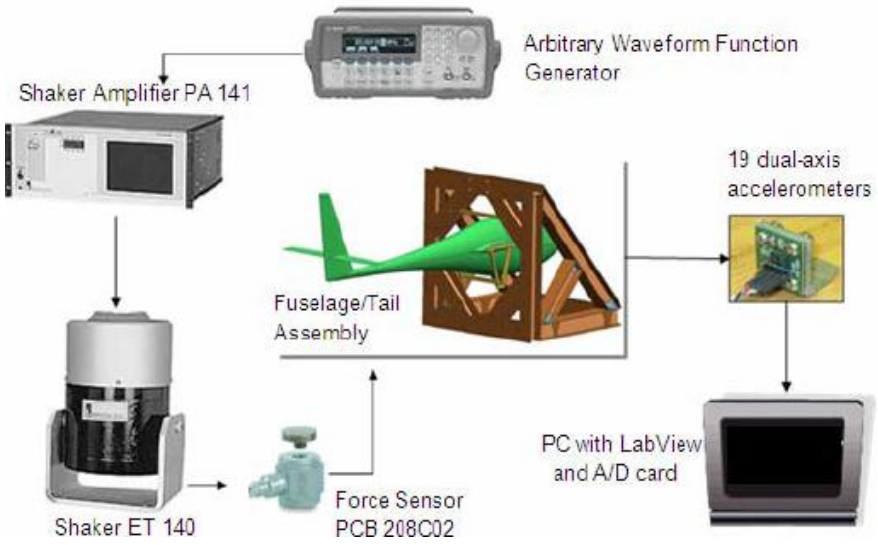

Figure 2.6. GVT Setup [5]

The phase resonance method, otherwise known as normal mode testing, has been used for the past three decades. This method is well suited for the separation of modes that are very close to each other. It involves single sine excitation at natural frequencies. Although there are many advantages to this technique, it is a very time-consuming process, which directly impacts the cost of aircraft development. Hence, the phase resonance method was replaced by the phase

separation technique, where modes are evaluated by FRFs. Various input signals are used in this technique [2], including multi-sine, periodic chip, stepped sine, and burst random (Figure 2.7).

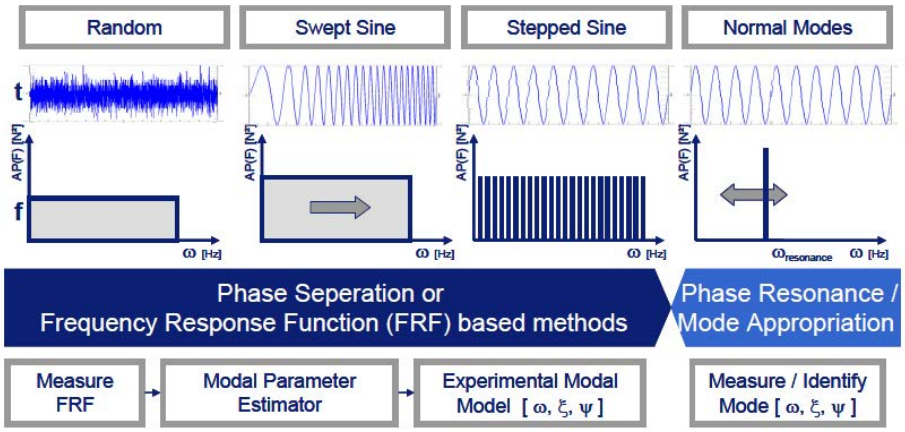

Figure 2.7. Different Signal Inputs for GVT [2]

Napolitano and Linehan [8] mention a method to perform multi-reference sine-sweep tests. The objective of multi-sine excitation is to combine the speed of burst random excitation with the data quality of sine-sweep excitation. The results of their research are shown in Figures 2.8 and Figure 2.9.

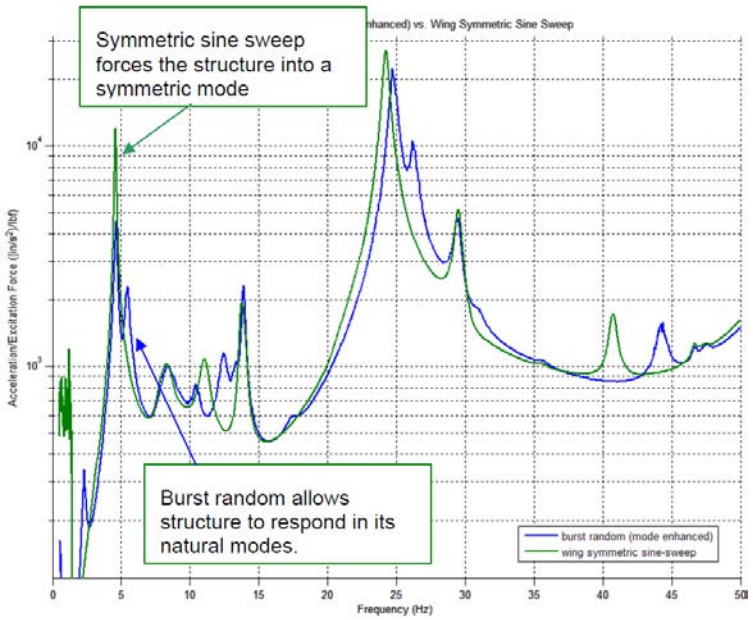

Figure 2.8. Comparison of Burst Random and Multi-Sine Sweep [8]

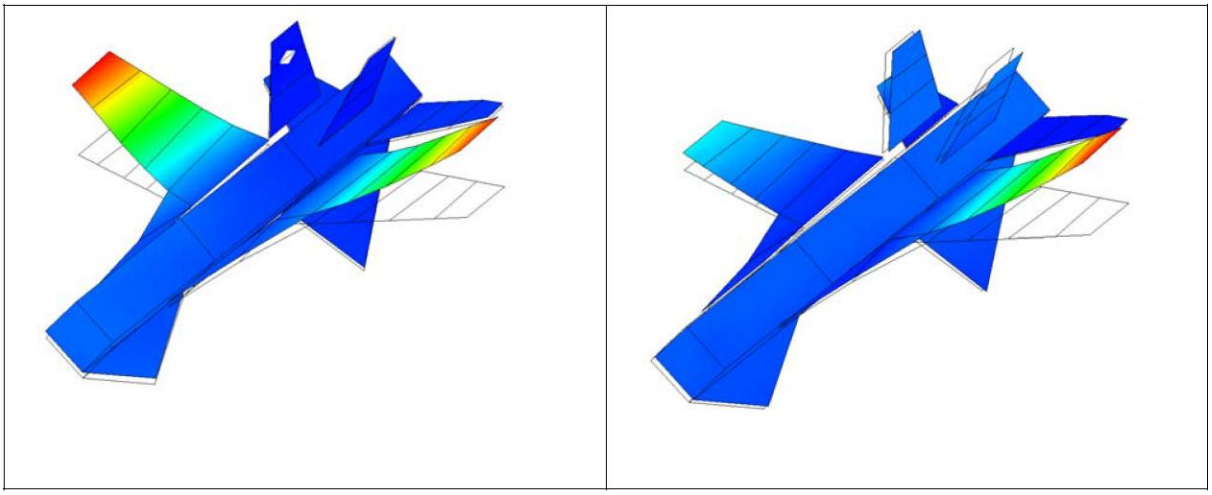

Figure 2.9. Comparison of Wing Bending Mode: Sine Sweep (left) and Burst Random (right) [8]

Lau et al. [9] stress the importance of time in good signal processing. LMS is one such company that offers expertise in a solution for this. One of the most popular modal parameter estimators, LMS Polymax (a solver), plays an important role in reducing analysis time.

Goge et al. [12] discuss the amount of GVT over the years on Airbus airplanes using the phase separation method (PSM) and the phase resonance method (PRM), as shown in Figure 2.10.

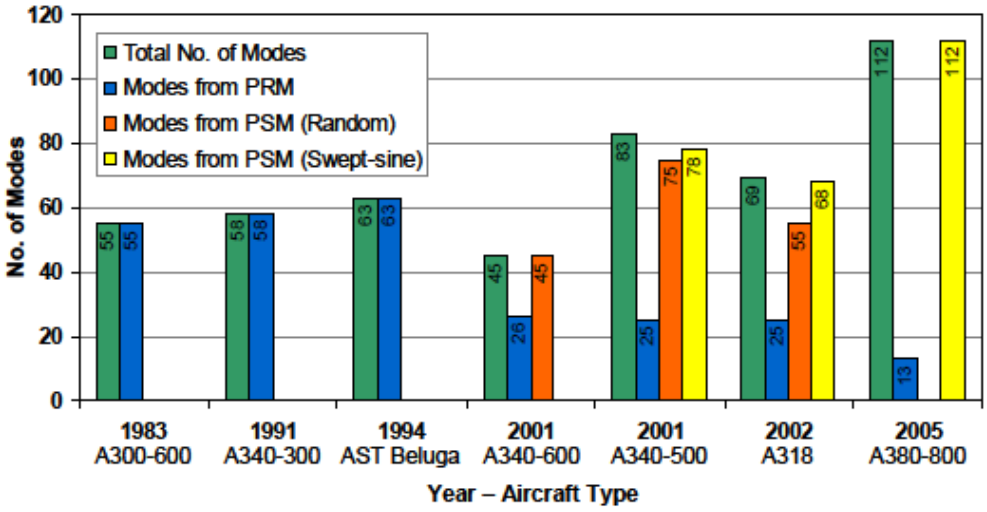

Figure 2.10. Modes Identified by Different Methods [12]

Kerschen [13] reports nonlinearities that occur along with linearity while measuring modal frequencies and shapes. Common nonlinearities include backlash and friction on control surfaces and joints, saturation effects in hydraulic actuators, etc. Salehi and Ziaei-rad [16] performed a study using different excitations on a structure using an impact hammer, random burst, and sine tests. Dieckelman et al. [17] discuss excitation force rtelative to frequencies. Their research concludes that frequencies of the structure converge with force levels.

2.2.2 Finite Element Model and Correlation

Several research studies have been performed using FE models for structural dynamics in the area of modeling GVT. Vittala et al. [6] employs a full coarse FEM of an airplane for dynamic analysis, using QUAD4 and TRIA3 shell elements of MSC NASTRAN [7]. The total degrees of freedom of the model was 672,000, and a proper check was made to compare the total mass and center of gravity of the structure. The dynamic frequency spectrum of the complete airplane (modes and mode shapes) was obtained using the FE model, as shown in Figure 2.11.

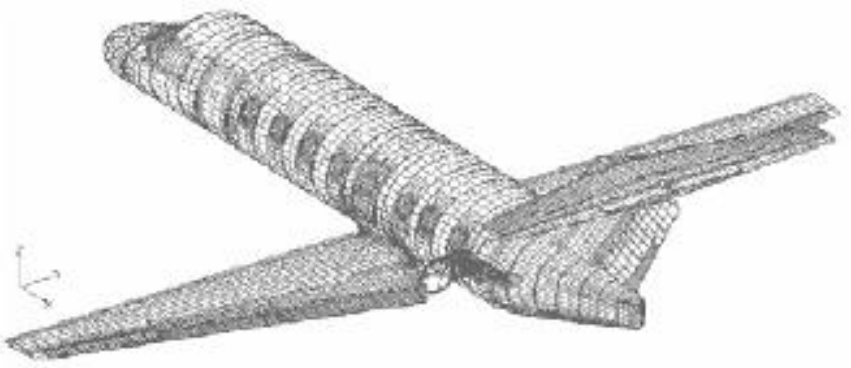

Figure 2.11. Finite Element Model [6]

Szkudlarek et al. [3] modeled a hobby airplane using NASTRAN and discretized it by using CBAR and CQUAD4 elements. The properties used were 2D PCOMP for composite

materials and CONM1 for lumped masses attached to the structure. The correlation analysis [18] was performed using the MAC. Figure 2.12 shows one such comparison.

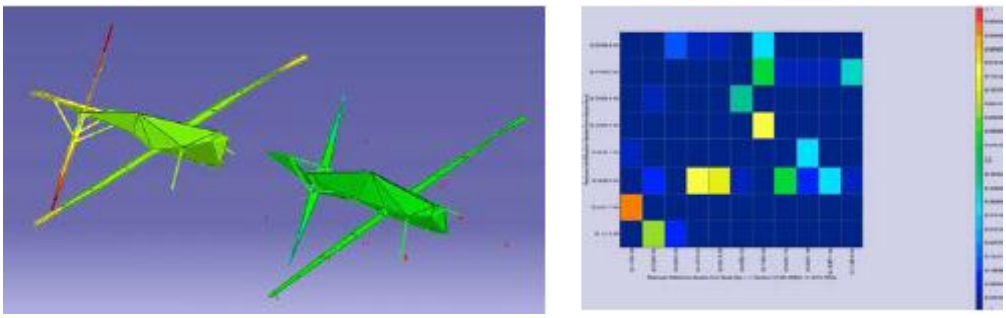

Figure 2.12. Analysis and Test Mode Shape (left) and MAC matrix (right) [3]

Ozkok and Weltin [14] proposed to support the results of an experimental modal analysis on an aircraft with a corresponding FE model, in order to detect missing and/or local vibration modes, which could not be found experimentally with GVT methods by iterative FEM updating. Goge [15] validated an FE model of a four-engine airplane with this test. Salehi and Ziaei-rad [16] conducted testing and FEA on an airplane-like structure, as shown in Figure 2.13. The FE model was constructed in ANSYS using 32 beam elements. A comparison of the analysis and test results using various excitations is shown in Figure 2.14. The measured FRFs were almost identical for the impact hammer and random results.

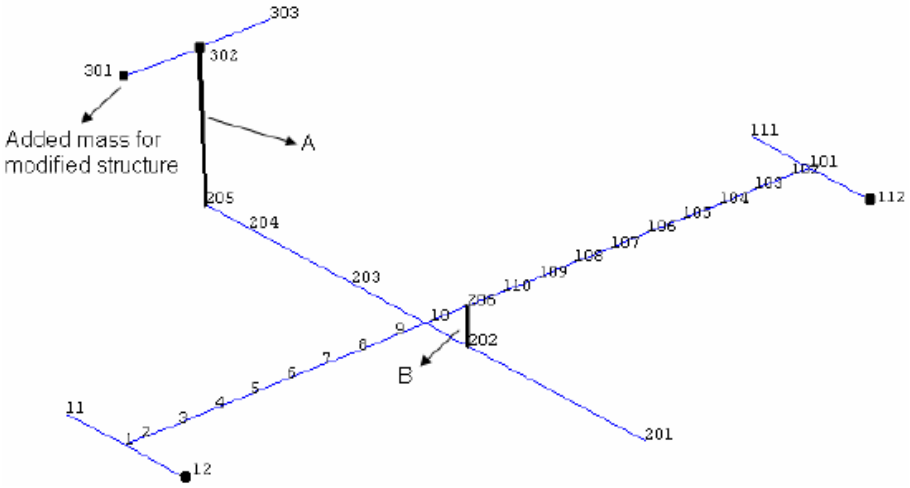

Figure 2.13 Finite Element Model with Beams [16]

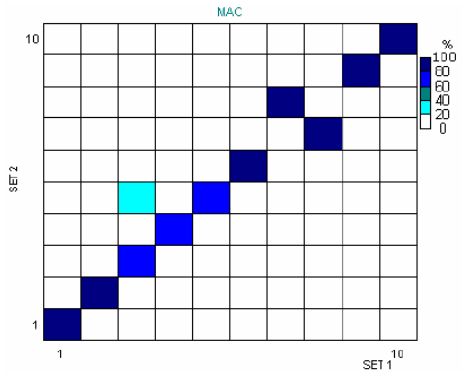

Figure 2.14. Comparison of Test Results Using FEM [16]

2.3 Free Vibration without Damping

From Newton's equation of motion (in x-direction), consider the forces on a spring-mass system [17]. The stiffness of k and mass of m is

$$m\frac{d^2x}{dt^2} + kx = 0 \tag{2.2}$$

where $x = 0$ is the equilibrium position. The solution of the above equation is given by

$$x = Asin\sqrt{\frac{k}{m}}t + Bcos\sqrt{\frac{k}{m}}\ t \tag{2.3}$$

where $\sqrt{\frac{k}{m}}$ is the angular natural frequency represented as ω. The sinusoidal oscillations of the mass repeats continuously, and the time interval to complete once cycle is

$$\tau = \frac{\omega}{2\pi} \tag{2.4}$$

2.3.1 Vibration Analysis of Plates

The classical differential equation of motion of transverse displacement, ω, [19, 20, 21] is

$$\frac{E.h^3}{12.(1-\vartheta^2)}\nabla^4\omega + \rho\frac{\delta^2 w}{\delta t^2} = 0 \tag{2.5}$$

where E is Young's modulus, h is the plate thickness, υ is Poisson's ratio, ∇ is the Laplace operator, and ω is the circular frequency. The frequency parameters are expressed in terms of

$$\lambda = \omega.a^2.\sqrt{\frac{\rho}{D}} \tag{2.6}$$

$$D = \frac{Eh^3}{12(1-v^2)} \tag{2.7}$$

where a is the length dimension, E is Young's modulus, h is the plate thickness, v is Poisson's ratio, and ρ is the mass density per unit area of the cantilever plate (Figure 2.15).

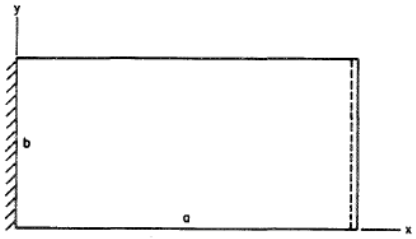

Figure 2.15. Cantilever Plate [25]

Wu et al. [26] and Werfalli and Karound [27] used the separation of variables to solve eigenvalues and to obtain mode shapes for all combinations of simple supported and clamped boundary conditions for a rectangular plate. Young [22] used the products of beam functions and the Raleigh-Ritz method to obtain precise bounds for frequencies in the case of a square cantilever plate. Barton [23, 24] performed additional work to obtain the results for rectangular plates. Five sets of mode shapes and frequencies for a/b = 0.5, 2, and 5 were determined, as well as frequency parameters.

Frequency parameters, mode shapes (node lines), and amplitude coefficients for the first five modes are shown in Tables 2.1 to Table 2.5. Werfalli and Karound [27] obtain the natural frequency by solving the mathematical model that governs the vibration behavior of the plate using a Galerkian-based finite element method. Kalita and Dutta [28] compared the frequency parameters for plates with different edge boundary conditions using their ANSYS finite element model and compared it to the work of Leissa and Kang [29]. For one-edge-clamped rectangular plates, the frequency parameters were very close for different geometric aspect ratios. Kapania and Liu [30], in their analysis of plate vibrations, used NASTRAN to determine the modes.

TABLE 2.1

FREQUENCY PARAMETER, AMPLITUDE COEFFICIENTS, AND MODE SHAPE OF FIRST MODE FOR CANTILEVER PLATE [25]

First mode

a/b	1/2	2	5	Mode shape
$\omega a^2\sqrt{\rho/D}$	3.508	3.472	3.450	
A_{11}	1. 0000	1. 0000	1. 0000	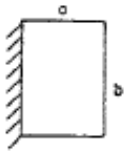
A_{13}	−. 0151	−. 0027	−. 0004	
A_{14}	−. 0028	−. 0002	. 0000	
A_{21}	−. 0011	−. 0040	−. 0048	
A_{23}	−. 0040	−. 0032	−. 0008	
A_{25}	−. 0023	−. 0004	−. 0001	
A_{31}	. 0001	−. 0003	−. 0010	
A_{33}	−. 0005	−. 0015	−. 0005	
A_{35}	−. 0008	−. 0003	−. 0001	

TABLE 2.2

FREQUENCY PARAMETER, AMPLITUDE COEFFICIENTS, AND MODE SHAPE OF SECOND MODE FOR CANTILEVER PLATE [25]

Second mode

a/b	1/2	2	5	Mode shape
$\omega a^2\sqrt{\rho/D}$	5.372	14.93	34.73	
A_{12}	1. 0000	1. 0000	1. 0000	
A_{14}	−. 0509	−. 0027	−. 0004	
A_{16}	−. 0056	−. 0001	. 0000	
A_{22}	. 0436	. 2040	. 2555	
A_{24}	. 0045	. 0011	. 0001	
A_{26}	. 0007	. 0002	. 0000	
A_{32}	−. 0012	. 0059	. 0215	
A_{34}	−. 0014	−. 0005	−. 0001	
A_{36}	−. 0010	−. 0002	. 0000	

TABLE 2.3

FREQUENCY PARAMETER, AMPLITUDE COEFFICIENTS, AND MODE SHAPE OF THIRD MODE FOR CANTILEVER PLATE [25]

Third mode

a/b	1/2	2	5	Mode shape
$\omega a^2\sqrt{\rho/D}$	21.96	21.61	21.52	
A_{11}	0. 0008	0. 0042	0. 0048	
A_{13}	−. 0465	. 0346	. 0054	
A_{15}	. 0725	. 0027	. 0004	
A_{21}	1. 0000	1. 0000	1. 0000	
A_{23}	. 0271	. 0206	. 0050	
A_{25}	. 0196	. 0024	. 0005	
A_{31}	−. 0011	−. 0058	−. 0068	
A_{33}	. 0001	. 0010	−. 0007	
A_{35}	. 0024	−. 0003	−. 0001	

TABLE 2.4

FREQUENCY PARAMETER, AMPLITUDE COEFFICIENTS, AND MODE SHAPE OF FOURTH MODE FOR CANTILEVER PLATE [25]

Fourth mode

a/b	1/2	2	5	Mode shape
$\omega a^2\sqrt{\rho/D}$	10.26	94.49	563.9	
A_{11}	0. 0155	0. 0034	0. 0006	
A_{13}	1. 0000	1. 0000	1. 0000	
A_{15}	−. 0357	−. 0031	−. 0004	
A_{21}	. 0459	−. 0389	−. 0065	
A_{23}	. 1120	. 2359	. 2469	
A_{25}	. 0088	. 0009	. 0001	
A_{31}	−. 0091	. 1025	. 0104	
A_{33}	. 0020	. 0351	. 0381	
A_{35}	−. 0018	−. 0003	−. 0002	

TABLE 2.5

FREQUENCY PARAMETER, AMPLITUDE COEFFICIENTS, AND MODE SHAPE OF FIFTH MODE FOR CANTILEVER PLATE [25]

Fifth mode

a/b	1/2	2	5	Mode shape
$\omega a^2\sqrt{\rho/D}$	24.85	48.71	105.9	
A_{12}	−0. 0529	−0. 2053	−0. 2639	
A_{14}	−. 1989	. 0128	. 0016	
A_{16}	. 0448	. 0017	. 0002	
A_{22}	1. 0000	1. 0000	1. 0000	
A_{24}	−. 1069	−. 0168	−. 0028	
A_{26}	. 0000	−. 0005	−. 0001	
A_{32}	. 0261	. 2222	. 3893	
A_{34}	. 0001	. 0048	. 0004	
A_{36}	. 0040	. 0012	. 0002	

2.3.2 Beam Vibration

Two popular beam theories are Euler-Bernoulli and Timoshenko. The Euler-Beroulli beam theory assumes that plane cross sections normal to the neutral axis before deformation continue to remain a plane and normal to the neutral axis before deformation. Shear deformation effects are negligible and hence valid for only slender beams. When beams are thick, that is, when shear-deformation effects are considered, Timoshenko beam theory comes into use [35]. The bending vibration of a beam, as shown in Figure 2.16, where L is the length of the beam, is given by [31]

$$EI\frac{\partial^4 y}{\partial x^4} + \rho A\frac{\partial^2 y}{\partial t^2} = 0 \tag{2.8}$$

where E, I, ρ, and A are the Young's modulus, second moment of area of the cross section, density, and area of the beam, respectively.

Figure 2.16. Bending Vibration of Beam

The solution of equation (2.8) can be represented as

$$y(x,t) = w(x).U(t) \tag{2.9}$$

$$w(x) = C1\sin(kx) + C2\cos(kx) + C3\sinh(kx) + C4\cosh(kx) \tag{2.10}$$

$$\omega^2 = \frac{EIg}{\rho A}k^4 \tag{2.11}$$

For solving and incorporating the boundary conditions for a free-free beam, the values of the frequency parameters *kL* for each mode [25] are provided in Table 2.6. Labonnote and Malo use an impact hammer to measure the damping of a wooden floor beam [36]. De Haro Silva et al. use FEM and test results to measure and compare modes [37]. Another such comparison on a theoretical and software-based comparison of a cantilever beam is shown in the research of Chaudhari et al. [38]. Azoury et al. describe the same kind of comparison between the experimental method and FEM in their research [39]. Both Emory and Zhu[40] and Sawant [41] mention the experimental verification of transverse vibrations of a free-free beam. Vaziri et al. [42] explain the use of an FFT analyzer in determining the modes of a cantilever beam and comparing them with the analytical results. Malekjafarian et al. [43] propose methodologies for determining various rigid body modes from modal output data. To determine the rigid body modes, FRFs of the structure from different excitation points were obtained, and all six rigid body modes could not be detected in one FRF. Klopper et al. [44] propose an experimental procedure that measures rigid body modes in approximately 1 minute. Figure 2.17 shows the setup where the test structure is suspended by elastic wires.

TABLE 2.6

VALUES OF *kL* FOR DIFFERENT BOUNDARY CONDITIONS OF BEAM [25]

SUPPORTS	MODE n	(A) SHAPE AND NODES (NUMBERS GIVE LOCATION OF NODES IN FRACTION OF LENGTH FROM LEFT END)	(B) BOUNDARY CONDITIONS EQ (7.16)	(C) FREQUENCY EQUATION	(D) CONSTANTS EQ (7.16)	(E) kl EQ (7.14) $\omega_n = k^2\sqrt{\frac{EIg}{A\gamma}}$	(F) R RATIO OF NON-ZERO CONSTANTS COLUMN (D)
HINGED-HINGED	1	0.50	$x=0\begin{cases}X=0\\X''=0\end{cases}$	SIN kl=0	A = 0	3.1416	1.0000
	2				B = 0	6.283	1.0000
	3	0.333 0.667			$\frac{C}{D}=1$	9.425	1.0000
	4	0.25 0.50 0.75	$x=l\begin{cases}X=0\\X''=0\end{cases}$			12.566	1.0000
	n>4					$\approx n\pi$	1.0000
CLAMPED-CLAMPED	1	0.50	$x=0\begin{cases}X=0\\X'=0\end{cases}$	(COS kl)(COSH kl) = 1	A = 0	4.730	-0.9825
	2				C = 0	7.853	-1.0008
	3	0.359 0.641			$\frac{D}{B}=R$	10.996	-1.0000-
	4	0.278 0.50 0.722	$x=l\begin{cases}X=0\\X'=0\end{cases}$			14.137	-1.0000+
	n>4					$\approx\frac{(2n+1)\pi}{2}$	-1.0000-
CLAMPED-HINGED	1	0.558	$x=0\begin{cases}X=0\\X'=0\end{cases}$	TAN kl = TANH kl	A = 0	3.927	-1.0008
	2				C = 0	7.069	-1.0000+
	3	0.386 0.692			$\frac{D}{B}=R$	10.210	-1.0000
	4	0.294 0.529 0.765	$x=l\begin{cases}X=0\\X''=0\end{cases}$			13.352	-1.0000
	n>4					$\approx\frac{(4n+1)\pi}{4}$	-1.0000
CLAMPED-FREE	1	0.783	$x=0\begin{cases}X=0\\X''=0\end{cases}$	(COS kl)(COSH kl) = -1	A = 0	1.875	-0.7341
	2				C = 0	4.694	-1.0185
	3	0.504 0.868			$\frac{D}{B}=R$	7.855	-0.9992
	4	0.358 0.644 0.906	$x=l\begin{cases}X''=0\\X'''=0\end{cases}$			10.996	-1.0000+
	n>4					$\approx\frac{(2n-1)\pi}{2}$	-1.0000-
FREE-FREE	1	0.224 0.776	$x=0\begin{cases}X''=0\\X'''=0\end{cases}$	(COS kl)(COSH kl) = 1	B = 0	0 (REPRESENTS TRANSLATION)	
	2				D = 0	4.730	-0.9825
	3	0.132 0.50 0.868			$\frac{C}{A}=R$	7.853	-1.0008
	4	0.094 0.356 0.644 0.906	$x=l\begin{cases}X''=0\\X'''=0\end{cases}$			10.996	-1.0000-
	5	0.0734 0.277 0.50 0.723 0.927				14.137	-1.0000+
	n>5					$\approx\frac{(2n-1)\pi}{2}$	-1.0000-

Figure 2.17. Experimental Setup to Determine Rigid Body Modes [44]

Masoumi et al. [45] determine the inertia matrix from a rigid-body property estimation using a modal method (FRFs). Schedlinski and Link [46] present a procedure to identify the rigid body properties of an elasto-mechanical system based on modal analysis. Arndt, M. et al. [33] discuss various commonly used FEM techniques in vibration analysis. Versions *h* and *p* are two refinement techniques they used. The first consists of a refinement of the element mesh, and the second consists of a higher-order shape function in the element domain without any change in mesh.

The torsional vibration of a beam is shown in Figure 2.18.

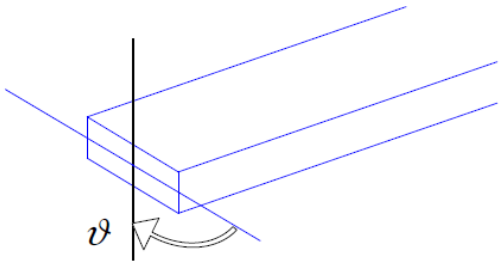

Figure 2.18. Torsional Vibration of Beam [32]

The change in angular orientation $\vartheta(x,t)$ for the cross section of a beam is represented by

$$\frac{\partial^2 \vartheta}{\partial t^2} - \frac{G\gamma}{\rho J_p}\frac{\partial^2 \vartheta}{\partial x^2} = 0 \tag{2.12}$$

where G is the shear modulus, υ is Poisson's ratio, γ is the torsional constant for a rectangular cross section, and J_p is the polar moment of the area of the cross section:

$$G = \frac{E}{2(1+\vartheta)} \tag{2.13}$$

$$\gamma = bh^3\left(\frac{1}{3} - 0.21\frac{h}{b}\left(1 - \frac{h^4}{12b^4}\right)\right) \tag{2.14}$$

$$J_p = \frac{bh}{12}(b^2 + h^2) \tag{2.15}$$

where b is the width of the beam, and h is the height of the beam.

$$\vartheta(x,t) = \theta(x)\, u(t) \tag{2.16}$$

$$\theta(x) = A_1\, sin(kx) + A_2 cos(kx) \tag{2.17}$$

$$k = \frac{\omega}{C_T} = \frac{n\pi}{L} \tag{2.18}$$

where n is the nth mode and

$$C_T = \sqrt{\frac{G\gamma g}{\rho J_p}} \tag{2.19}$$

Little research has been performed on characterizing in-phase and out-of-phase modes of attached secondary structures.

CHAPTER 3

MOTIVATION, OBJECTIVES, AND METHODOLOGY

3.1 Motivation

Solving real-time problems with knowledge acquired from early high school days up until today has been interesting. Along with development of skills, various other factors are very favorable, including colleagues with an immense amount of knowledge relative to topics of interest on which they work on a daily basis, great mentors, and obviously time.

Ground vibration testing is one of the most critical testing procedures for airplane certification. One of the primary purposes of GVT is to "tune" the stiffness distribution of each component and its compliance so that a better analytical model can be developed for flutter analysis. Flutter, a function of stiffness, mass, and aerodynamics, is a catastrophic event that occurs during flight. Proper GVT can determine the stiffness, natural frequencies, mode shapes, and structural damping of each airplanecomponent. Hence, results from GVT is highly important. The problem defined here is one that can be misleading and may lead to catastrophe, if proper attention is not given to GVT results. During GVT, most technicians and engineers instrument most of the primary components of the airplane but totally avoid secondary structures, such as bungees, gears, control surfaces, etc. Secondary surfaces are of equal important as primary surfaces, in order to have knowledge of in-phase and out-of-phase modes with the primary structures. If attention is not paid to secondary surfaces, then tuning the stiffness may be incorrect. This dissertation tries to illustrate one such example, where a primary structure's natural frequencies without instrumenting the secondary structure, like a flexible link attached to the primary structure, leads to wrong tuning of the primary structure's stiffness. This worsens if in-phase and out-of-phase modes involving the secondary structure are near the

torsional frequency of the primary structure. While performing GVT on a fully assembled airplane with gear that is not instrumented, there is a strong chance of tuning the torsional stiffness of the wing to the out-of-phase torsional mode of the main landing gear, missing the in-phase torsional mode of the wing with the gear. In this case, the wing torsional stiffness used in flutter for an airplane flying with gears retracted will not be conservative at all, and the flutter analysis will show a wing of relatively high flutter speed for a simple bending and torsion flutter. In reality, the real wing torsion stiffness is determined by the in-phase mode with the gear.

3.2 Objectives

The primary objectives of this dissertation are as follows:

- To determine the natural frequency and mode shape of a cantilever plate and compare the results with FEA.
- To determine the natural frequency and mode shape of a free-free beam and compare the results with FEA.
- To determine the natural frequencies and mode shapes of a cantilever plate and a free-free beam with attached an link including in-phase and out-of-phase modes of a secondary structure.
- To develop a finite element model to match the secondary structure modes and frequencies.
- To determine the variation of in-phase and out-of-phase torsional frequencies with the change in rotational compliant stiffness and location of the secondary structure.

3.3 Methodology

Vibration tests were initially conducted without a secondary structure attached to the primary structure, and later, tests were conducted with a secondary structure attached to the

primary structure. In doing this, the stiffness distributions of the primary structure were well determined before tuning the in-phase and out-of phase modes of the secondary structure. Steps to achieve the objectives are shown in Figure 3.1.

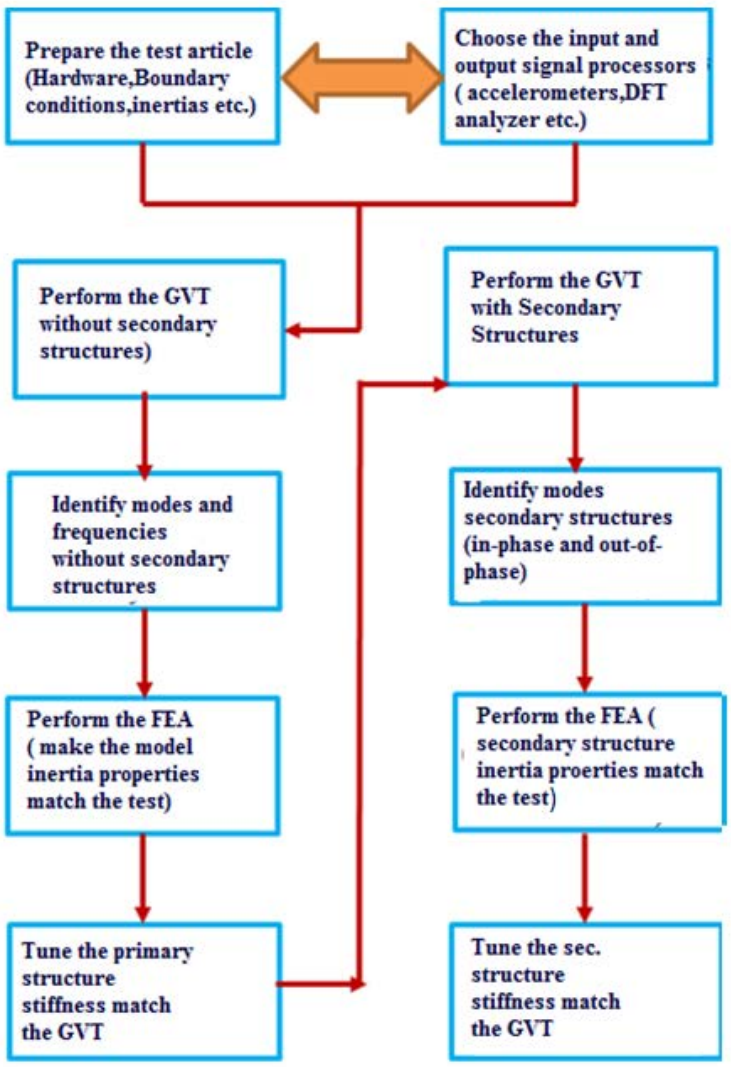

Figure 3.1. Methodology Used to Determine In-Phase and Out-of-Phase Modes of Secondary Structure with Primary Structure

The methodology involves performing a component GVT of the primary structure and FEA before performing the 'full GVT' of the assembled structure. This is performed to 'tune' the stiffness of the primary structure.

CHAPTER 4

GROUND VIBRATION TESTING OF FREE-FREE BEAM AS WELL AS SECONDARY STRUCTURE

4.1 GVT of Free-Free Beam

GVT of the free-free beam alone was performed by hanging it to a rigid structure using bungees, as shown in Figure 4.1. The dimensions of the beam and the location of accelerometers are shown in Figures 4.2 and 4.3, respectively.

Figure 4.1. GVT Setup of Beam

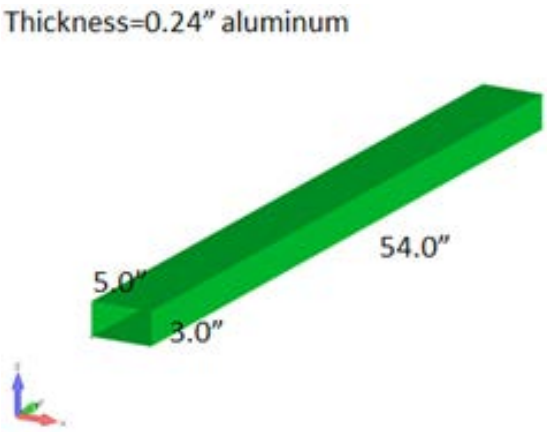

Figure 4.2. Dimensions of Beam

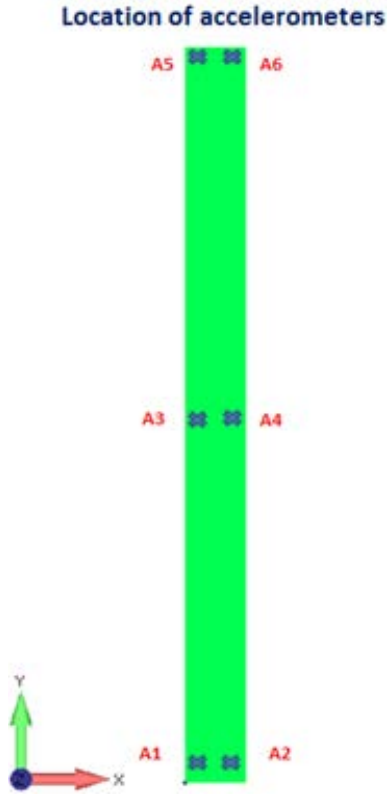

Figure 4.3. Location of Accelerometers on Beam

Figures 4.4 and 4.5 show the magnitude and phase responses of accelerometers A1, A2, and A3 when force is applied on accelerometer A5. Figures 4.6 and 4.7 show the magnitude and phase responses of accelerometers A1, A2, and A3 when force is applied on accelerometer A6.

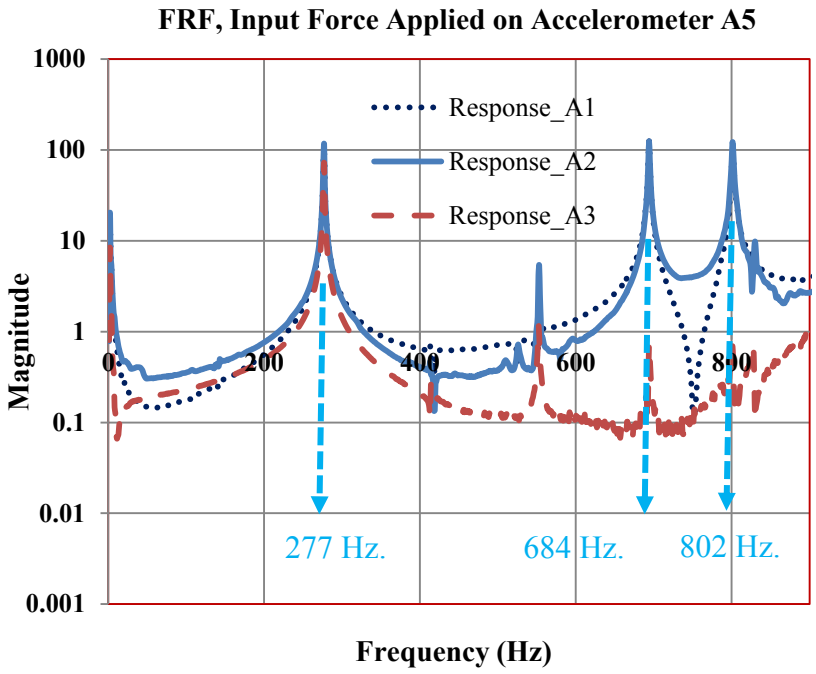

Figure 4.4. FRF, Magnitude, Input Force Applied on Accelerometer A5, and Responses of Accelerometers A1, A2, and A3

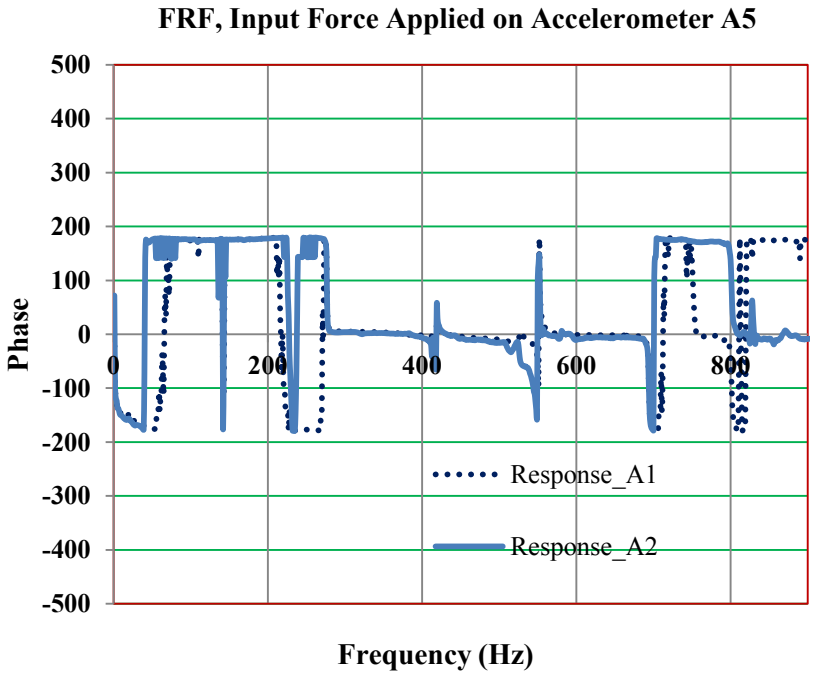

Figure 4.5. FRF, Phase, Input Force Applied on Accelerometer A5, and Responses of Accelerometers A1 and A2

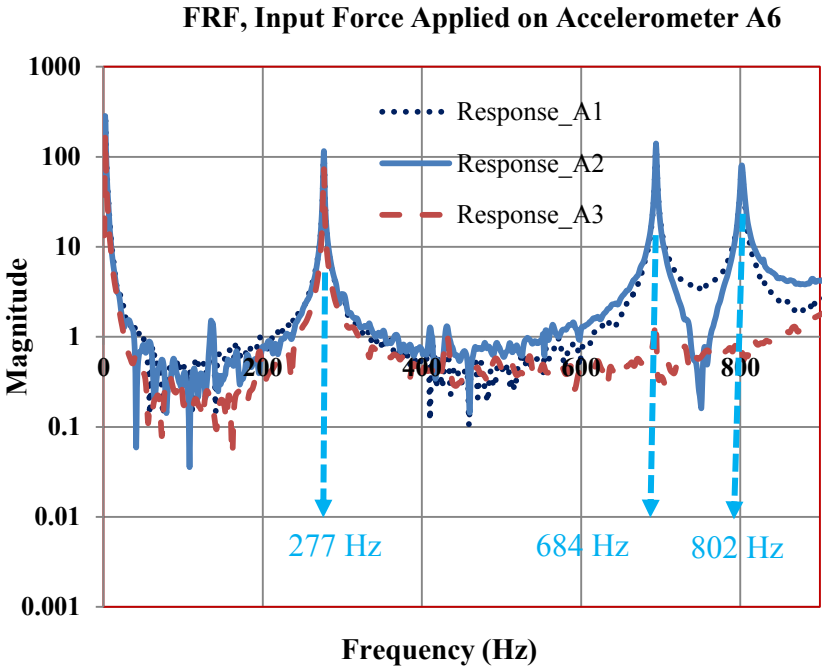

Figure 4.6. FRF, Magnitude, Input Force Applied on Accelerometer A6, and Responses of Accelerometers A1, A2, and A3

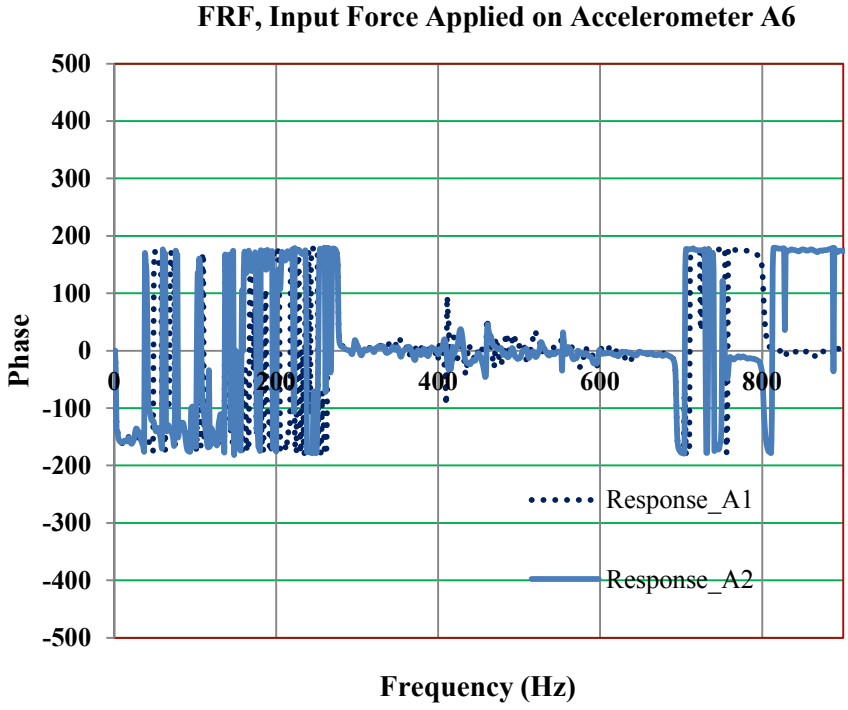

Figure 4.7. FRF, Phase, Input Force Applied on Accelerometer A6, and Responses of Accelerometers A1 and A2

At 277 Hz, Figure 4.8 shows that A1 and A2, as well as A5 and A6 are in phase, and that A1 and A2 are in phase with A5 and A6, respectively, which indicates that the mode at 277 Hz is evidence of symmetric bending. At 694 Hz, Figure 4.9 shows that the reponse from A1 and A2 is in phase but out of phase with A5 and A6, respectively, which makes the mode unsymmetric bending. Near 802 Hz, Figure 4.10 shows that A1and A2, and A5 and A6 are out of phase, but that A1 is in-phase with A6 and that A2 is in phase with A5, thus indicating a torsion mode.

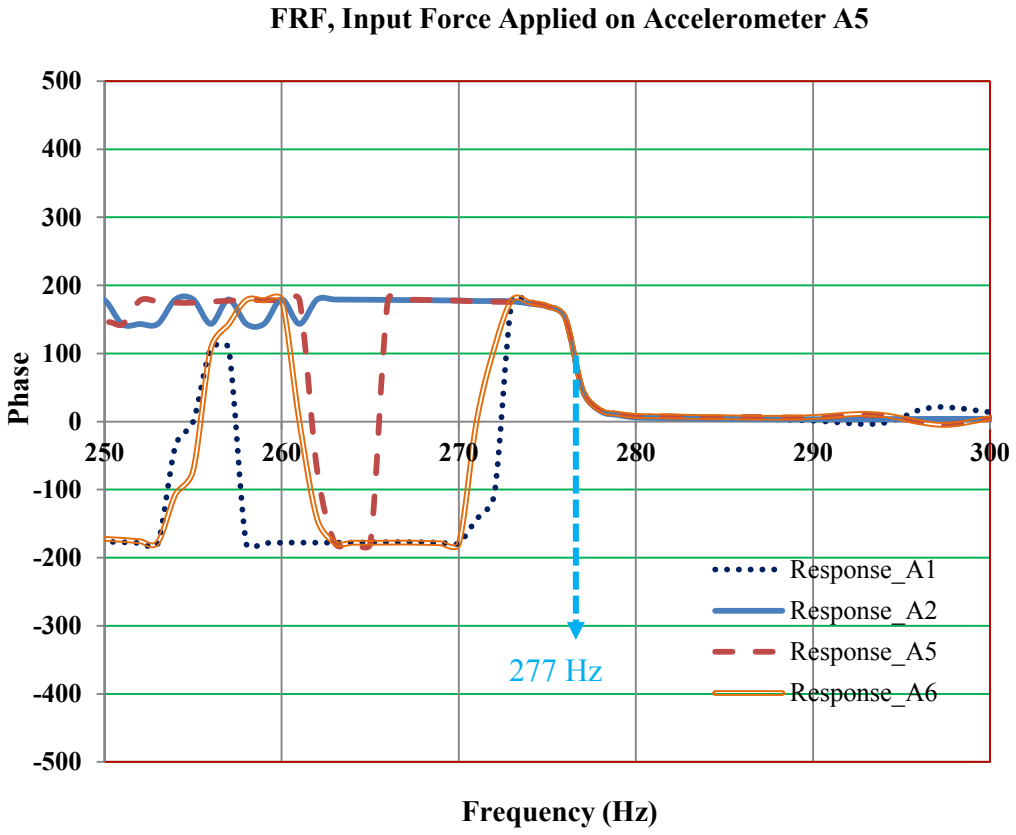

Figure 4.8. FRF, Phase, Input Force Applied on Accelerometer A5, and Responses of Accelerometers A1, A2, A5, and A6 Showing Symmetric Bending Mode at 277 Hz

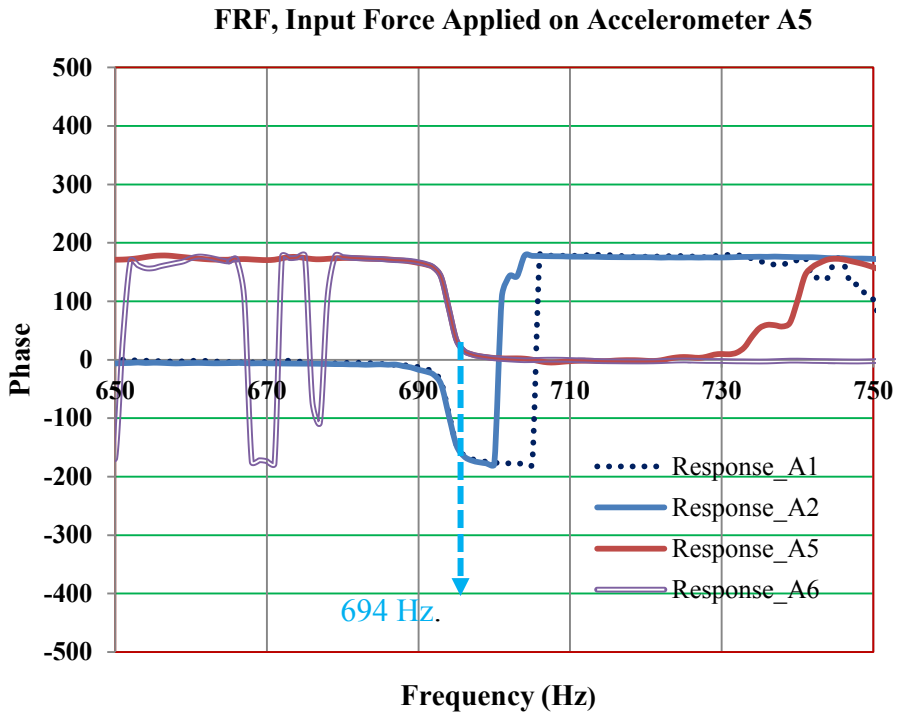

Figure 4.9. FRF, Phase, Input Force Applied on Accelerometer A5, and Phase Responses of Accelerometers A1, A2, A5, and A6 Showing Unsymmetric Bending Mode at 694 Hz

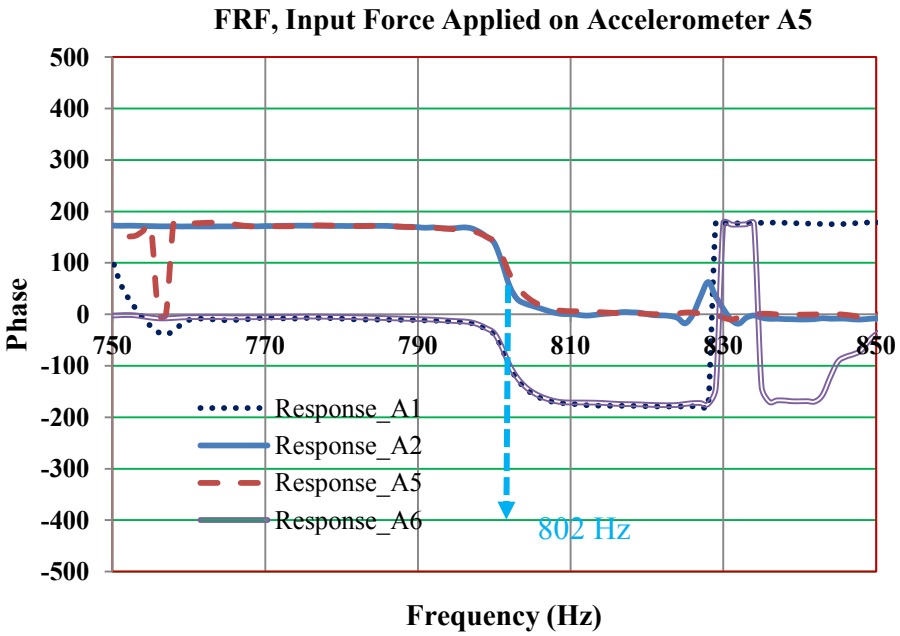

Figure 4.10. FRF, Phase, Input Force Applied on Accelerometer A5, and Responses of Accelerometers A1, A2, A5, and A6 Showing Torsion Mode at 802 Hz

4.2 GVT of Free-Free Beam with Attached Secondary Structure/Links

Figure 4.11 shows the test setup of a beam with two 0.6-pound links attached. As can be seen, accelerometers A7 and A8 are attached to the links in the fore-aft direction (direction 1). The average FRFs and magnitude responses, and FRFs and phase responses of the accelerometers for force input near A5 are shown in Figures 4.12 and 4.13, respectively. From Figure 4.12, it can be seen that there are two peaks at 75 Hz and 113 Hz, and the magnitude peaks at accelerometers A7 and A8 are greater than at the other accelerometers, thus indicating that this mode is primarily associated with the links.

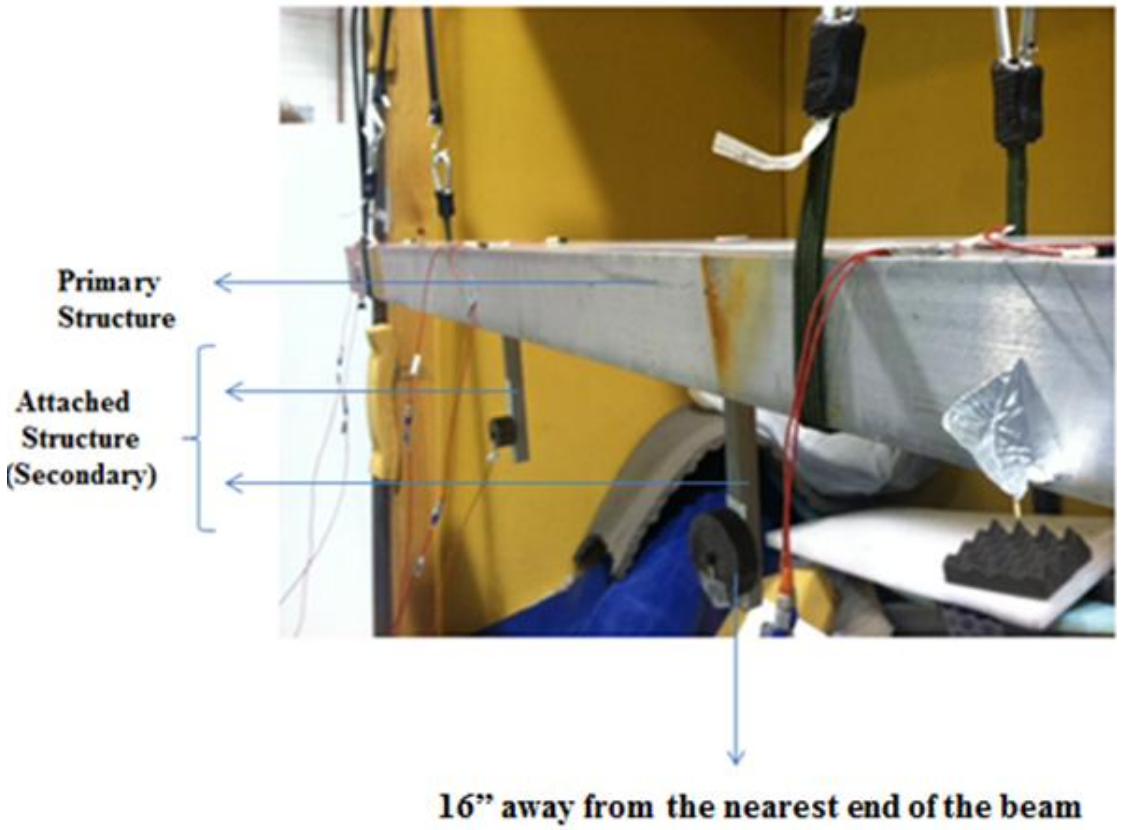

Figure 4.11. GVT Setup of Beam with Attached Secondary Structure

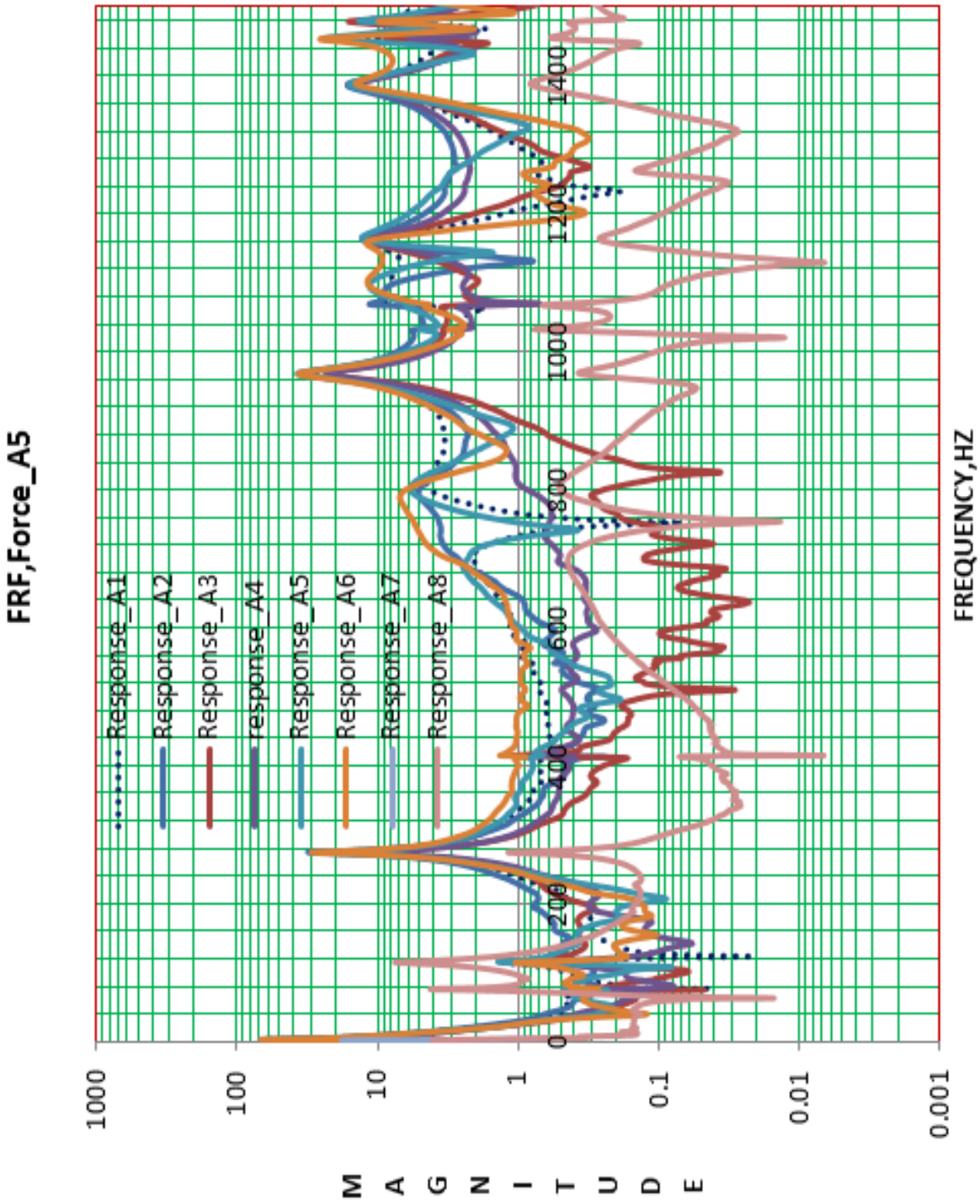

Figure 4.12. FRF and Magnitude Responses of all Accelerometers with Input Force Applied on Accelerometer A5

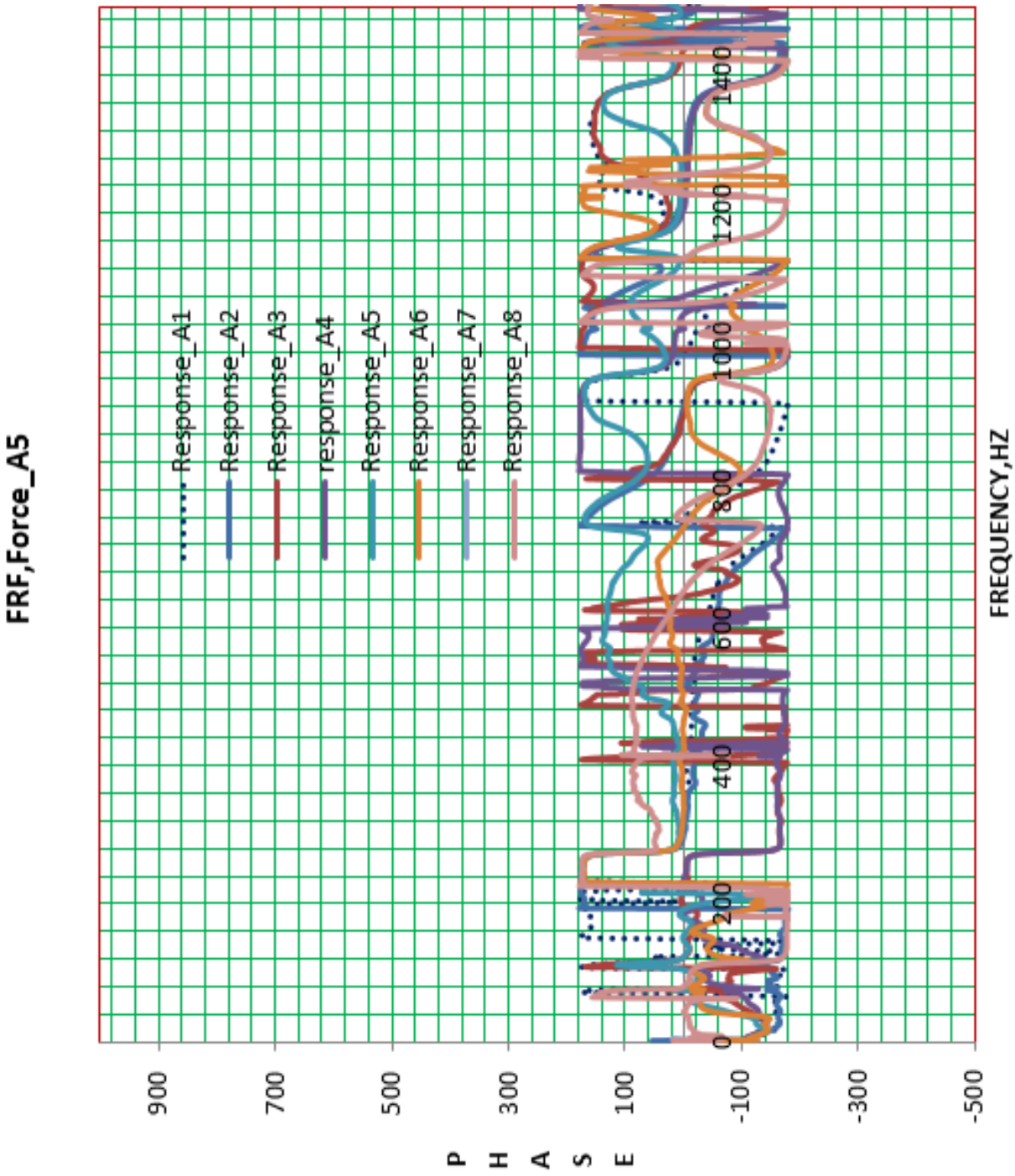

Figure 4.13. FRF and Phase Responses of all Accelerometers with Input Force Applied on Accelerometer A5

It can be seen from Figure 4.14 that at 73 Hz, A7 and A8 are out of phase, and at 113 Hz, they are in phase. From Figure 4.15, it is evident that the other peaks on the beam are at 273 Hz, 686 Hz, and 784 Hz.

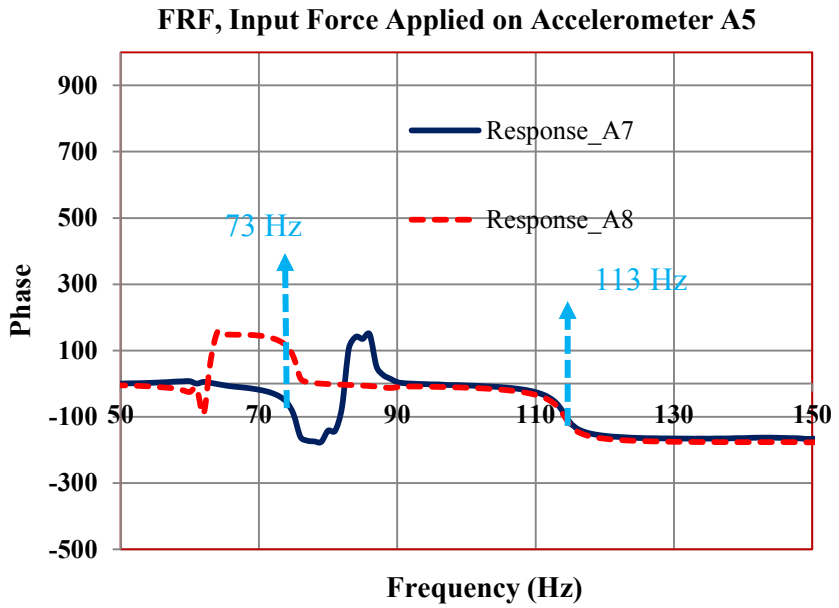

Figure 4.14. FRF, Phase, Input Force Applied on Accelerometer A5, and Responses of Accelerometers A7 and A8

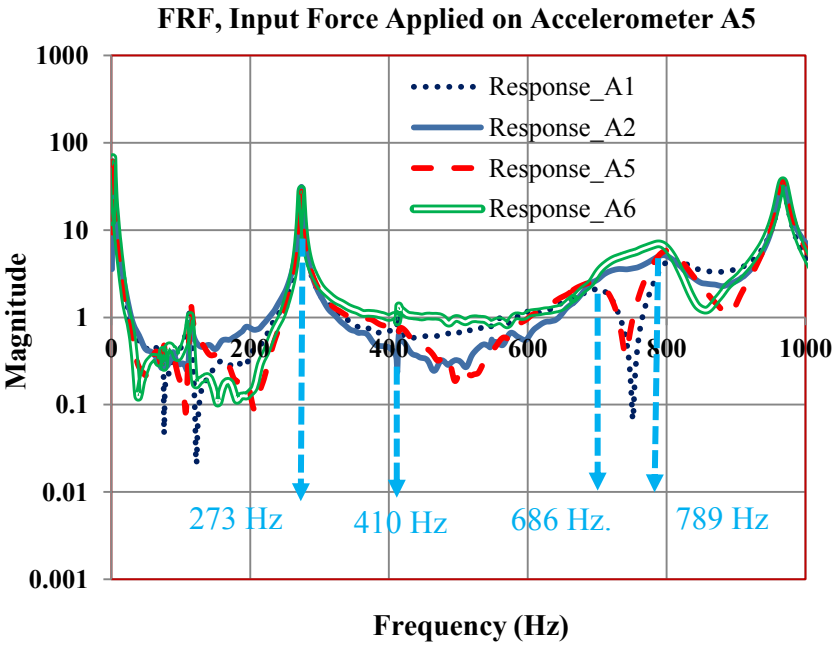

Figure 4.15. FRF, Magnitude, Input Force Applied on Accelerometer A5, and Responses of Accelerometers A1, A2, A5, and A6

To identify the characteristics of those modes, Figure 4.16 shows that at 273 Hz, all accelerometers are in phase, which indicates a symmetric bending mode. Figure 4.17 shows that

A1and A2 accelerometers are in phase, and accelerometers A5 and A6 are in-phase, but A1 is out of phase with A5, which indicates an asymmetric bending mode. Figure 4.18 shows that A1 and A2 accelerometers are out of phase, as are A5 and A6, while accelerometers A1 and A6 are in phase, which indicates a torsion mode.

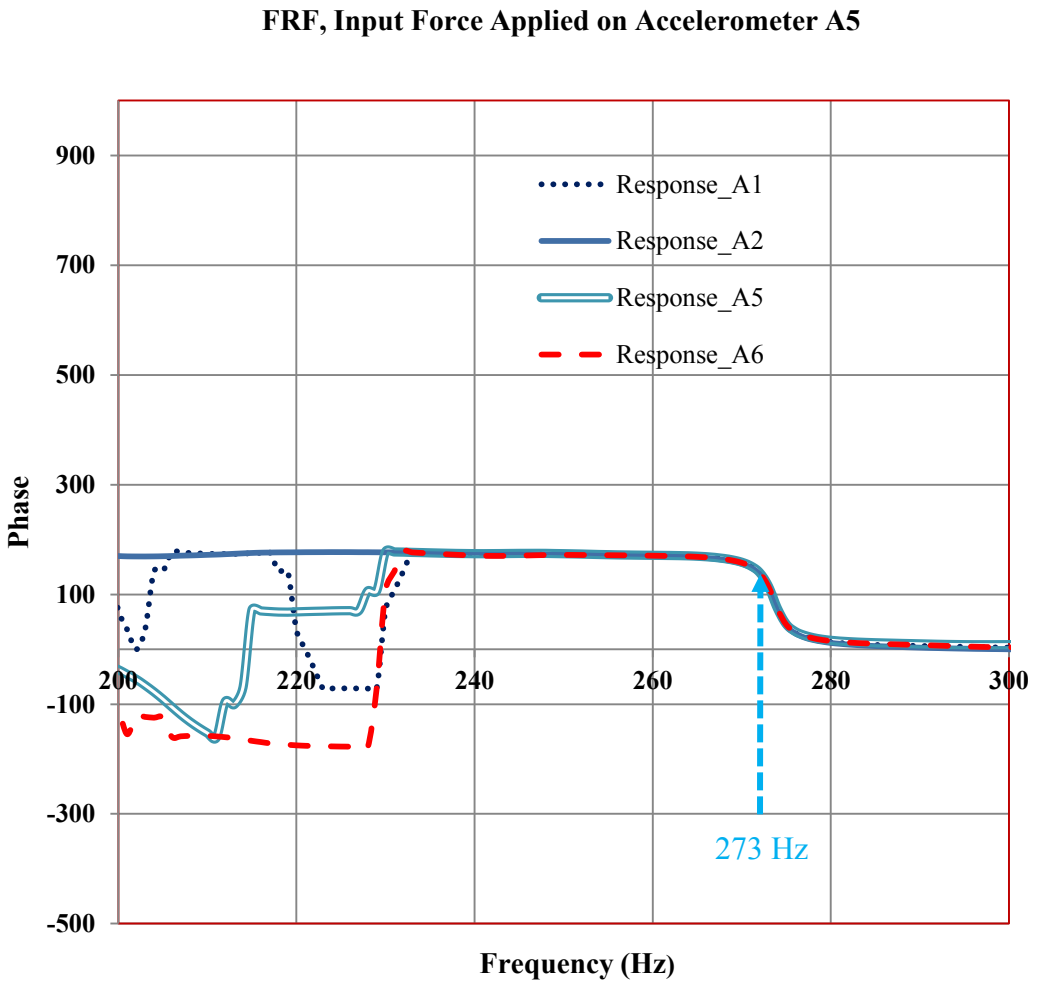

Figure 4.16. FRF, Phase, Input Force Applied on Accelerometer A5, and Phase Characteristics of Accelerometers A1, A2, A5, and A6 at 273 Hz Mode

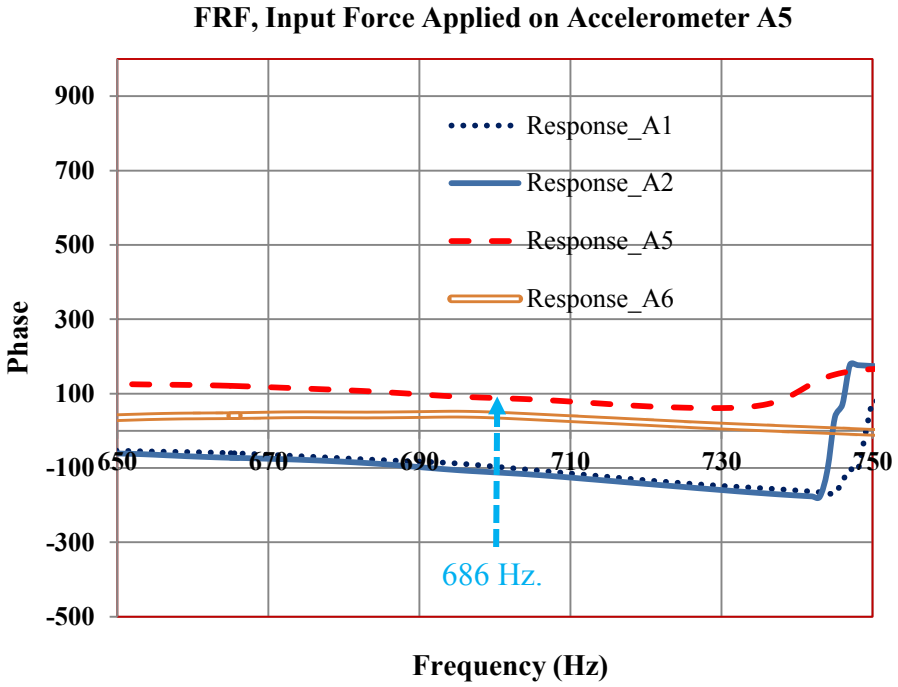

Figure 4.17. FRF, Phase, Input Force Applied on Accelerometer A5, and Phase Characteristics of Accelerometers A1, A2, A5, and A6 at 686 Hz Mode

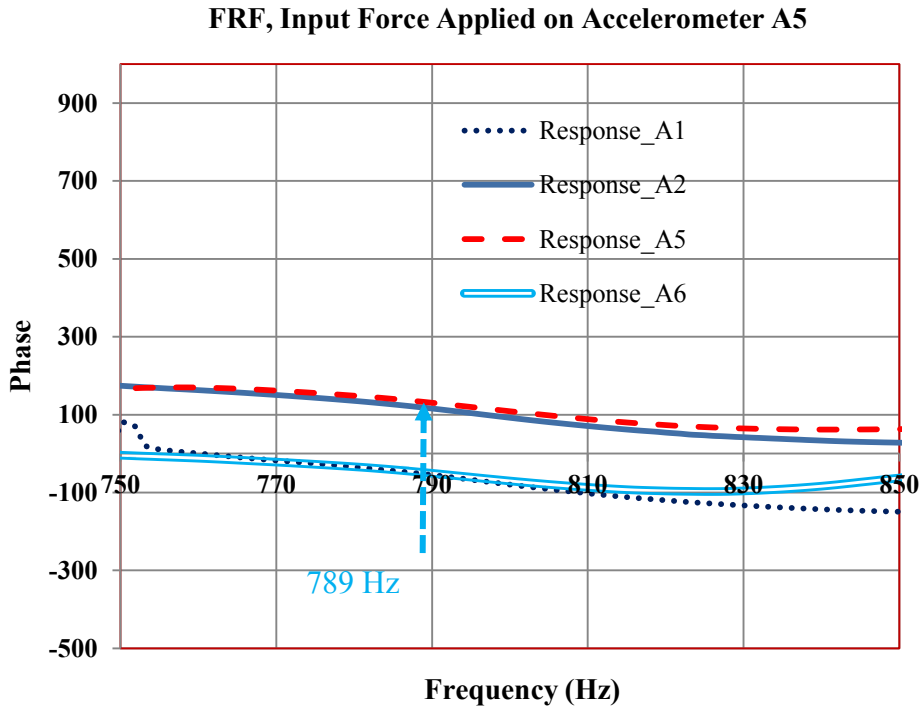

Figure 4.18. FRF, Phase, Input Force Applied on Accelerometer A5, and Phase Characteristics of Accelerometers A1, A2, A5, and A6 at 789 Hz Mode

CHAPTER 5

ANALYSIS RESULTS AND DISCUSSION OF FREE-FREE BEAM AND SECONDARY STRUCTURE

5.1 Vibration Analysis of Free-Free Beam (FEM)

A finite element modal analysis was performed on the free-free beam. Bungees are represented by spring elements in Figure 5.1. This model was built using FEMAP with the solver MSC NASTRAN. A total of 1,296 CQUAD elements with a thickness of 0.24 in. and 1,322 grid points were used in the model. The spring stiffness used to represent bungees were of relatively low values in order to represent the rigid body modes of frequencies close to 1 Hz, which is a much lower value than the first structural mode.

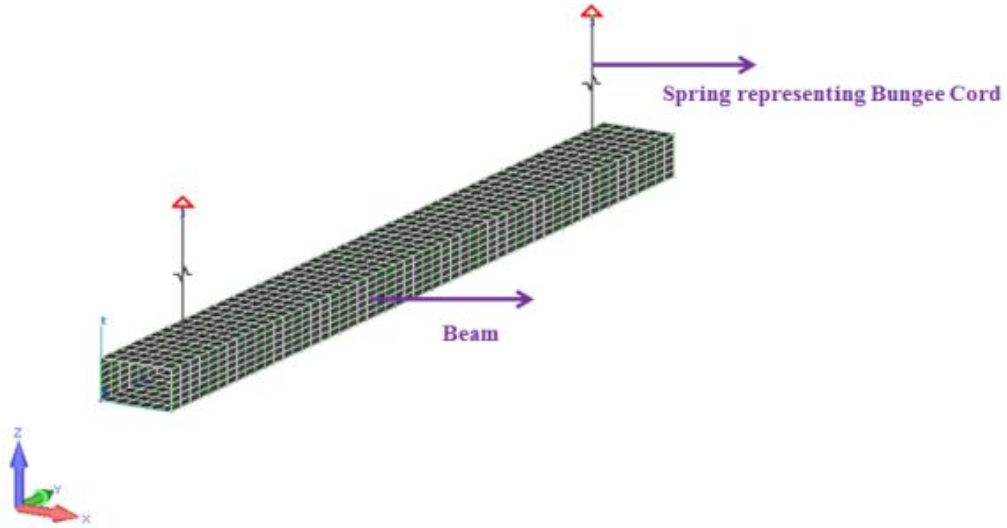

Figure 5.1. Finite Element Model of Beam

The NASTRAN SOL 103 program was used on the model, and the natural frequencies were extracted to match up with the test results. The mode shapes of all those natural frequencies are shown in Figures 5.2 to 5.5.

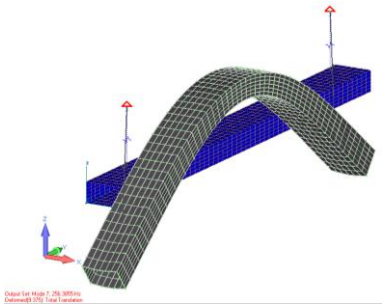

Figure 5.2. First Natural Frequency of Beam, 256 Hz.

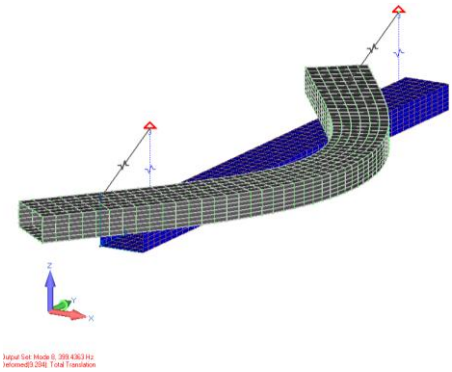

Figure 5.3. Second Natural Frequency of Beam, 399 Hz.

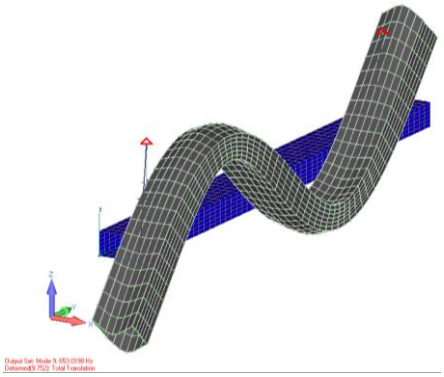

Figure 5.4. Third Natural Frequency of Beam, 653 Hz

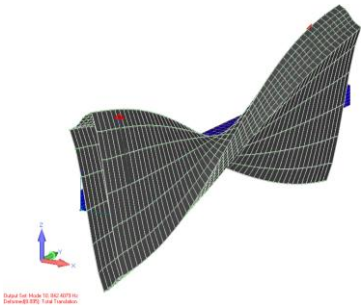

Figure 5.5. Fourth Natural Frequency of Beam, 842 Hz.

5.2 Vibration Analysis of Stick Model

A stick model was developed so that the whole hollow beam could be represented by equivalent beam elements. To develop this simplified model, the detailed coarse model was divided into separate equidistant bays, where the shear center of the cross section was connected to the various points in the structure by RBE3 (Rigid bars in NASTRAN), as shown in Figure 5.6. A moment of 100 lb-in was applied at one end, and the other end was constrained in three degrees of freedom (x, y, and z). From the output file, the rotational displacements were measured to determine the section properties: EI1, EI2, and GJ. For the given Young's modulus and shear modulus, the section properties of the cross section, I1, I2, and J can be determined. Property I1 mostly determines the vertical bending frequency, I2 determines the fore-aft frequency, and J contributes to the torsional frequency. This methodology was explained previously in Chapter 1.

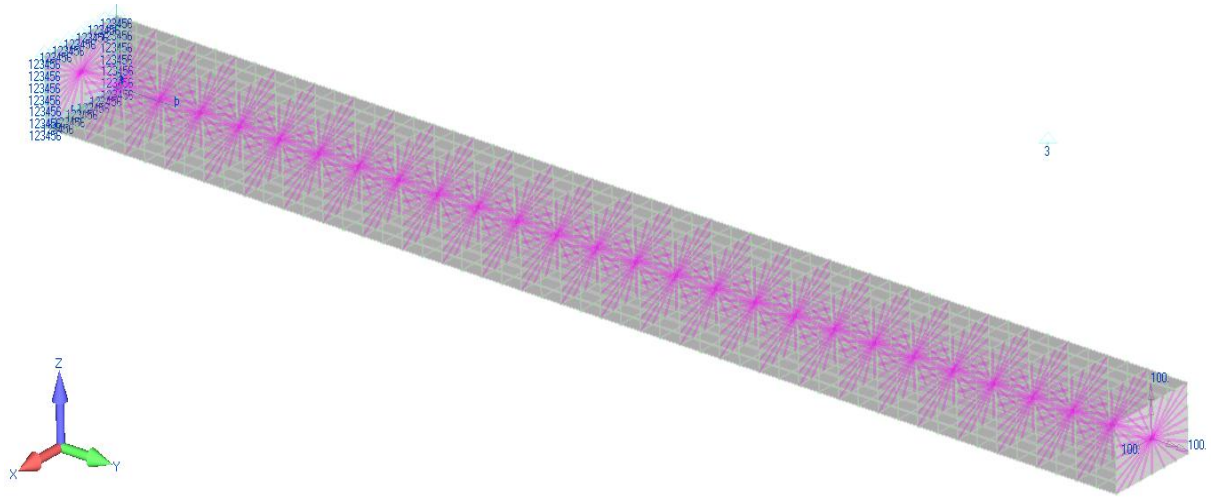

Figure 5.6. Load-Deflection Model of Beam

The simplified stick model of the beam is shown in Figure 5.7. The stiffness distribution of the beam, from the above methodology, is shown in Figure 5.8. Using the previously

mentioned methodology, the section moduli were determined to be, I1 = 3.9 in^4, I2 = 9.8 in^4, and J = 8.3 in^4.

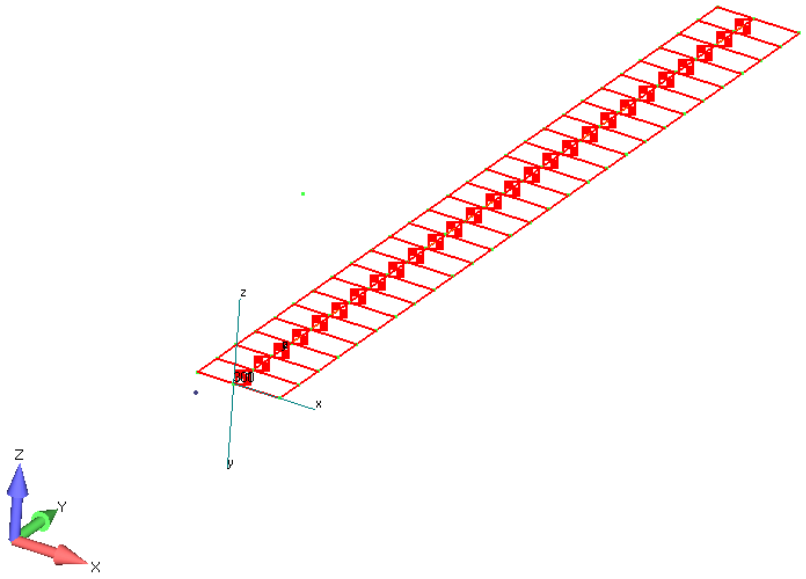

Figure 5.7. Stick Model of Beam

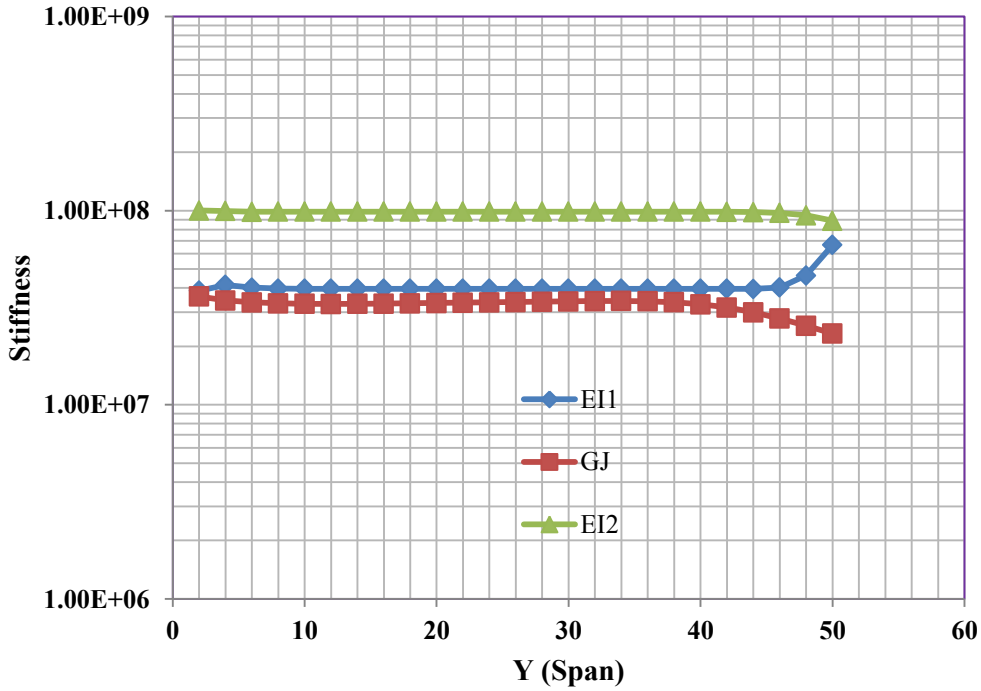

Figure 5.8. Stiffness Distribution of Beam

A modal comparison of the stick model was also performed. Figures 5.9 to 5.12 show the mode shapes and frequencies associated with each mode on the stick model.

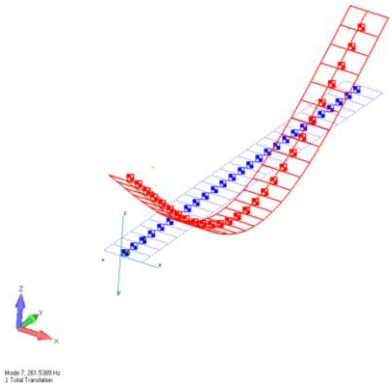

Figure 5.9. First Vertical Bending Mode at 261 Hz.

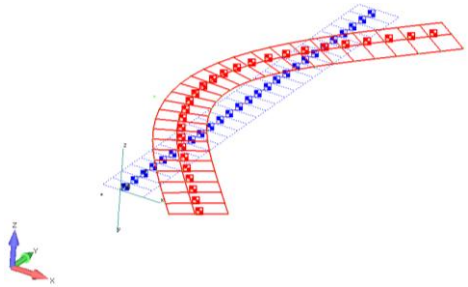

Figure 5.10. First Fore-Aft Mode at 400 Hz.

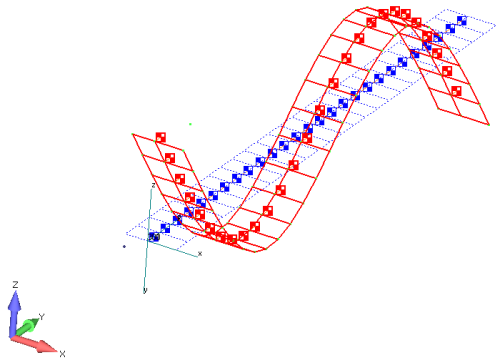

Figure 5.11 Second Vertical Bending Mode at 710 Hz

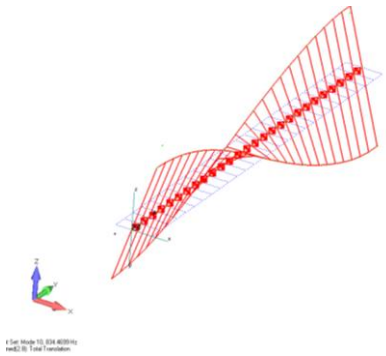

Figure 5.12. First Torsion Mode at 835 Hz

A comparison of the transfer function of the two beam models (coarse FE model and stick model) with test results is shown in Figure 5.13.

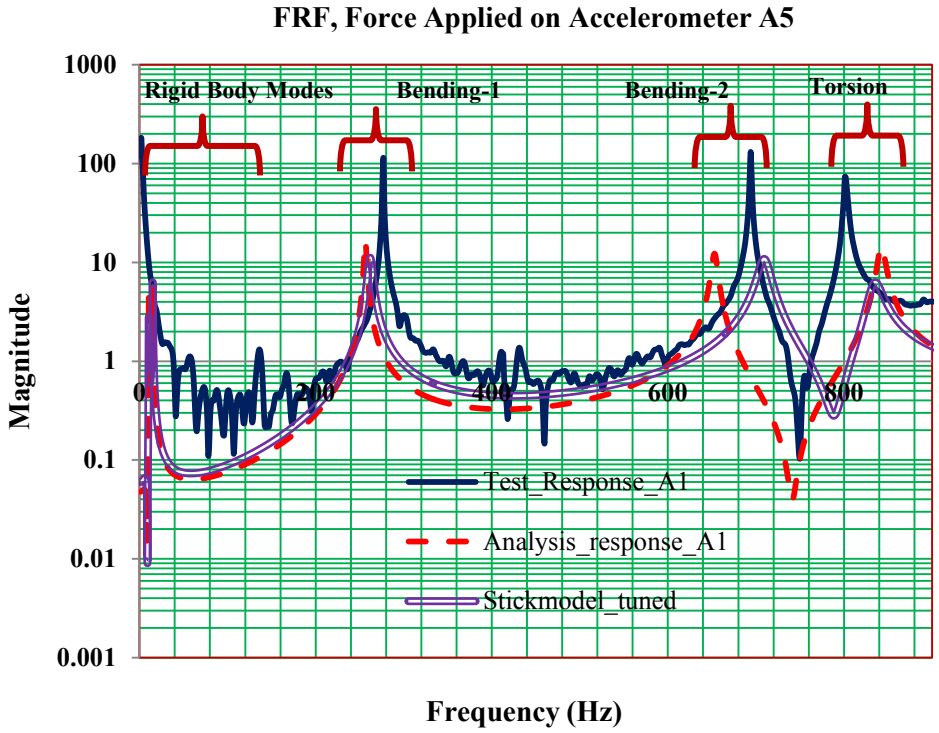

Figure 5.13. Transfer Function Comparison of Two Beam Models (Coarse FE Model and Stick Model) with Test Results

5.3 Analytical Approach to Determine Natural Frequency of Parametric Free-Free Beam

Analytically, natural frequencies of the free-free beam bending were determined using the mathematical expressions mentioned in the literature review in Chapter 2. Previously shown Table 2.6 indicates the values of *kL* (frequency parameter) for bending. For torsion mode,

equations (2.18) and (2.19) were applied to determine the natural frequency. Table 5.1 shows the natural frequencies of the bending modes as well as torsion mode of the free-free beam. Details of the calculations can be found in Appendix A. Table 5.2 provides the natural frequencies determined by the coarse FE model, stick model, and analytical method, all compared to the test data.

TABLE 5.1

NATURAL FREQUENCIES OF MODES OF FREE-FRFEE BEAM
DETERMINED ANALYTICALLY

Parameters	Bend. Mode 1	Bend. Mode 2	Bend. Mode 3	Parameters	Torsion mode 1
L (Length of the beam,Inches)	54.00	54.00	54.00	L	54.00
b1 (Outer width of the cross section,Inches)	5.00	5.00	5.00	b1	5.00
h1(Outer height of the cross section)	3.00	3.00	3.00	h1	3.00
t (Thickness,Inches)	0.24	0.24	0.24	t	0.24
b2 (Inner width of the cross section,Inches)	4.52	4.52	4.52	b2	4.52
h2 (Inner height of the cross section,Inches)	2.52	2.52	2.52	h2	2.52
A (Area of cross section)	3.61	3.61	3.61	A	3.61
I1 (Section modulus,vertical bending)	3.50	3.50	3.50	J	8.33E+00
p (density,lb/in^3)	0.10	0.10	0.10	p	0.10
E (Young's modulus,psi)	1.00E+07	1.00E+07	1.00E+07	G (Shear Modulus)	4.00E+06
v (poisson's ratio)	0.30	0.30	0.30	v	0.30
KL(freq.parameter)	4.73	7.85	11.00	Jp	17.08
K	0.09	0.15	0.20	Ct	86777.37
ω (Angular Frequency)	1484.34	4088.37	8021.95	ω	5045.94
f (Natural frequency,ω/(2*3.14)	236.36	651.01	1277.38	f	803.49

TABLE 5.2

COMPARISON OF NATURAL FREQUENCIES OF FREE-FREE BEAM
WITH TEST RESULTS

	TEST(HZ)	ANALYSIS, COARSE FEM(HZ)	%diff	ANALYSIS,STICK MODEL (HZ)	%diff	Analytical	%diff
BENDING 1	277	257	-7.22	261	-5.78	236	-14.80
BENDING-2	694	652	-6.05	710	2.31	651	-6.20
TORSION-1	802	843	5.11	835	4.11	803	0.12

5.4 Vibration Analysis of Free-Free Beam with Flexible Link

Modal analysis of the free-free beam with flexible links was performed using the stick model. The flexible links were modeled as rigid elements with a spring and mass attached to the primary structure, thus making it flexible. The spring stiffness was tuned to match up with the test results, and the degrees of freedom whereby the spring stiffness was made flexible in the rotational direction 5 (rotation about the y-axis). Figure 5.14 shows the free-free beam model (stick model) and the two attached links.

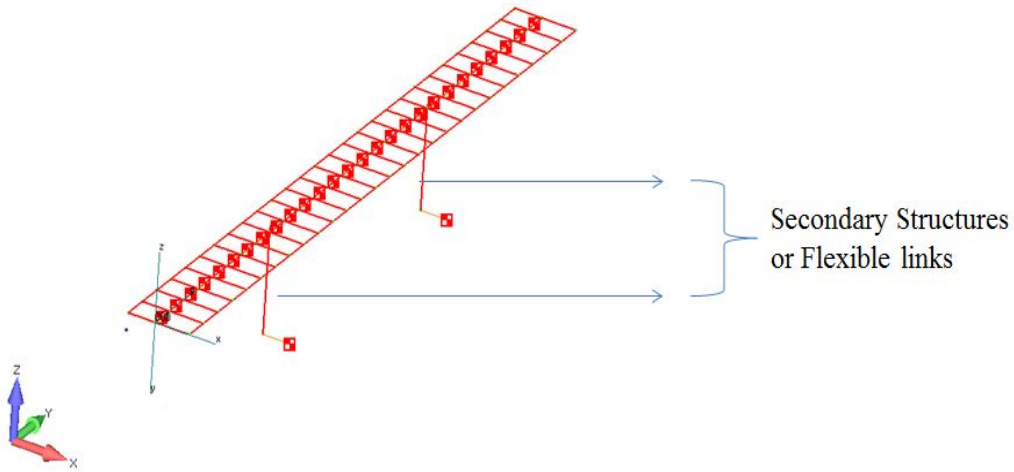

Figure 5.14. Stick Model with Flexible Links

The link structure frequencies are lower than the structural frequency of the beam. Natural frequencies of the system are the peaks shown in Figure 5.15. Figure 5.16 shows that at 73 Hz, the links are out of phase (asymmetric) with each other, and at 113 Hz, the links are in phase (symmetric) with each other. Figure 5.17 shows the response on accelerometers A7 and A8, which indicates that the two modes near 73 Hz and 113 Hz. Analysis results for those modes are shown in Figures 5.17 and 5.18, respectively. Figures 5.19 to 5.22 show the mode shapes of the other structural frequencies. A comparison of the transfer function on accelerometers A1 and A7 with input force applied on accelerometer A5 are shown in Figures 5.23 and 5.24, respectively. Table 5.3 shows a comparison of analysis frequencies with test results.

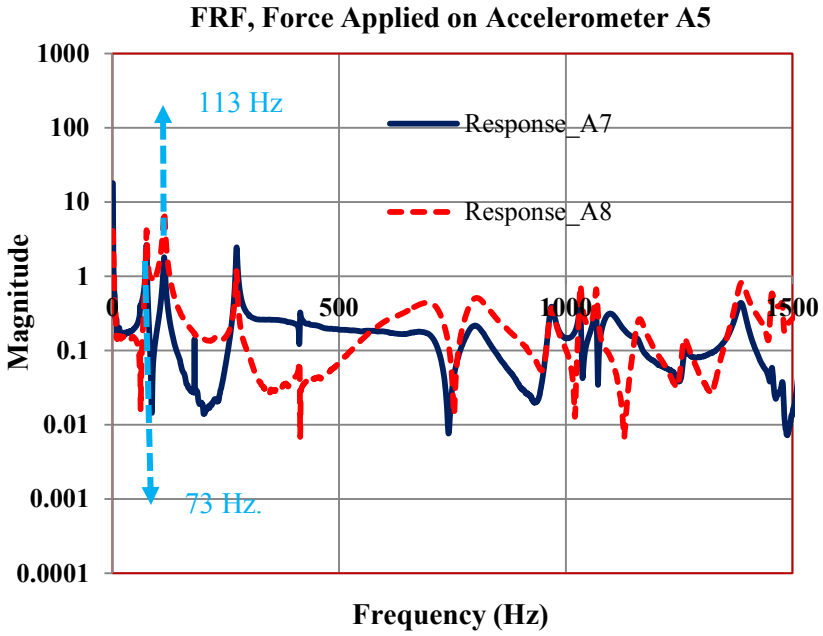

Figure 5.15. FRF, Magnitude, Force Applied on Accelerometer A5, and Transfer Function Responses of Accelerometers A7 and A8

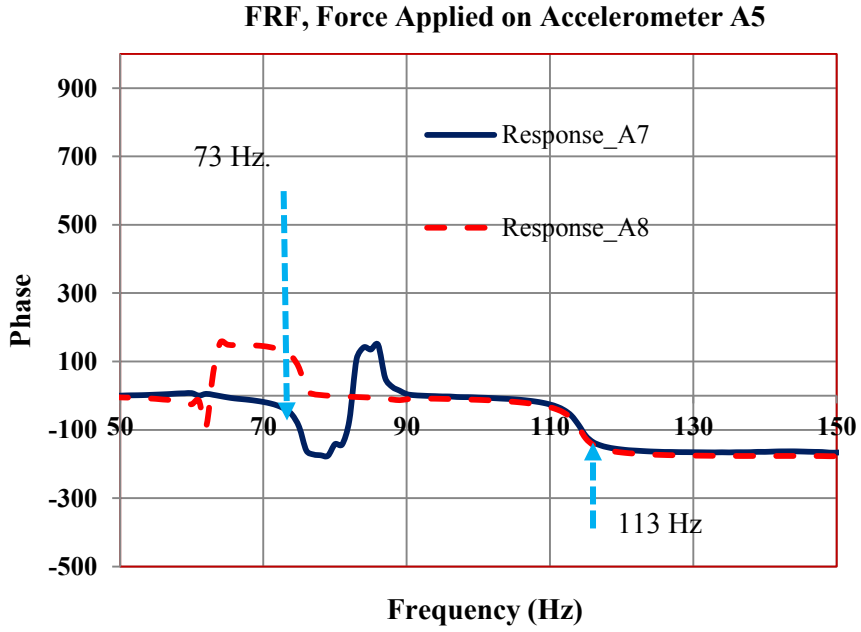

Figure 5.16. FRF, Phase, Force Applied on Accelerometer A5, and Phase Responses of Accelerometers A7 and A8

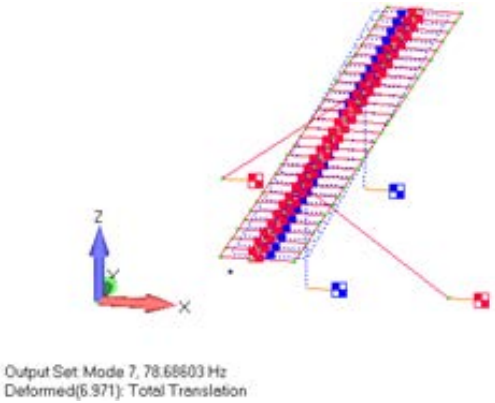

Figure 5.17. Mode Shape at 78.6 Hz

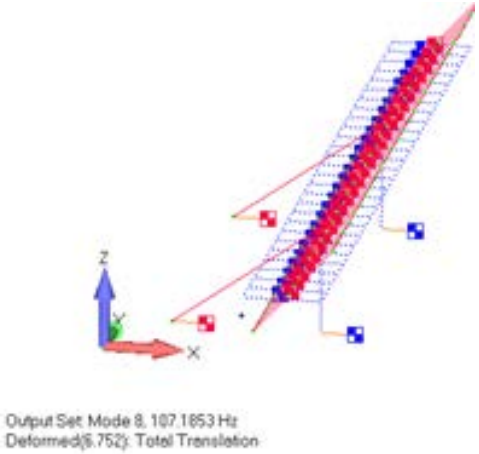

Figure 5.18. Mode Shape at 107.1 Hz

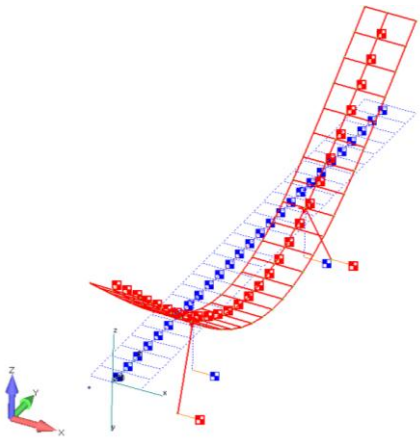

Figure 5.19. Bending Mode at 253.4 Hz

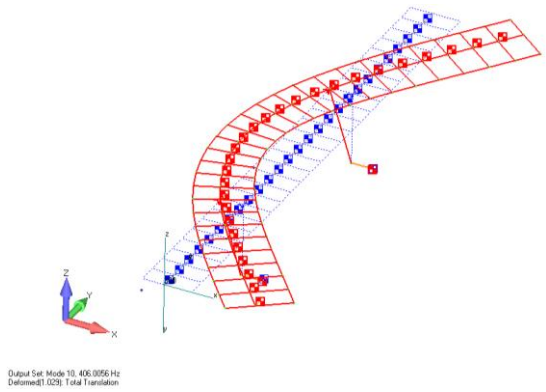

Figure 5.20. Fore-Aft Mode at 406 Hz

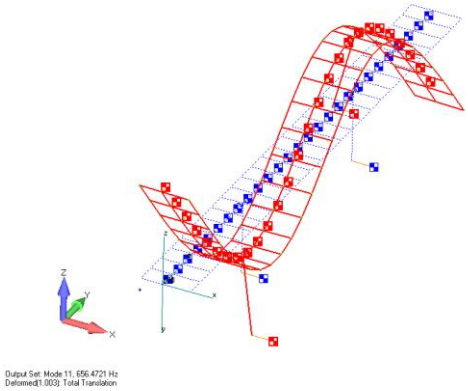

Figure 5.21. Second Bending Mode at 675 Hz

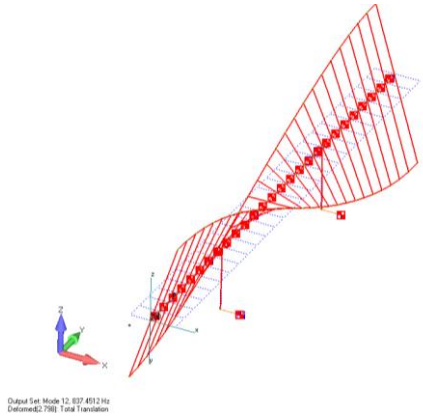

Figure 5.22. First Torsion Mode at 837 Hz

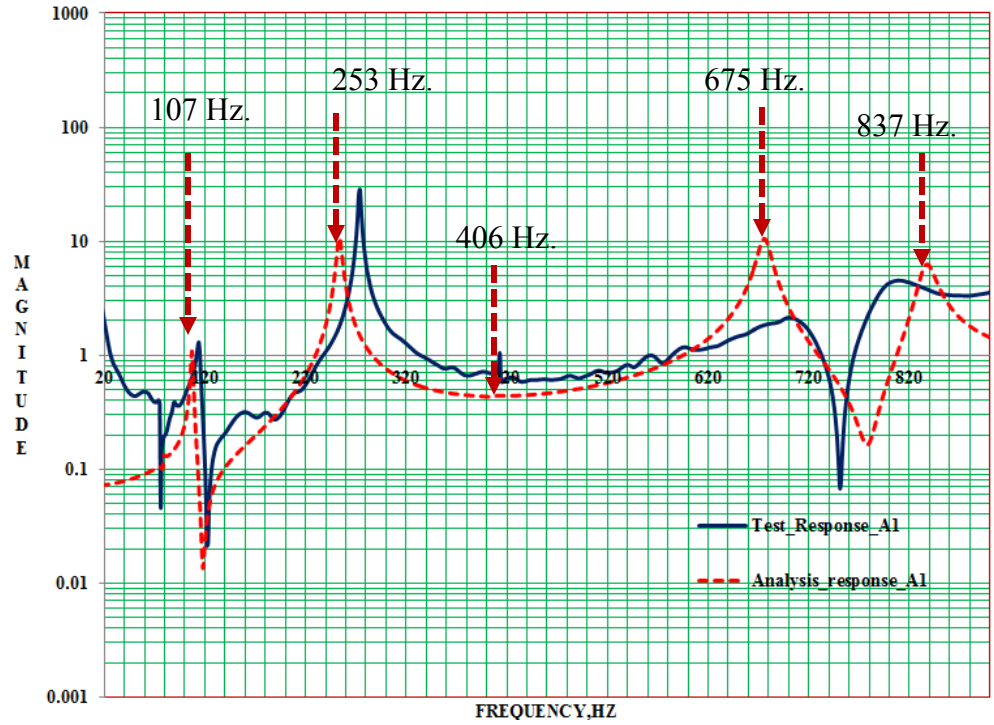

Figure 5.23. FRF, Magnitude, Input Force on Accelerometer A5, and Transfer Function Comparison on Accelerometer A1

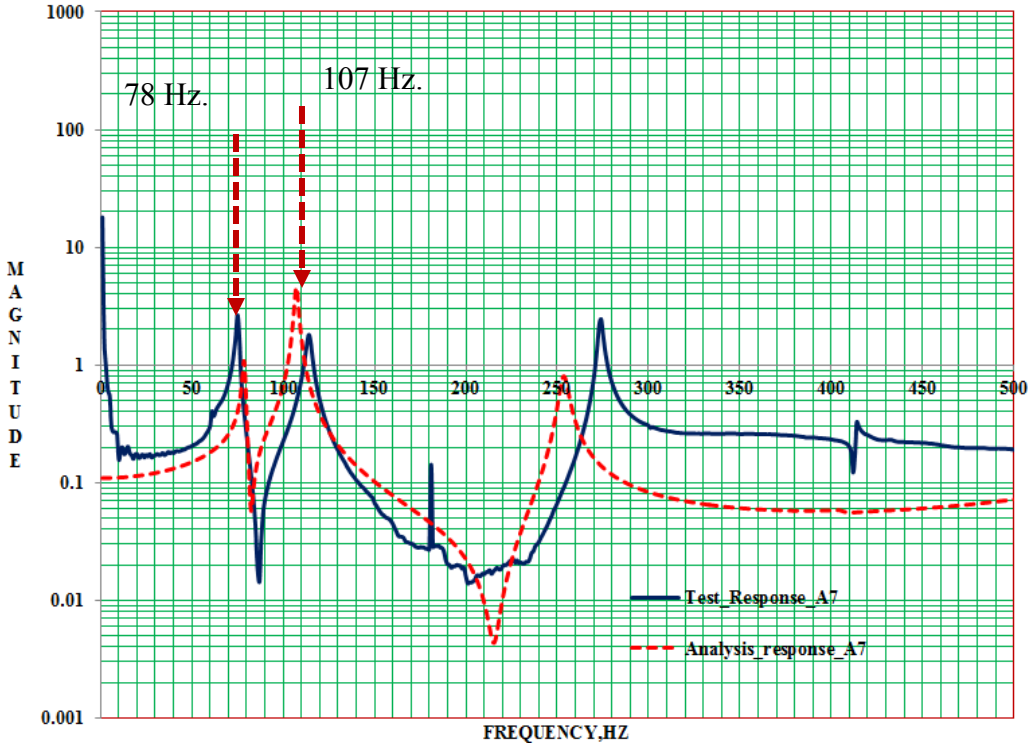

Figure 5.24. FRF, Magnitude, Input Force on Accerometer A5, and Transfer Function Comparison on Accelerometer A7

TABLE 5.3

COMPARISON OF ANALYSIS FREQUENCIES WITH TEST RESULTS

Mode	Test (Hz)	Analysis (Stick Model)	Difference (%)
Link Out-of-Phase Mode	73	78.6	7.67
Link In-Phase Mode	113	107.1	5.22
Bending-1	273	253.4	–7.16
Fore-Aft	410	406.6	–0.83
Bending-2	686	675.9	–1.47
Torsion	789	836.6	6.03

5.5 Parametric Study of Free-Free Beam Modes with Change in Flexible Link Compliant Stiffness

A parametric study was conducted on the variation of rotational stiffness (degrees of freedom-5) of the links on the link in-phase (symetrical) and out-of-phase (asymmetrical) mode with each other. The rotational stiffness was varied from 0.33 times the nominal stiffness to 100 times. The nominal rotational stiffness was tuned to be 3.0E4 lbf/rad. Results of the study are provided in Figure 5.25, which shows the increase in the frequency of the symmetric link (secondary structure) mode and asymmetric link (secondary structure) mode. As the rotational stiffness of the flexible link increases, the asymmetric beam torsion mode splits into two: in-phase and out-of-phase with asymmetric link modes. For the asymmetric beam torsion mode in phase with the link mode, the links move along with the motion of the beam (Figure 5.26), and for the out-of phase mode, the links moves in the opposite direction of the beam's direction of motion (Figure 5.27). For 33 times the rotational stiffness, the beam asymmetric torsional mode in phase with the links is at 356 Hz (Figure 5.26), and the beam asymmetric torsional mode out of phase with the links is at 929 Hz (Figure 5.27).

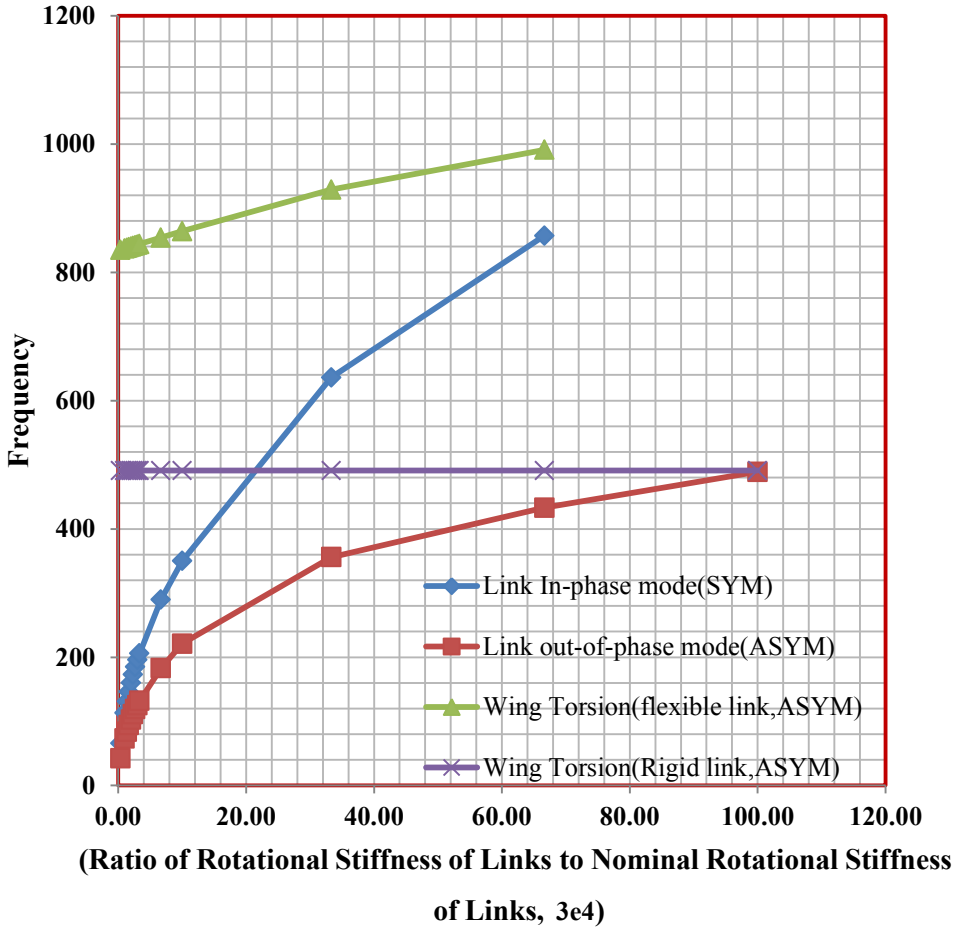

Figure 5.25. Variation of In-Phase and Out-of-Phase Modes with Stiffness

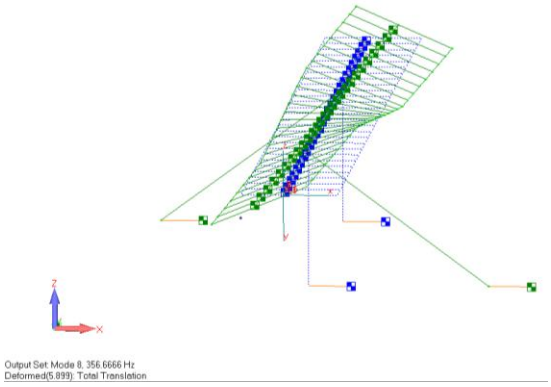

Figure 5.26. Asymmetric Beam Torsion Mode in Phase with Links

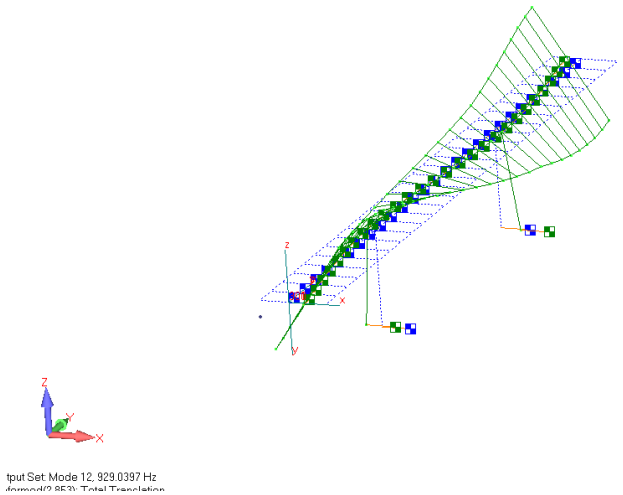

Figure 5.27. Asymmetric Beam Torsion Mode out of Phase with Links

While performing GVT, for a beam configuration with flexible links having 33 times the nominal rotational stiffness (Figure 5.25), engineers would see two peaks for beam torsion, one at 356 Hz and one at 929 Hz. If there are no accelerometers on the links, it would be difficult to tune or determine the correct beam torsional stiffness. In this case, there is a high probability that the wing torsional stiffness is tuned to 929 Hz. It can be seen in Figure 5.25 that the asymmetric beam torsion mode in phase with the links converges as the compliant stiffness of the links to the beam becomes stiffer (rigid); in this case, that frequency converges to 491 Hz. The stiffness distribution of the beam which shows 491 Hz when the link masses are rigidly attached is the real torsional stiffness. But if the beam torsional stiffness is tuned to 929 Hz, then the flutter analysis following GVT will be highly non-conservative—the higher the torsional frequency, the higher the flutter speed. At the same time, if the wing torsional stiffness is tuned to 356 Hz, then the flutter analysis performed will be highly conservative—the lower the torsional frequency, the lower the flutter speed. This will most probably result in over stiffening the beam to obtain a higher torsion mode. Therefore, for a beam having a secondary structure, it is necessary to perform GVT without the secondary structure attached and perform a GVT on the assembled

structure with accelerometers installed on the flexible secondary structures, to determine the in-phase and out-of-phase modes of the secondary structure with the beam mode.

5.6 Parametric Study of Free-Free Beam Modes with Change in Flexible Link Location

A parametric study was conducted to determine the change in torsional frequencies that are in phase and out of phase with the links, when the flexible links are moved to a different spanwise location on the beam (Figure 5.28). Case 1 is the nominal location of the flexible links. Case 2 is the location of the flexible links outboard of the nominal location, and Case 3 is the location of the flexible links inboard of the nominal location. This study was performed on flexible stiffness, 33 times the nominal (1E6 lbf/rad), so that a definite difference could be made on the torsion modes.

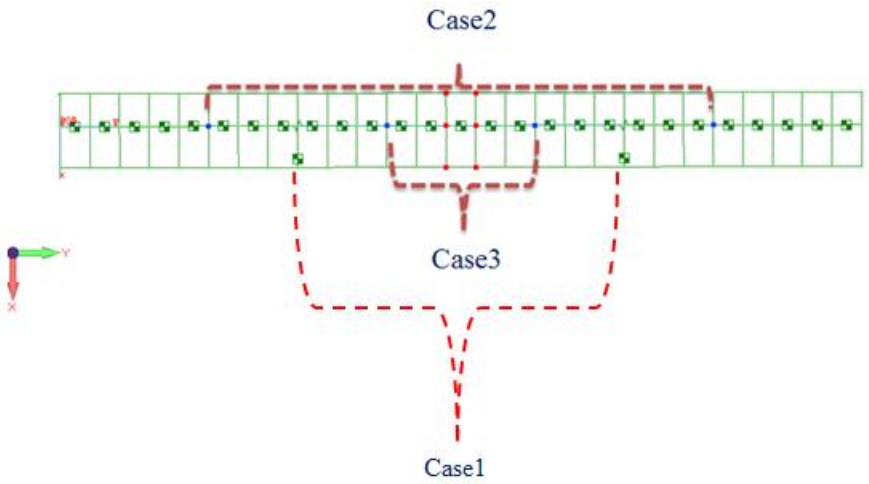

Figure 5.28. Location of Flexible Links (Spanwise Location)

Figure 5.29 shows that by moving the flexible link location more inboard, so that the beam torsion is in phase with the flexible link mode, the frequency increases, and for the beam torsion mode out of phase with the links, the frequency increases. This is shown in Figure 5.30. A summary of the change in frequencies is shown in Figure 5.31.

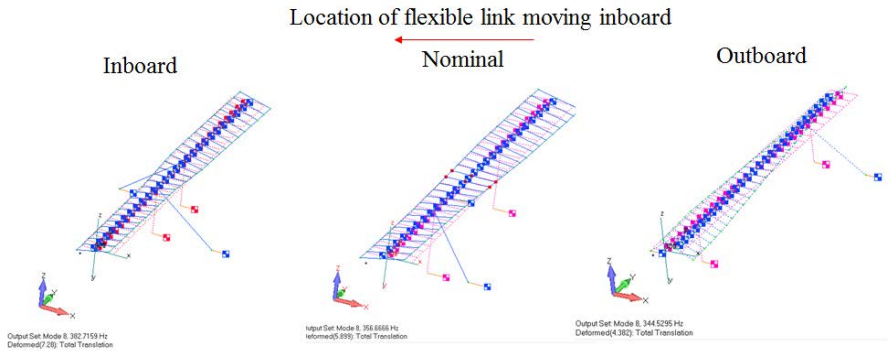

Figure 5.29. Change in Frequency on Beam Torsion Mode in Phase with Flexible Link

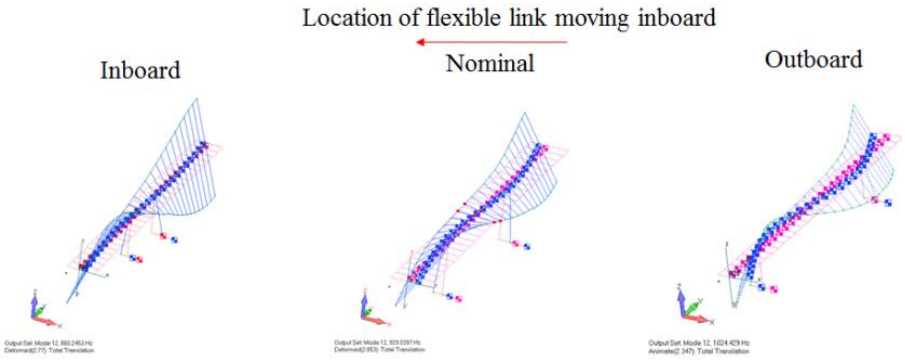

Figure 5.30. Change in Frequency on Beam Torsion Mode Out of Phase with Flexible Link

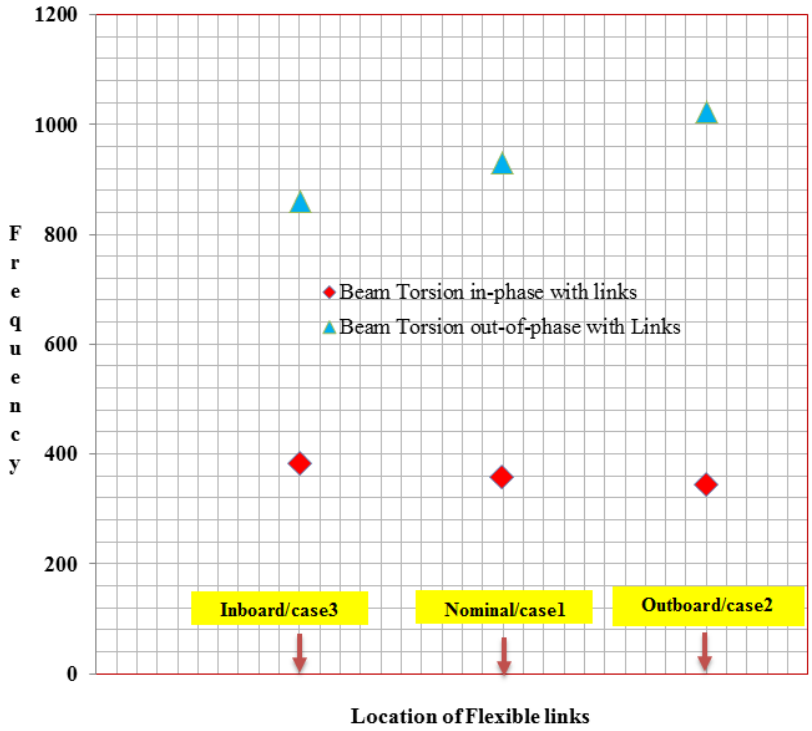

Figure 5.31. Change in Frequency due to Change in Spanwise Location of Flexible Links

Another parametric study was conducted to determine the change in the two torsional frequencies (in phase and out of phase with links), when the center of gravity of the flexible links changes its location. Three cases were considered: Case 1 is the nominal location, Case 2 is when the location of the mass (flexible link) is closer to the elastic axis of the beam, and Case 3 is when the mass is further away from the elastic axis of the beam, as shown in Figure 5.32. The nominal case has a compliance stiffness of 1E6 lbf/rad. Figure 5.33 shows that by moving the CG of the secondary structure (flexible links), the further the CG is from the elastic axis, the lower the frequencies.

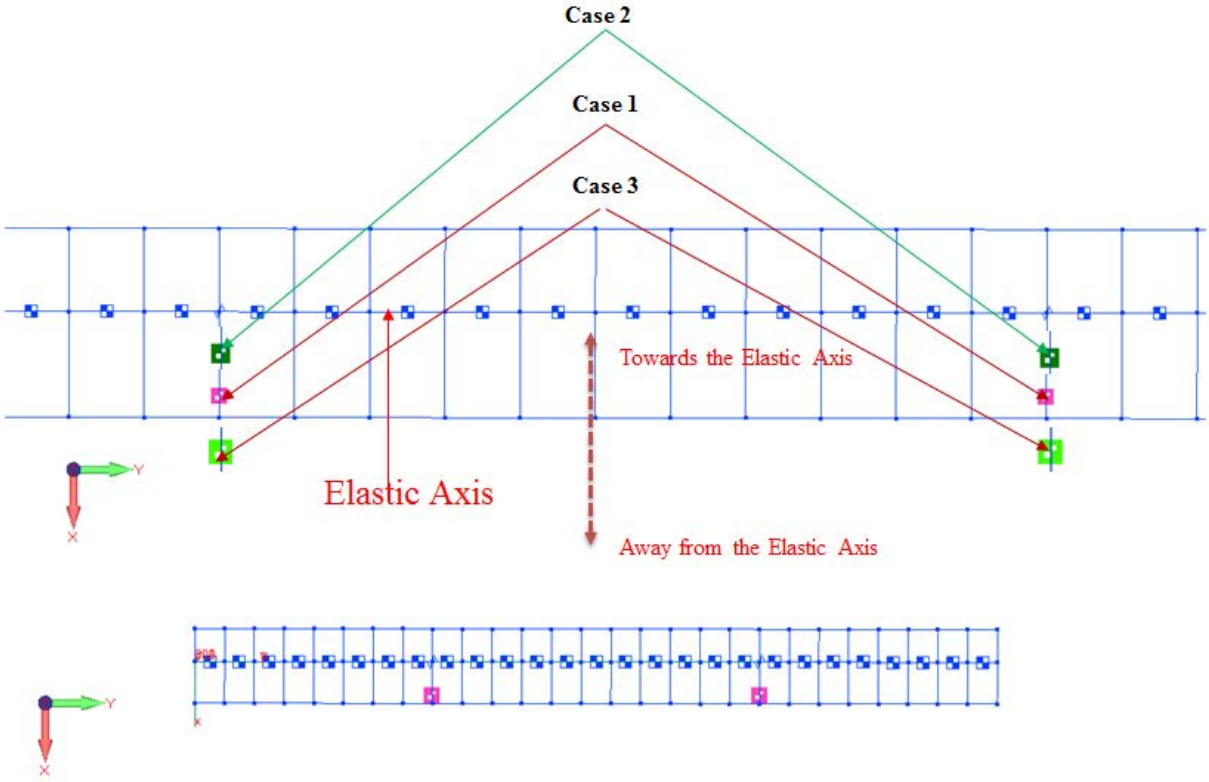

Figure 5.32. Flexible Link Location Change (Chordwise) with Respect to Elastic Axis

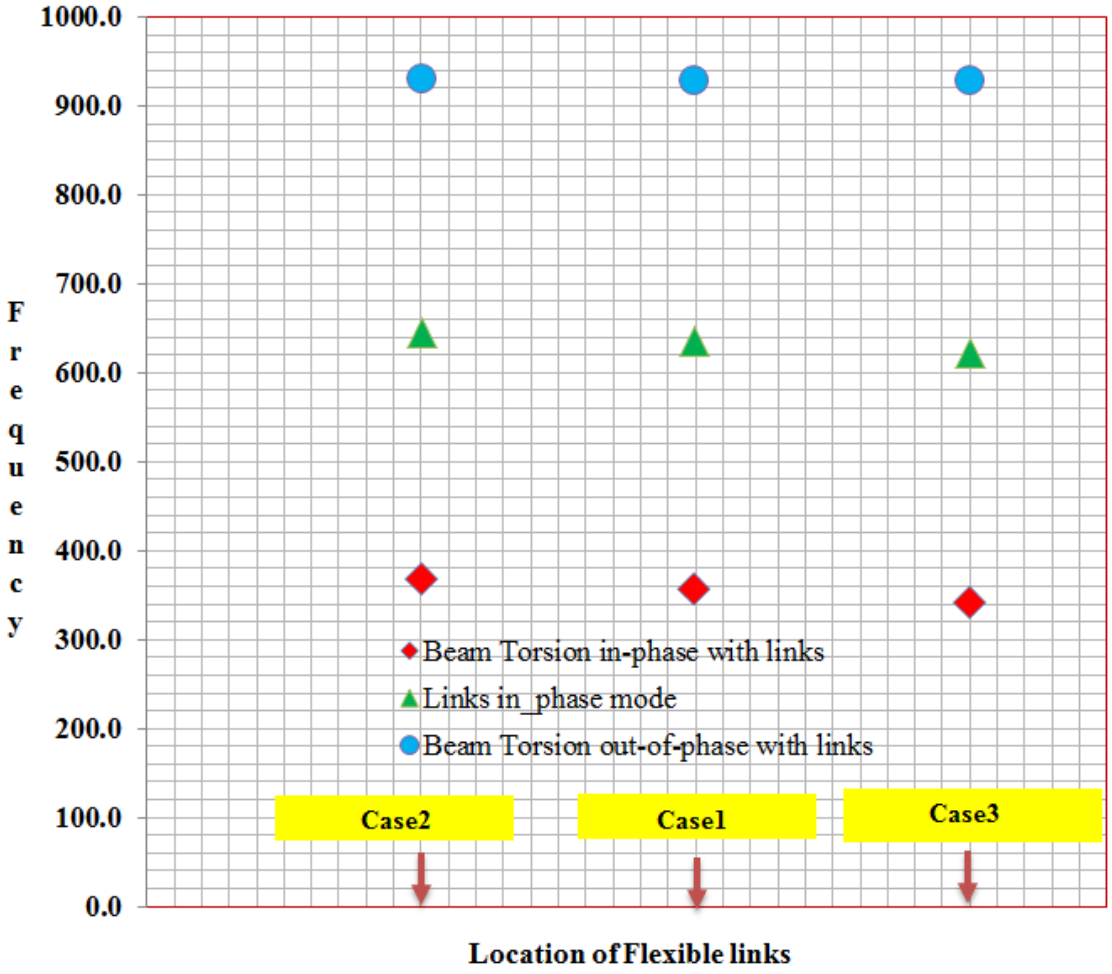

Figure 5.32. Change in Frequency on Chordwise Flexible Link Location

CHAPTER 6

GROUND VIBRATION TESTING OF CANTILEVER PLATE AS WELL AS SECONDARY STRUCTURE

6.1 GVT of Cantilever Plate

The GVT setup for the cantilever plate alone is shown in Figure 6.1. The plate, made out of aluminum 6061 of size 17" x 14" with thickness 0.115" was firmly clamped on one end. Three unidirectional (z-direction, vertical direction of input force) accelerometers were placed at the three ends as shown in Figure 6 1. Force input was done using an impact hammer (0 to 8,000 Hz), and the respective FRFs and phase plots were recorded. Labview PXI-1000B was used for signal processing, Dytran 5850B was used as the impact hammer, and the accelerometers were Endevco model 2222. All accelerometers were uniaxial, i.e., measuring acceleration in the z-direction (perpendicular to the plane of the plate).

Figure 6.1. GVT Setup for Cantilever Plate

Ten impacts were made, each near the location of accelerometers A1, A2, and A3. The average of the FRFs are shown in Figures 6.2 and 6.3. Figure 6.2 shows the magnitude response and Figure 6.3 shows the phase response of each accelerometer reading.

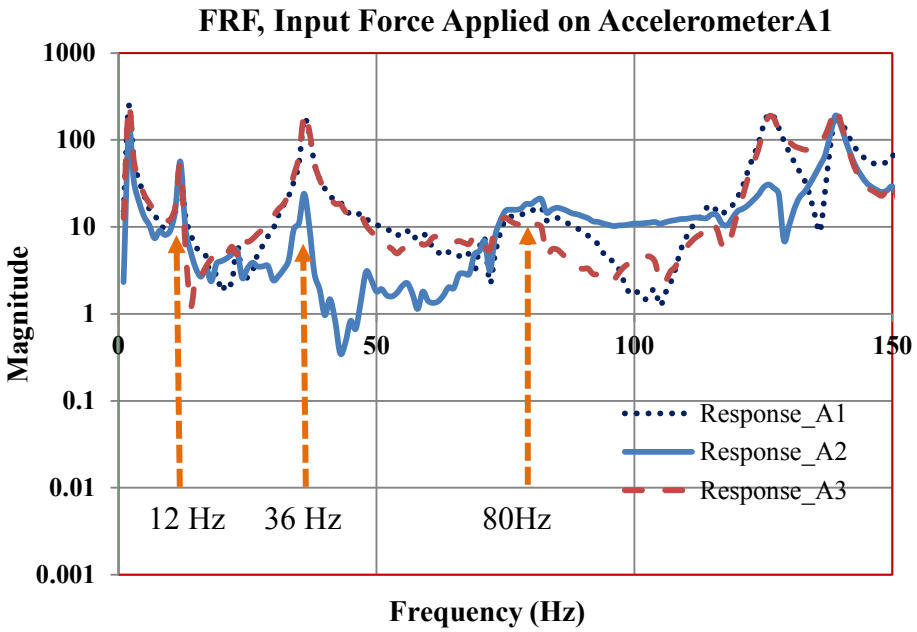

Figure 6.2. FRF, Magnitude, Input Force Applied on A1, and Responses of Accelerometers A1, A2, and A3

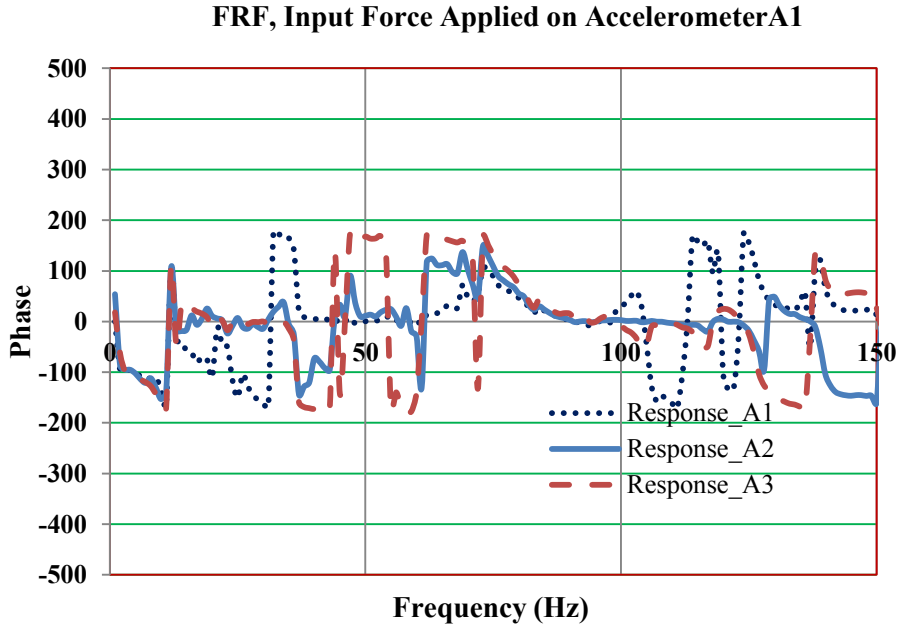

Figure 6.3. FRF, Phase, Input Force Applied on A1, and Responses of Accelerometers A1, A2, and A3

From the magnitude graph shown in Figure 6.2, it can be seen that near 12 Hz, the responses (acceleration in z-direction) of all three accelerometers are of the same magnitude. Near 36 Hz, accelerometers A1 and A3 (at the ends) show more response in the z-direction than accelerometer A2 at the center. In the vicinity of 80 Hz, all three accelerometers show a relatively equal response in the z-direction. As shown in Figure 6.4, from the phase response, near 12 Hz, the z-direction responses of the three accelerometers are in phase, which indicates a bending mode. Near 36 Hz, Figure 6.5 shows that the accelerometer A1 response is almost out of phase with the accelerometer A3 response, also indicating a bending mode. At 80 Hz, Figure 6.6 shows that the responses of all three accelerometers are in phase, indicating a bending mode. Figures 6.7 and 6.8 show the magnitude and phase response of the three accelerometers with force input near A2.

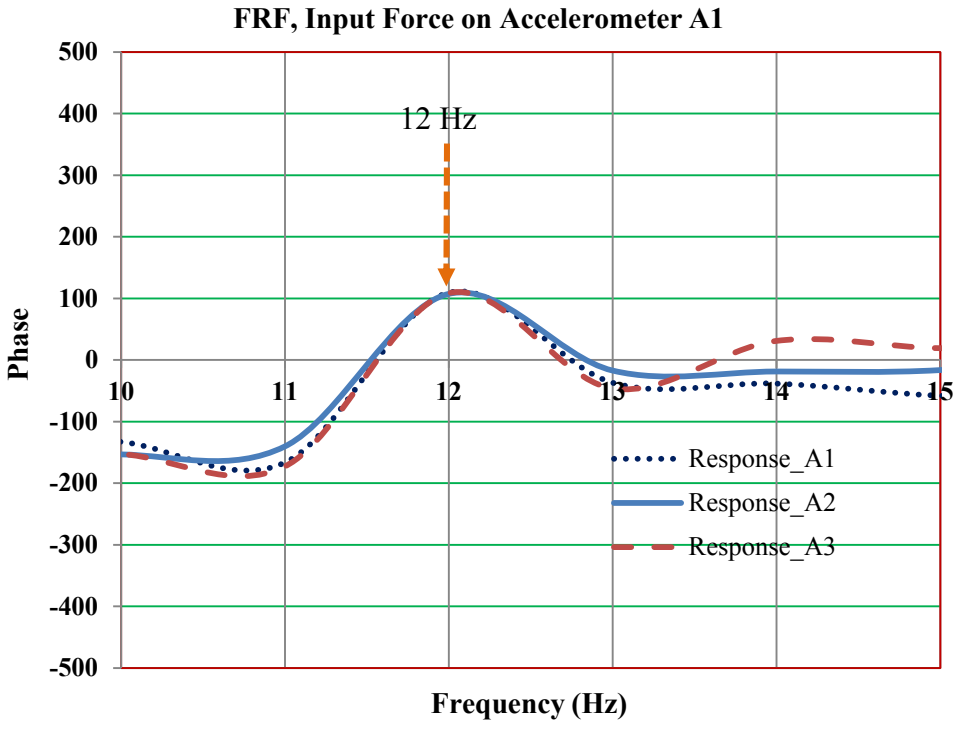

Figure 6.4. FRF, Phase, Input Force on Accelerometer A1, and Responses of Accelerometers A1, A2, and A3 Showing Bending Mode at 12 Hz

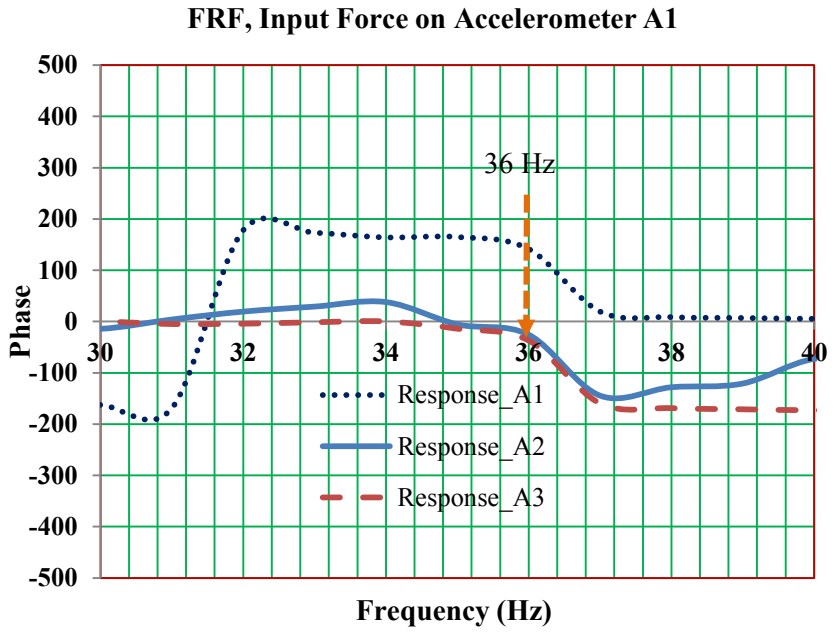

Figure 6.5. FRF, Phase, Input Force on Accelerometer A1, and Responses of Accelerometers A1, A2, and A3 Showing Torsion Mode at 36 Hz

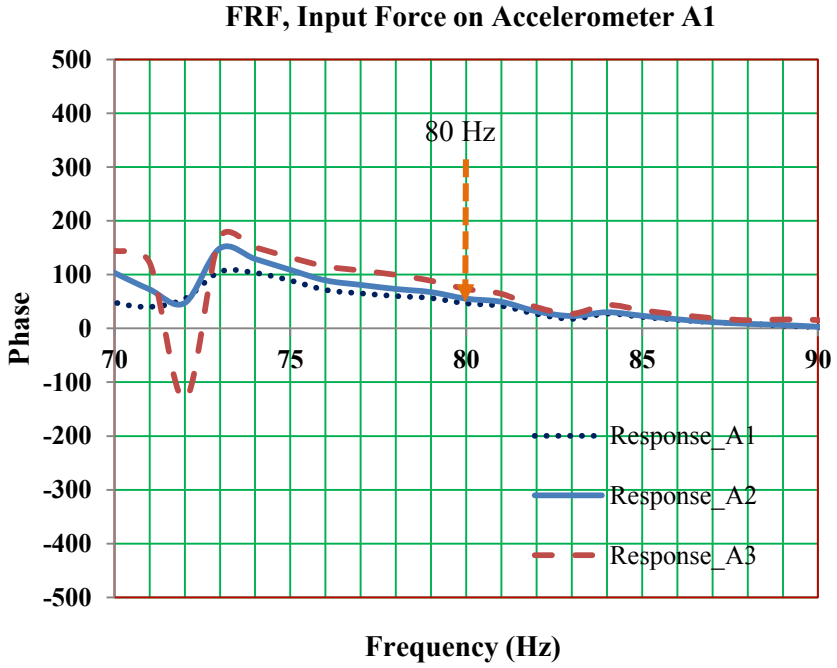

Figure 6.6. FRF, Phase, Input Force on Accelerometer A1, and Responses of Accelerometers A1, A2, and A3 Showing Bending Mode at 80 Hz

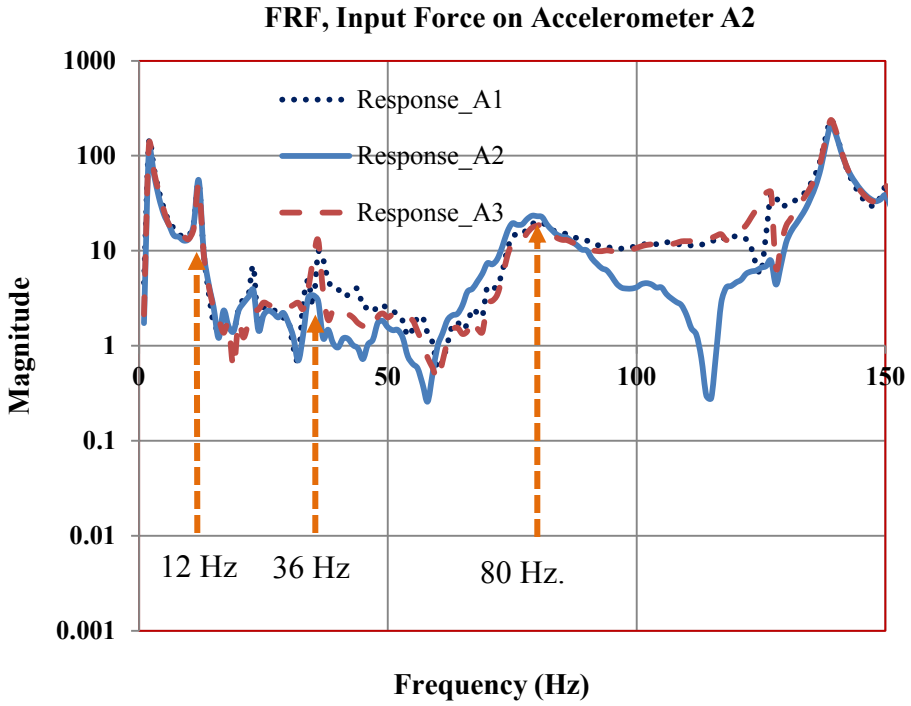

Figure 6.7. FRF, Magnitude, Input Force on Accelerometer A2, and Responses of Accelerometers A1, A2, and A3

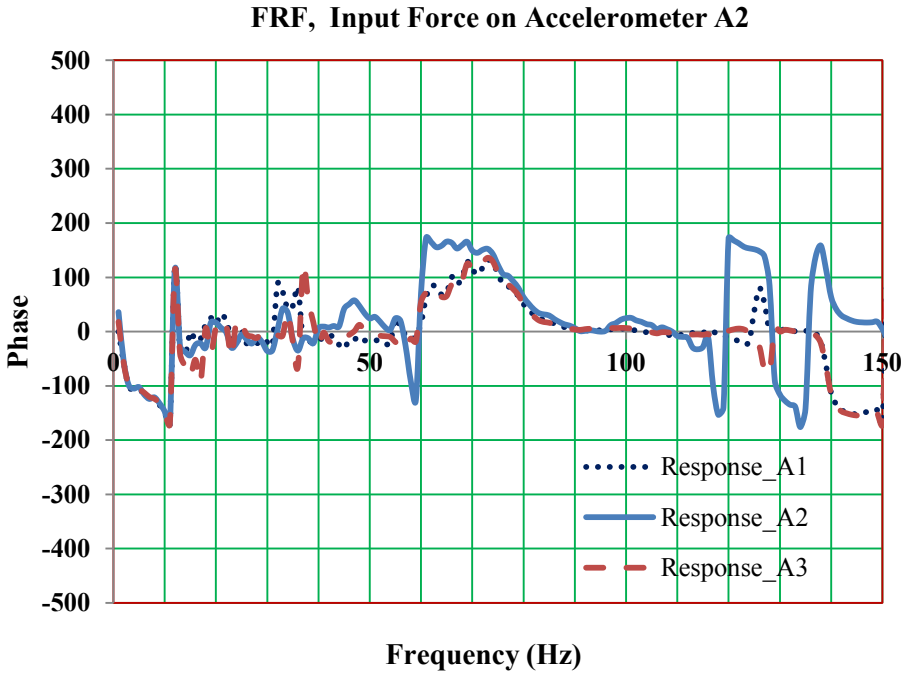

Figure 6.8. FRF, Phase, Input Force on Accelerometer A2, and Responses of Accelerometers A1, A2, and A3

6.2 GVT of Cantilever Plate with Attached Secondary Structure/Link

In order to study the effect of modes resulting from the attachment of an additional structure, a link was attached to the primary structure (cantilever plate), as shown in Figure 6.9. The link's translation degrees of freedom were restricted in directions 1, 2, and 3, and the rotational degrees of freedom were restricted in directions 4 and 6.

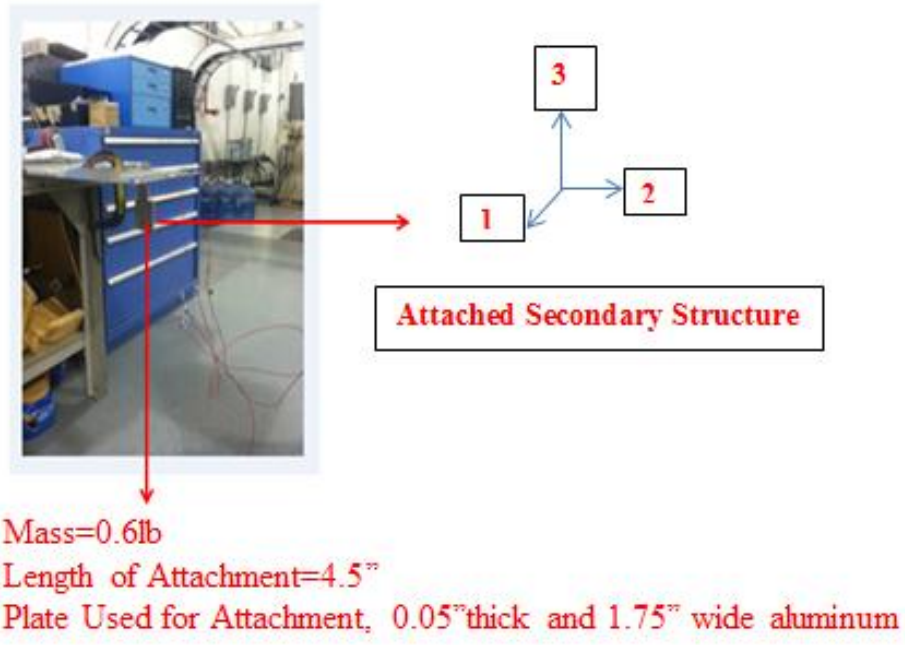

Figure 6.9. Test Setup of Cantilever Plate with Attached Secondary Structure

A new accelerometer, A4, was placed in the x-direction (direction 1 on the attached link). Responses were recorded from all accelerometers with input forces near A1 (Figures 6.10 and 6.11) and near A2 (Figures 6.12 and 3.13). At 11 Hz, Figure 6.14 shows that the responses of accelerometers A1, A2, and A3 are in phase, thus indicating a bending mode. Figure 6.15 shows that at 27 Hz and 39 Hz, A1 and A3 responses are out of phase, which means that both are in torsion mode, one in phase (27 Hz) with the attachment structure and the other out of phase (39 Hz) with the attachment structure.

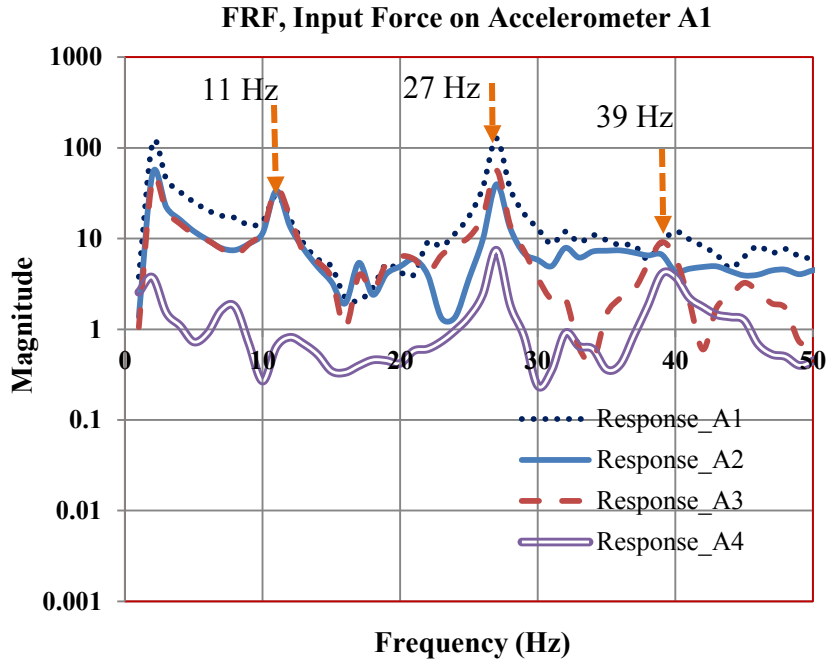

Figure 6.10. FRF, Magnitude, Input Force on A1, and Responses of Accelerometers A1, A2, A3, and A4

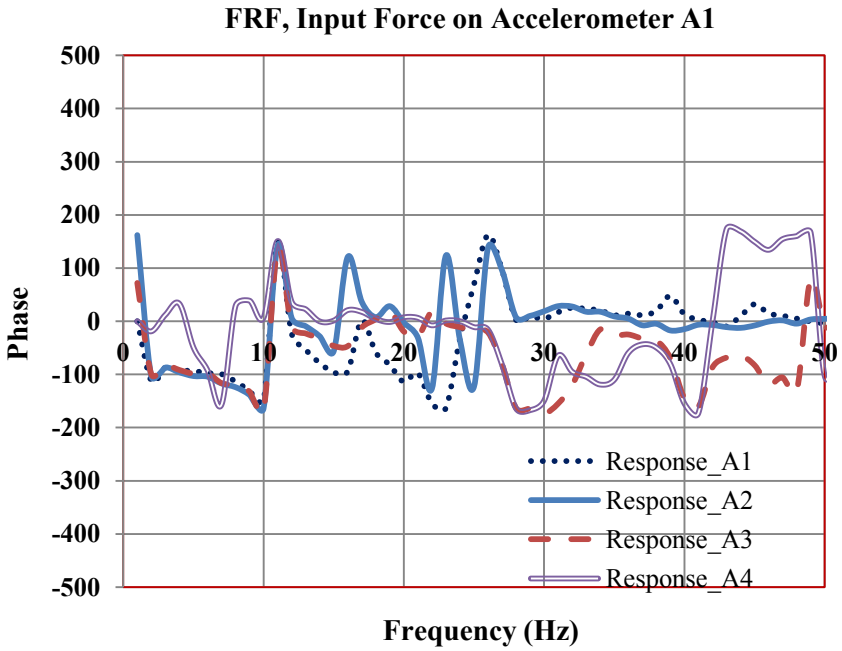

Figure 6.11. FRF, Phase, Input Force on A1, and Responses of Accelerometers A1, A2, A3, and A4

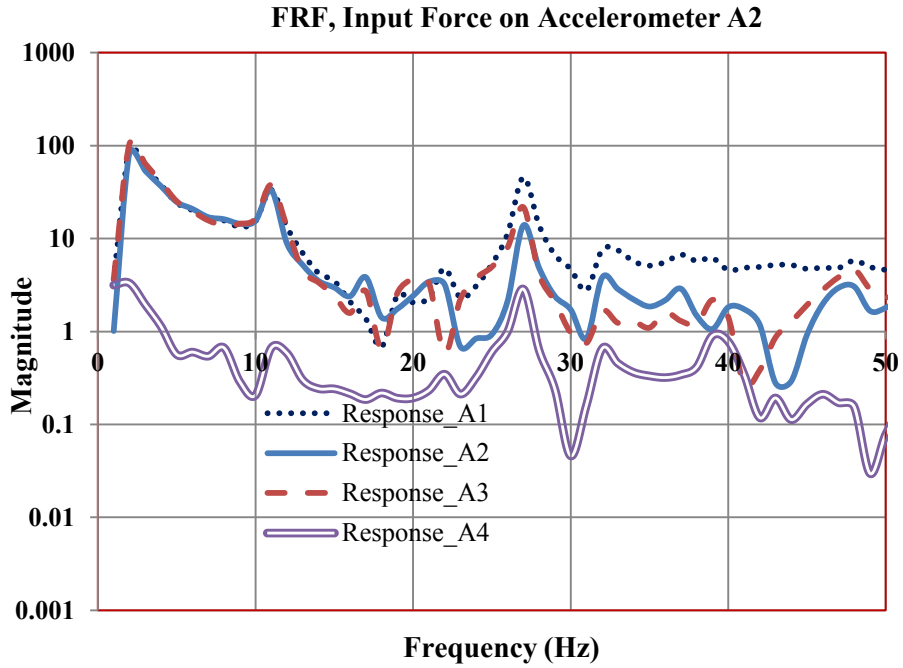

Figure 6.12. FRF, Magnitude, Input Force on Accelerometer A2, and Responses of Accelerometers A1, A2, A3, and A4

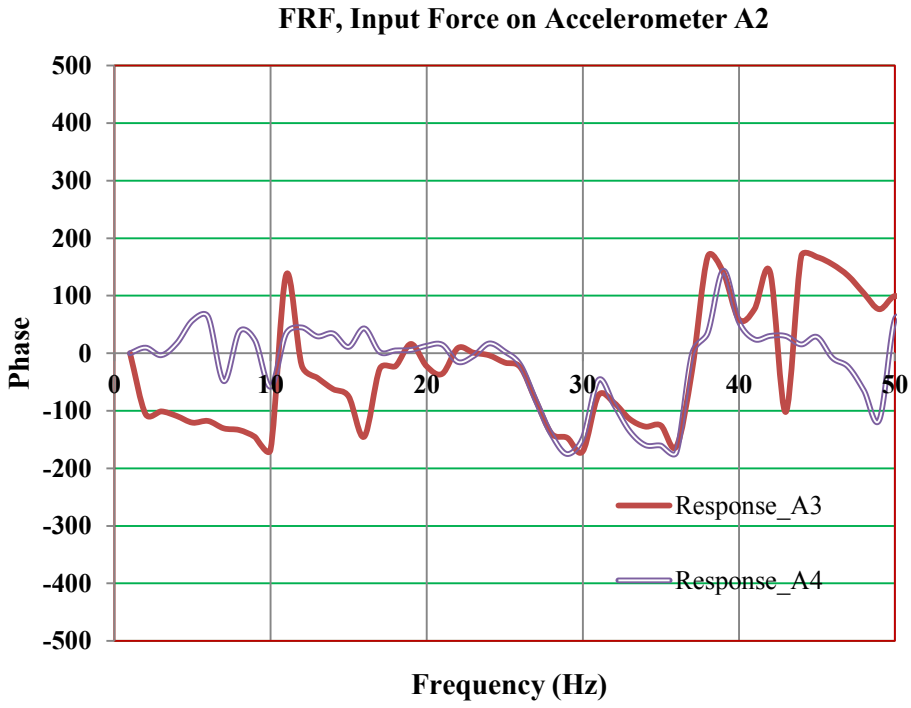

Figure 6.13. FRF, Phase, Input Force on Accelerometer A2, and Responses of Accelerometers A3 and A4

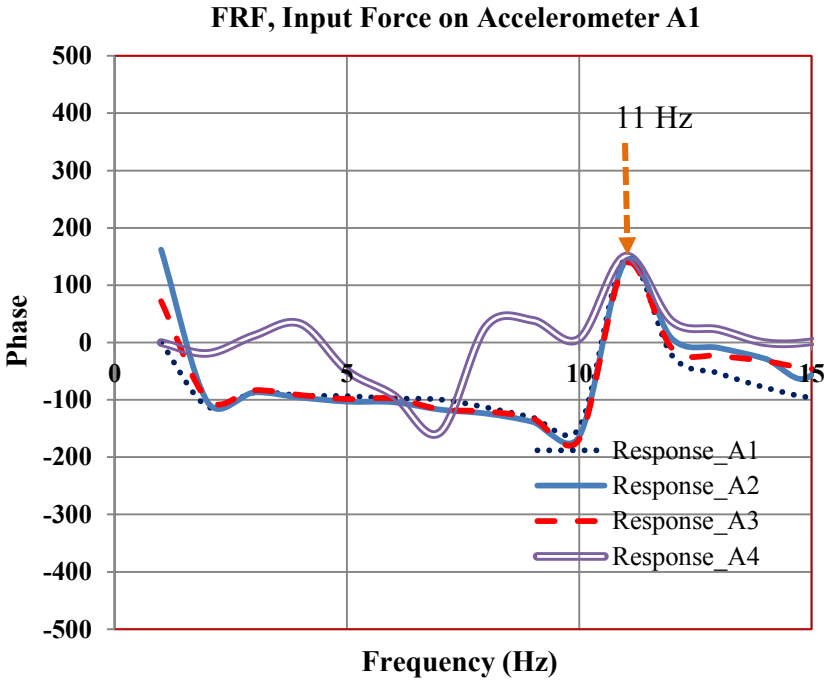

Figure 6.14. FRF, Phase, Input Force on Accelerometer A1, and Responses of Accelerometers A1, A2, and A3 Showing Bending at 11 Hz

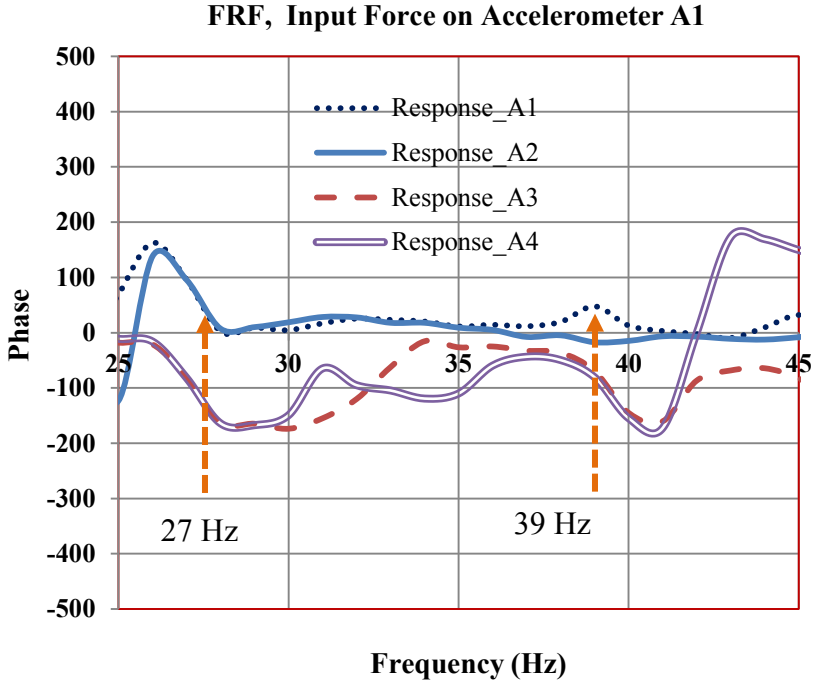

Figure 6.15. FRF, Phase, Input Force on Accelerometer A1, and Responses of Accelerometers A1, A2, and A3 Showing Torsion at 27 Hz and 39 Hz

CHAPTER 7

ANALYSIS RESULTS AND DISCUSSION OF CANTILEVER PLATE GVT

7.1 Vibration Analysis of Cantilever Plate

Figures 7.1 to 7.3 show the finite element model of the cantilever plate of the same dimensions as the test plate. The total weight and CG of the cantilever plate were compared with that of the test. The NASTRAN SOL 103 program was used to obtain the eigenvalues and eigenvectors (natural frequencies and mode shapes) of the system. The NASTRAN plate element, CQUAD4, was used for the analysis. A total of 96 QUAD elements and 117 nodes exist in the finite element model. One of the edges of the model is constrained in all degrees of freedom, because it is clamped at that edge. Figures 7.4 to 7.6 show the natural frequency and mode shapes of the plate. A NASTRAN SOL 111 program was used to analyze and compare the transfer function (FRF).

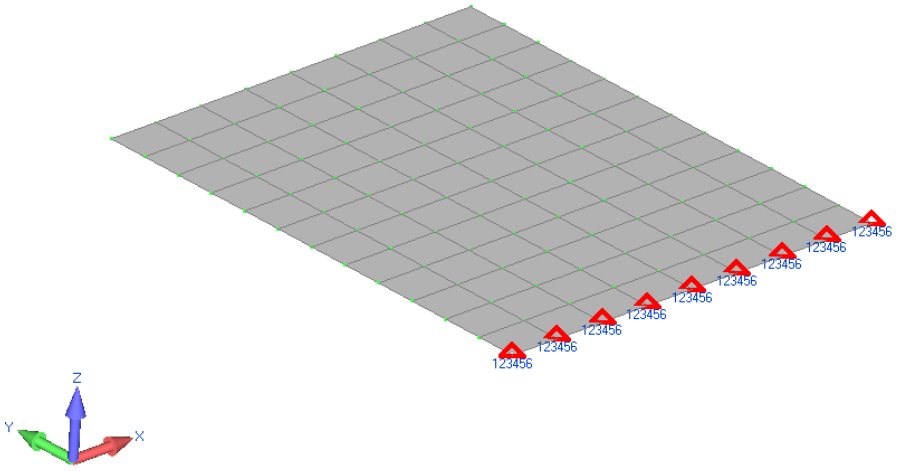

Figure 7.1. Finite Element Model of Cantilever Plate

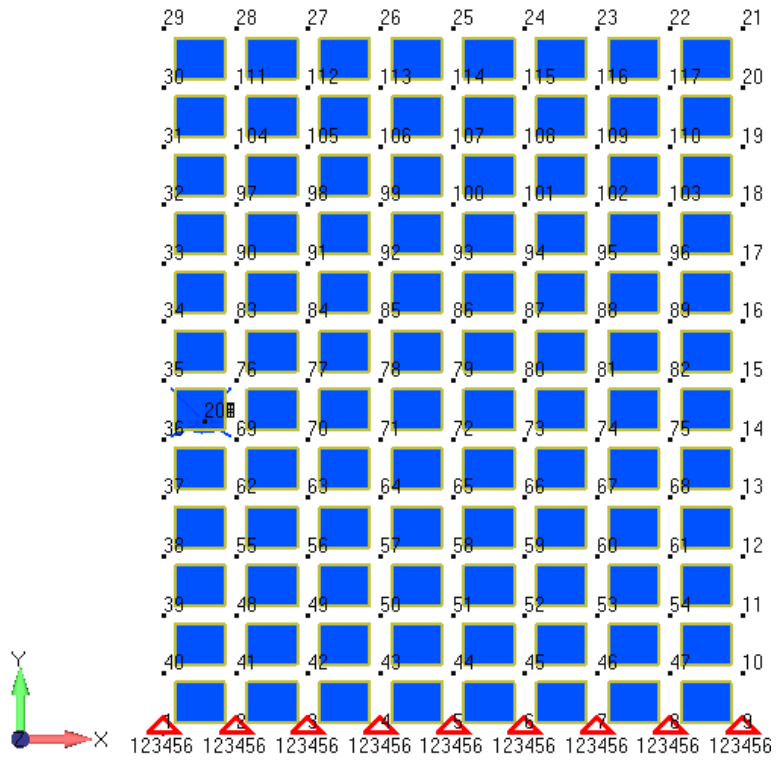

Figure 7.2. Shrink Top View of Finite Element Model of Cantilever Plate with Grid Points (Nodes)

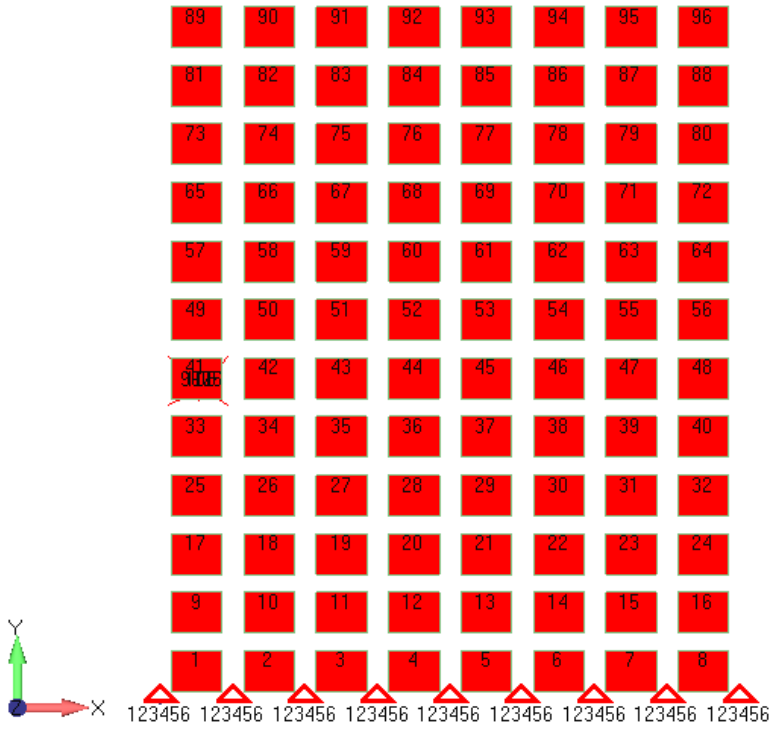

Figure 7.3. Shrink Top View of Finite Element Model of Cantilever Plate with Element IDs

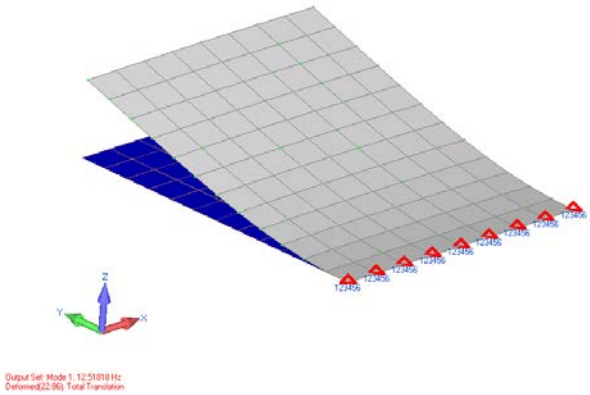

Figure 7.4. First Bending Mode at 12.51 Hz

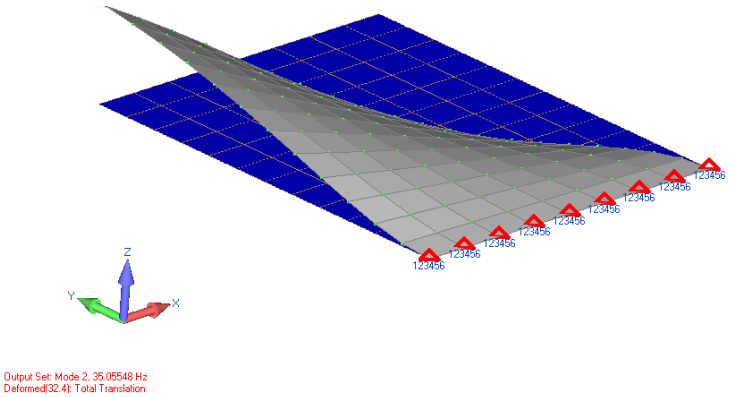

Figure 7.5. First Torsion Mode at 35.05 Hz

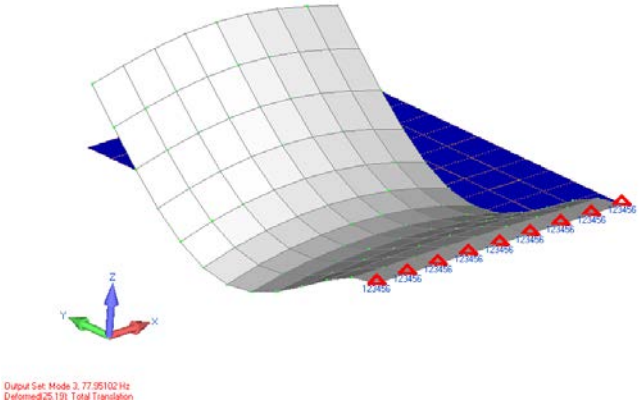

Figure 7.6. Second Bending Mode at 79 Hz

To perform an FRF comparison between the test and the analysis, the frequency response, was extracted from node 117 (point A1 on test), where the plate was impacted using the impact hammer, as shown in Figure 7.7. On the NASTRAN deck, both force and response points were defined on node 117 in the z-direction.

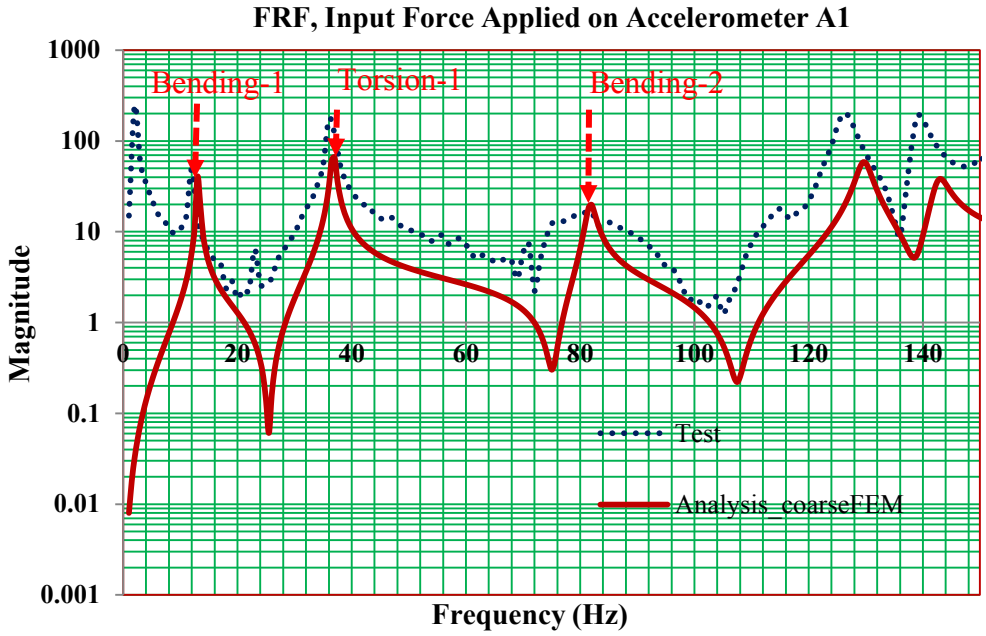

Figure 7.7. Comparison of Transfer Function Responses on Accelerometer A1, Test vs. Analysis

From equation (2.6), the frequency parameters, taken from *Harris' Shock and Vibration Handbook* [25], are compared in Figure 7.8. The a/b ratio is the length-to-width ratio of the frequency parameter.

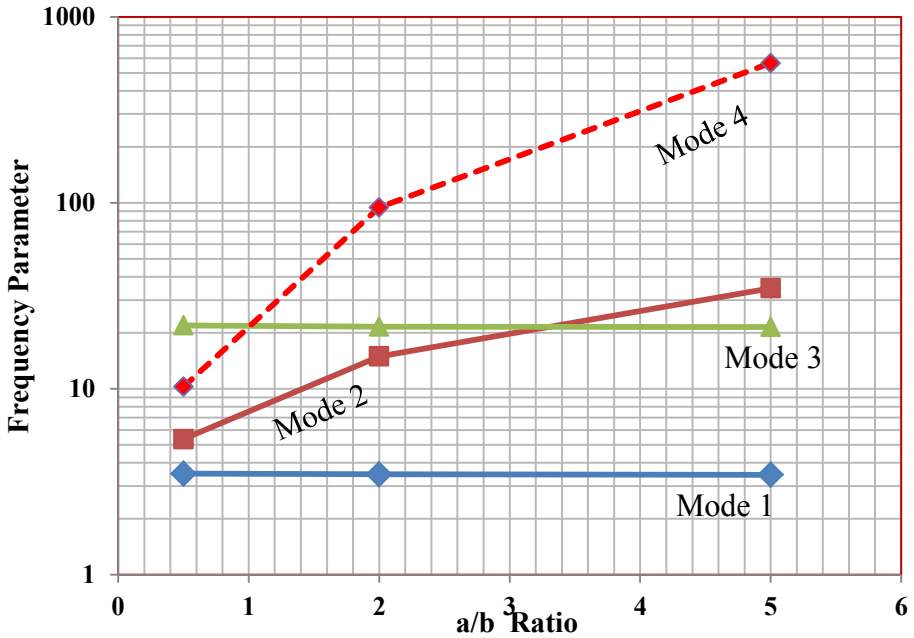

Figure 7.8. Frequency Parameter vs. Length/Width Ratio of Plate for Different Modes

For the plate geometry of 17 x 14 x 0.115, the a/b ratio is 1.21, and for different modes, the frequency parameter was interpolated. The respective frequency parameter is 3.48, 9.83, 21.79, and 49.56 for modes 1 to 4, respectively (includes ending and torsion modes). Table 7.1 shows the natural frequency values calculated from the frequency parameter values from *Harris' Shock and Vibration Handbook* [25], as shown in Appendix B. A comparison of the NASTRAN-generated FRFs with the test results is also shown in Figure 7.7. A summary of the natural frequency comparison for the cantilever plate is given in Table 7.2. For all modal frequencies, the percentage difference between the analytical FEM with respect to the test is also shown in Table 7.2.

TABLE 7.1

NATURAL FREQUENCIES OF CANTILEVER PLATE CALCULATED FROM *HARRIS' SHOCK AND VIBRATION HANDBOOK* [25]

Parameters	Mode 1	Mode 2	Mode 3	Mode 4
λ (interpolated freq. Parameter)	3.486	9.831	21.79	49.56
E (Young's Modulus,Pa)	7.23E+10	7.23E+10	7.23E+10	7.23E+10
h (Plate thickness,m)	2.92E-03	2.92E-03	2.92E-03	2.92E-03
v (Poisson's ratio)	0.3	0.3	0.3	0.3
a/b (ratio of length/width of plate)	1.23	1.23	1.23	1.23
a (length,m)	0.44	0.44	0.44	0.44
b (width,m)	0.36	0.36	0.36	0.36
ρ (mass density,kg/m^3)	2821.00	2821.00	2821.00	2821.00
$D=(E.h^3/12.(1-v^2))$	164.84	164.84	164.84	164.84
sqrt($\rho h/D$)	0.22	0.22	0.22	0.22
sqrt $(\rho h/D)*a^2$	0.04	0.04	0.04	0.04
ω	81.29	229.24	508.10	1155.64
$f=\omega/2pi$	**12.94**	**36.50**	**80.91**	**184.02**

TABLE 7.2

COMPARISON OF TEST RESULTS AND FEM

parameters	Test	coarseFEM	Diff(FEM Vs.Test)	Analytical	Diff(Analy Vs.Test)
CG-x(In.)	7.00	7.00	0.00%	NA	
CG-y(In.)	8.50	8.50	0.00%	NA	
CG-z(In.)	0.06	0.00		NA	
Total weight(lbs)	3.00	3.01	0.37%	NA	
Ixx-CG	NA	72.00		NA	
Iyy-CG	NA	48.40		NA	
Izz-CG	NA	120.40		NA	
mode-1/Bending,Hz	12.00	12.50	4.17%	12.94	7.83%
mode-2/Torsion,Hz	36.00	35.05	-2.64%	36.50	1.39%
Mode-3/bending,Hz	80.00	77.90	-2.62%	80.91	1.14%

7.2 Vibration Analysis of Cantilever Plate with Rigid Link

Figure 7.9 shows the effect of an eccentric mass on the transfer function of the system. Whenever there is an extra mass added to a vibrating system, it lowers the natural frequency. If the mass is eccentric to the elastic axis of the system, then there will be more reduction in torsional frequency compared to the bending frequency. Figure 7.9 shows this effect. This is applicable when the mass is rigidly attached to the system.

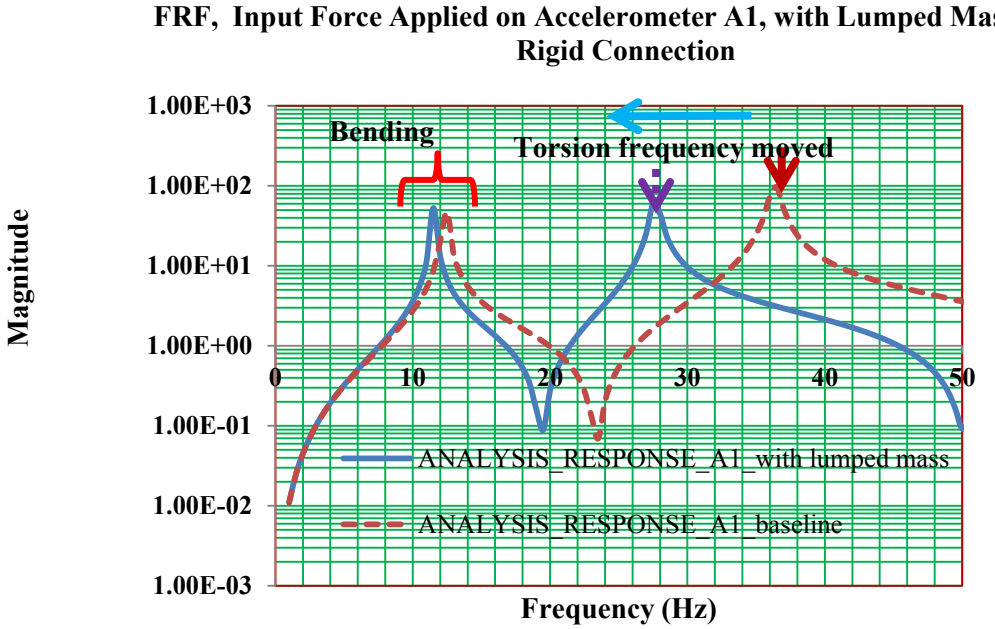

Figure 7.9. Effect of Eccentric Mass on System

7.3 Vibration Analysis of Cantilever Plate with Flexible Link

When an eccentric mass is attached to the plate through a flexible link, link modes are coupled with plate modes, which are associated with the system. Flexibility is modelled by introducing a CELAS spring element in NASTRAN, with 5 degrees of freedom, which is rotated about the y-axis. Details of the model are shown in Figures 7.10 and 7.11. Figures 7.12 to 7.14 show mode shapes of the structure for the respective natural frequency of the system. The in-phase and out-of-phase torsion mode of the plate with the link are shown in Figures 7.13 and 7.14, respectively. It is to be noted that the location of the mass on the link is represented correctly as shown in the test. The spring stiffness of the CELAS spring element was tuned to match with test results.

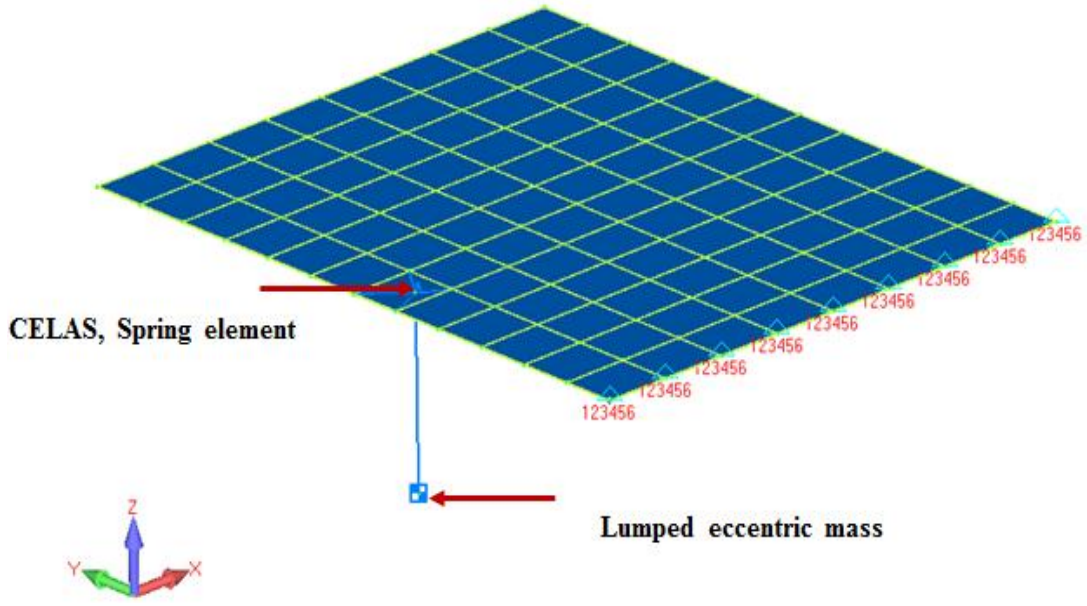

Figure 7.10. Finite Element Model of Plate with Flexible Link

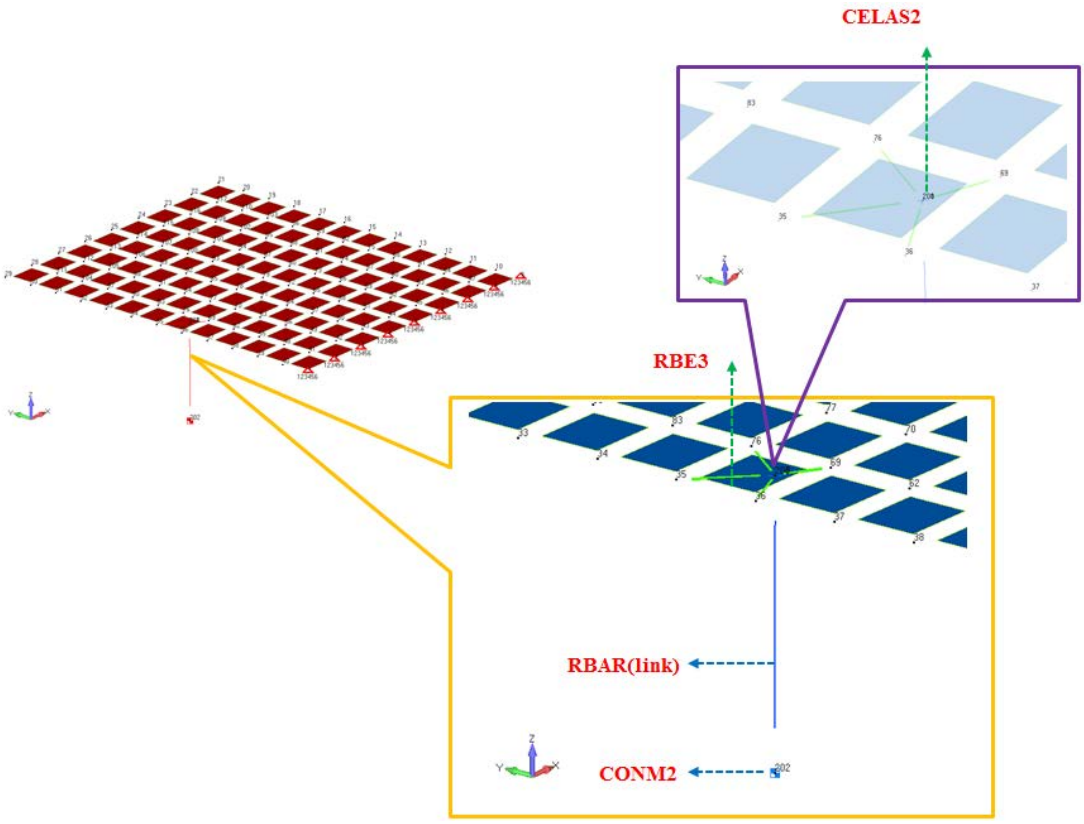

Figure 7.11. Details of Finite Element Model with Secondary Structure (Flexible Link)

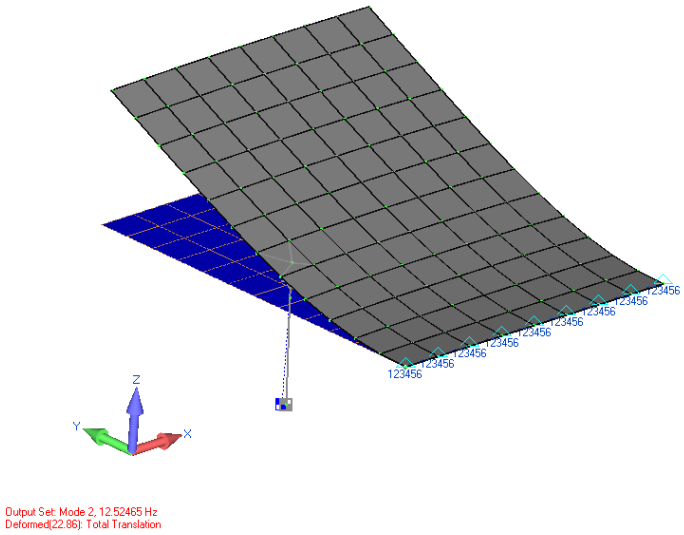

Figure 7.12. Natural Frequency Bending-1 at 12.5 Hz

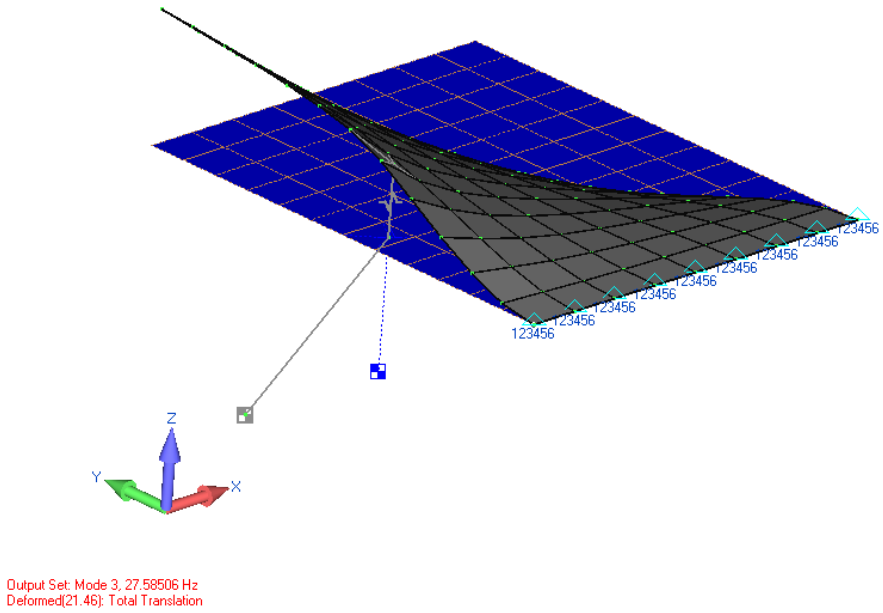

Figure 7.13. Natural Frequency Torsion in Phase with Link at 27.5 Hz

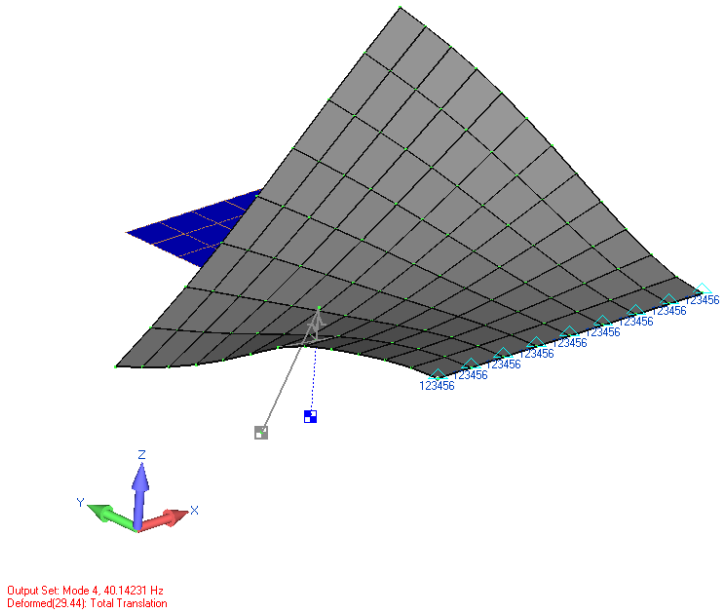

Figure 7.14. Natural Frequency Torsion out of Phase with Link at 40.1 Hz

A comparison of the test result and the analysis was made and is shown in Table 7.3. A transfer function comparison (NASTRAN SOL 111) of point A3 was also performed to validate the analysis with that of the test results, as shown in Figure 7.15.

TABLE 7.3

FREQUENCY COMPARISON OF ANALYSIS WITH TEST

	Test (Hz)	Analysis (Hz)	Difference in FEM vs.Test (%)
Bending-1	11	12.5	13.64
Torsion in Phase	27	27.5	1.85
Torsion Out of Phase	39	40.1	2.82

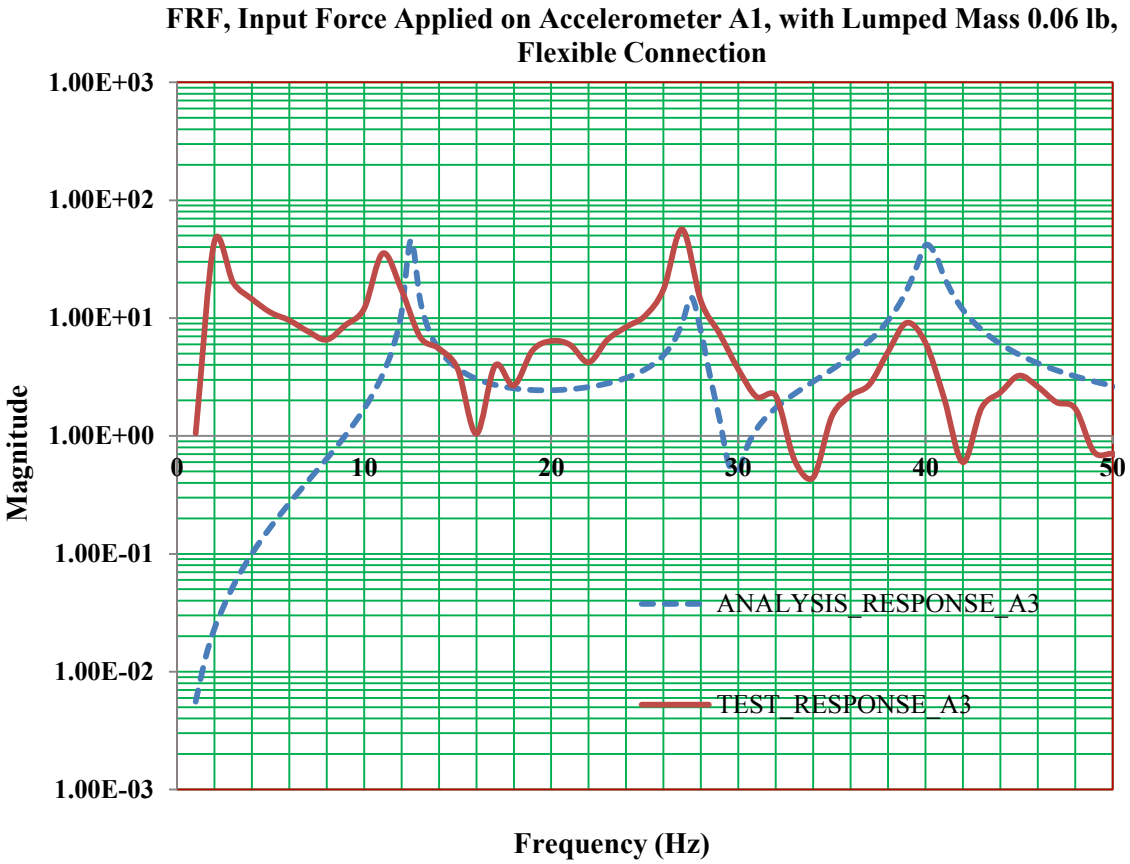

Figure 7.15. Transfer Function Comparison

7.4 Parametric Study of Structural Dynamics of Cantilever Plate with Flexible Link

A detailed study was performed to understand the frequency changes of the in-phase and out-of-phase torsion modes with a change in location, both chordwise and spanwise. The

attachment of the link and the lumped mass of the link were moved, as shown by dotted line in Figure 7.16, both in the direction of chord and spanwise. Both torsion frequencies are reduced when the attachment moves away from the elastic axis (elastic axis is x/c = 0.5), as shown in Figure 7.17. The in-phase frequency is reduced and the out-of-phase frequencies are increased when the attachment and mass move towards the outboard edge (Y/S = 1), as shown in Figure 7.18.

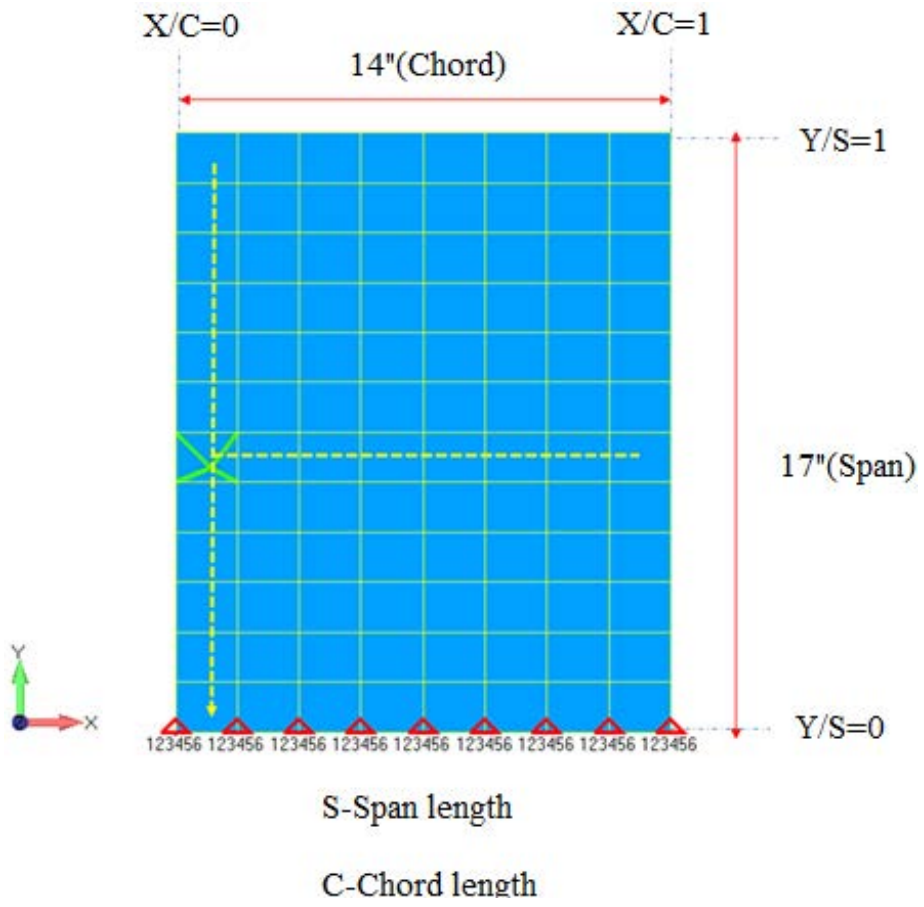

Figure 7.16. Location of Attachment for Parametric Study

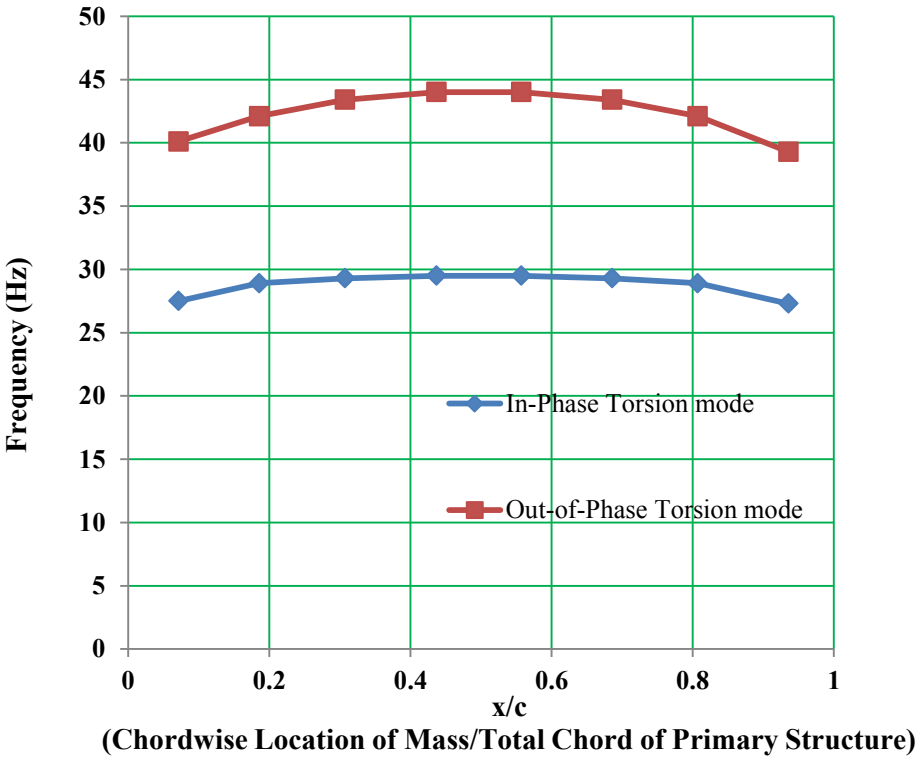

Figure 7.17. Change in Frequencies with Change in Chordwise Location of Attachment

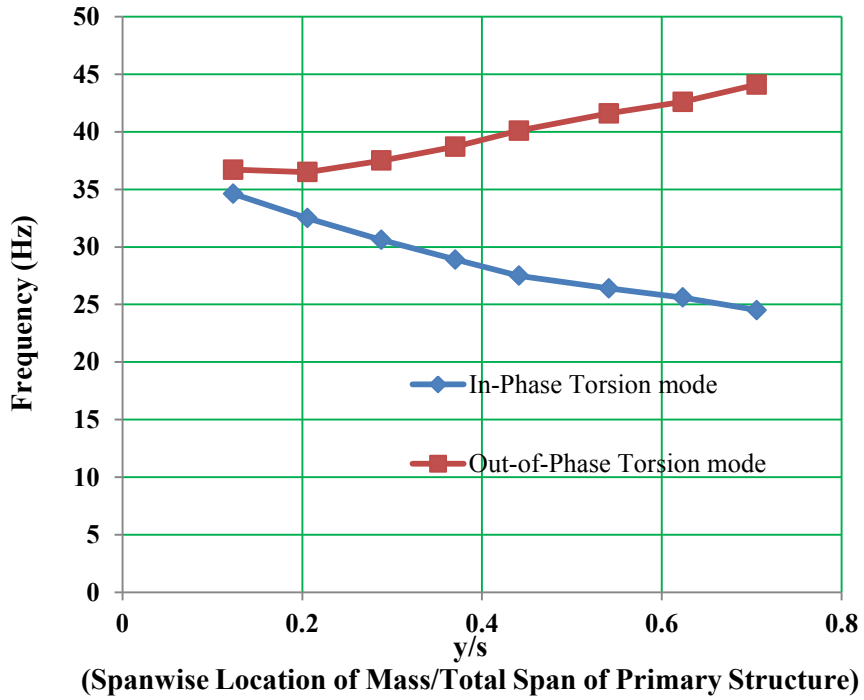

Figure 7.18. Change in Frequencies with Change in Spanwise Location of Attachment

With an increase in stiffness of the rotational spring, which represents the attachment of the link to the plate, frequencies increase, as shown in Figure 7.19. The nominal rotational stiffness is 2.0 E3.

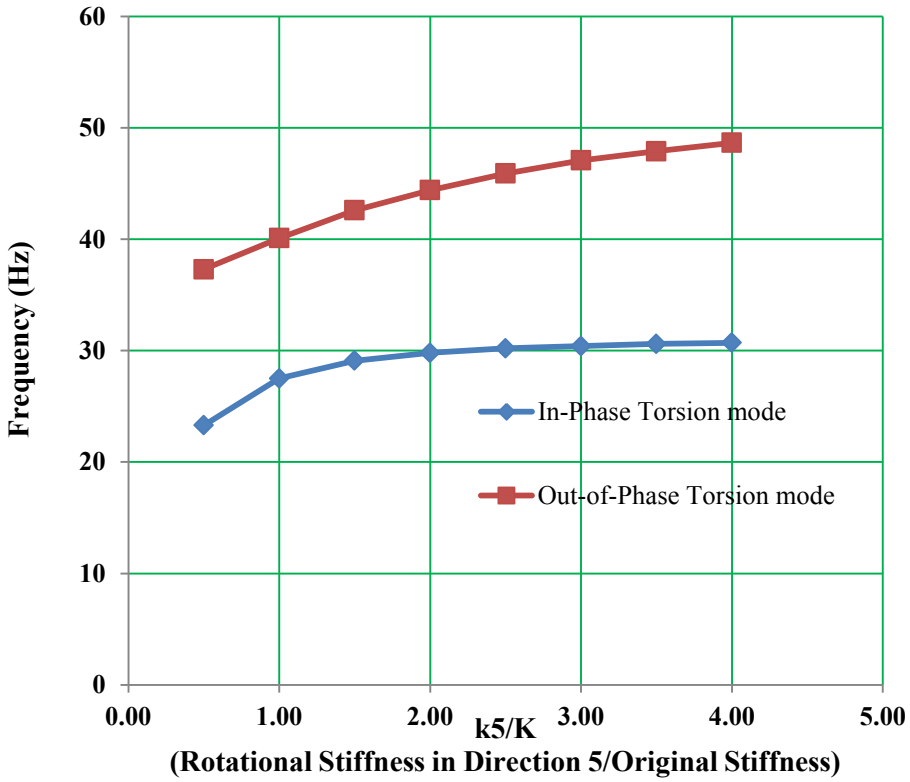

Figure 7.19. Change in Frequencies with Change in Rotational Stiffness of the Attachment

CHAPTER 8

CONCLUSIONS AND RECOMMENDATIONS

8.1 Conclusions

The objectives of this dissertation were to develop and validate simple FE models and procedures to assist in GVT and to quantify the effect of secondary structures in GVT. To achieve these objectives, the following tasks were identified:

- Determine the natural frequency and mode shape of a free-free beam and a cantilever plate, and compare the results with finite element analysis.
- Determine the natural frequencies and mode shape of the cantilever plate and a free-free beam with an attached link.
- Characterize the secondary structure modes and in-phase and out-of-phase modes of the secondary structure with the primary structure.
- Perform a study to determine the change in various natural torsional frequencies on a free-free beam and on a cantilever plate, with a change in location of the secondary structure and with a change in the compliant rotational stiffness of the secondary structure to the primary structure.

The purpose of these objectives was to demonstrate and prove the importance of ground vibration testing of a primary structure component by itself and the importance of instrumenting secondary structures during full GVT. An experimental methodology to determine the basic first-order natural frequencies of the free-free beam and a cantilever plate were successfully performed. Results were compared to the existing analytical methods and finite element analysis. Magnitude and phase responses from the test were carefully analyzed to differentiate the bending modes (symmetric and asymmetric) and torsion modes (both symmetric and asymmetric) to

compare them to mode shapes from FEA results. Natural frequencies and modes of flexible links attached to the free-free beam were analyzed on the basis of test data. Careful analysis and interpretation of the frequency response functions were performed to determine the in-phase and out-of-phase modes of the secondary structure (flexible ink) with the primary structure using FEA. The influence of secondary structure compliance stiffness and location to the in-phase and out-of-phase torsional modes was also determined.

A comparison of the free-free beam modal test results with respect to the two FEA results. One of the finite element analyses used a coarse mesh model and the other used a stick model. A comparison of FEA results and test results using the stick model with flexible links incorporated into it was also conducted. For a free-free beam, an acceptable range of frequency magnitude variation up to 10% was found between the test results of the FEM and analytical method. With a secondary structure attached to the beam, those frequencies were reduced by approximately 1.5% for bending and torsion. The comparison of test results and FEA is within 10%. with a secondary structure attached to the primary structure, with increase in the compliant rotational stiffness, the frequency of both in-phase and out-of-phase torsion modes with the secondary structure increases for both the free-free beam and the cantilever plate. A comparison of the natural frequencies from the calculations and test results for the cantilever plate without the links, and the ones with the links were also conducted. As the secondary structure moves more outboard (spanwise), in the case of the free-free beam when the secondary structure moves away from the center of gravity and for the cantilever plate when it moves outboard of the constraints, the frequency increases. When the secondary structure moves away from the elastic axis, the frequency is reduced.

It was demonstrated that for any parametric study to be performed on the model, analysts can use the simplified stick model. For GVT of the free-free beam with secondary structures, characterization of the in-phase and out-of-phase modes of the secondary structures were also analyzed along with the correlation with FEA. If the modal test was performed on the assembled structure without instrumenting the secondary structure, then analysts would see two peaks of torsional frequencies, if the secondary structure mode is near the vicinity of the real torsion mode—one in-phase torsion mode with flexible links and the other out-of-phase mode. If analysts do not have knowledge of in-phase and out-of-phase modes of the secondary structure compared to the primary structure, then there is a strong possibility that the tuning of the stiffness could occur in two ways: one that results in a lower frequency (in phase) and the other that results in a higher frequency (out of phase). If the stiffness of the primary structure is tuned to the in-phase torsion mode from the test, then this would be a very conservative approach from a flutter analysis perspective, which might result in increasing the stiffness by changing the cross section and probably result in increasing the weight of an aerostructure. Instead, if the primary structure stiffness is tuned to the out-of-phase torsion mode, this would be a very non-conservative approach for flutter analaysis and would affect the safety of the structure. Hence, to avoid both the weight impact and improve the safety and proper testing, instrumenting the secondary structure is essential together with the component GVT of the primary structure itself.

8.2 Recommendations for Future Work

This dissertation made use of a simple dynamic system representing an airplane structure instead of instead of the real aero-structure. It would be a good validation if the same philosophy and work being performed on a real wing –gear structure. The secondary structure involved here in this research is a single degree of freedom dynamic system. As a future work, a multi degree

of freedom dynamic system can be considered as a secondary structure. Another main task as a future work is performing an aeroelastic analysis of an assembled wing- gear structure and determining the effect of compliance stiffness of secondary structure like gear on wing , on the flutter speed .

REFERENCES

REFERENCES

[1] Office of the Federal Register, National Archives and Records, "Code of Federal Regulations, Aerospace and Space," January 2004.

[2] Peeters, B., Climent, H., de Diego, R., Alba, J. Ahlquist, J. R., Carreno, J. M., Hendricx, W., Rega, A., Garcia, G., Deweer, J., and Debille, J., "Modern Solutions for Ground Vibration Testing of Large Aircraft," 26th International Modal Analysis Conference, Orlando, FL, February 2008.

[3] Szkudlarek, W., Mizutani, A., Peeters, B., Luczak, M., and Kahsin, M., "Ground Vibration Testing, Finite Element Modeling and Correlation of a Composite Hobby Aircraft," 13th International Conference on Aerospace Sciences and Aviation Technology, Cairo, Egypt, May 2009.

[4] Kehoe, M. W., and Freudinger, L. C, "Aircraft Ground Vibration Testing at NASA Dryden Flight Research Facility," NASA Technical Memorandum, 1993.

[5] Simsiriwong, J., and Sullivan, W., "Vibration Testing of a Carbon Composite Fuselage," 23rd Technical Conference of the American Society for Composites, Memphis, TN, September 2008.

[6] Vittala, N. G. V., Pankaj, A. C., and Swarnalatha, R., "Dynamic and Aeroelastic Analysis of a Transport Aircraft," Proceedings of the International Conference on Aerospace Science and Technology, Bangalore, India, June 2008.

[7] MSC Software, *MSC NASTRAN 2014 Quick Reference Guide*, 2014.

[8] Napolitano, K., and Linehan, D., "Multi Sine Sweep Excitation for Ground Vibration Tests," 27th International Modal Analysis Conference, Orlando, FL, February 2009.

[9] Lau, J., Debille, J., Peeters, B., Giclais, S., Lubrina, P., Boeswald, M., and Govers, Y., "Advanced Systems and Services for Ground Vibration Testing—Application for Research Test on an Airbus A340-600 Aircraft," 15th International Forum on Aeroelasticity and Structgural Dynamics, Paris, France, June 2011.

[10] Hensley, D., Smith, K., Doane, B., and Dreyer, W., "Implementation of an Airbag Suspension System for the Global Hawk Vibration Test," 15th International Modal Analysis Conference, Orlando, FL, February 1997.

[11] Whitney, M. J., Panza, J. L. , and Brillhart, R. D., "GVT Suspension Effects on Correlation of the Predator B Vehicle," 20th International Modal Analysis Conference, Los Angeles, February 2002.

[12] Goge, D., Boswald, M., Fullekrug, U., and Lubrina, P., "Ground Vibration Testing of Large Aircraft-State-of-the-Art and Future perspectives," 25th International Modal Analysis Conference, Orlando, FL, February 2007.

[13] Kerschen, G., "Modal Analysis of Nonlinear Vibrating Systems: Recent Progress and Challenges," 8th International Conference on Structural Dynamics, EURODYN 2011, Leuven, Belgium, 2011.

[14] Ozkok, B., and Weltin, U. I., "Finite Element Model Updating Based on Ground Vibration Test Results," 3rd International Multi-Conference on Society, Cybernetics and Informatics, Orland, FL, July 2009.

[15] Goge, D., "Effective Validation of a Finite Element Model-Application of Computational Model Updating to a Civil Four-Engine Aircraft," 21st International Modal Analysis Conference, Kissimmee, FL, February 2003.

[16] Salehi, M., and Ziaei-rad, S., "Ground Vibration Test (GVT) and Correlation Analysis of an Aircraft Structure Model*," Iranian Journal of Science and Technology, Transaction B, Engineering*, vol. 18, no. B1, 2007, pp. 65–80.

[17] Dieckelman, R., Hauenstein, A. J., Hayes, W. B., and Ritzel, R. P., "High Force Experimental Modal Analysis," 21st International Modal Analysis Conference, Kissimmee, FL, February 2003.

[18] Pickrel, C. R., "Airplane Ground Vibration Testing—Nominal Modal Model Correlation," *Sound & Vibration*, November 2002.

[19] Leissa, A. W., *Vibration of Plates*, Office of Technology Utilization, NASA SP-160, Washington, 1969.

[20] Looker, J. R., and Sader, J. E., "Flexural Resonant Frequencies of Thin Rectangular Cantilever Plates," *Journal of Applied Mechanics*, vol. 75, no. 011007, January 2008.

[21] Pouladkhan, A. R., Emadi, J., Safamehr, M., and Habibolahiyan, H., "The Vibration of Thin Plates by Using Modal Analysis," *World Academy of Science, Engineering and Technology*, vol. 59, 2011.

[22] Young D., "Vibration of Rectangular Plates by Ritz Method," *Journal of Applied Mechanics*," vol. 17, no. 4, December 1950, pp. 159–160,.

[23] Barton, M. V., "Free Vibration Characteritics of Cantilever Plates," Defense Research Laboratory, The University of Texas Report, Defence Research Lab, December 1949.

[24] Barton, M. V., "Vibration of Rectangular and Skewed Cantilever Plates," *Journal of Applied Mechanics*, vol. 18, no. 1, June 1951, pp. 129–134.

[25] Harris, C. M., and Piersol, A. G., *Harris' Shock and Vibration Handbook*, McGraw Hill Handbooks, 2002.

[26] Wu, J. H., Liu, A. Q., and Chen, H. L., "Exact Solutions for Free-Vibration Analysis of Rectangular Plates Using Bessel Functions," *Journal of Applied Mechanics*, vol. 74, no. 6, November 2007, pp. 1247–1251.

[27] Werfalli, N. M., and Karound, A. A., "Free Vibration Analysis of Rectangular Plates Using Galerkian-Based Finite Element Method," *International Journal of Mechanical Engineering*, vol. 2, iss. 4, May 2012, pp. 59–67.

[28] Kalita, K., and Dutta, A., "Free Vibration Analysis of Isotropic and Composite Rectangular Plates," *International Journal of Mechanical Engineering Research,* vol. 3, no. 4, November 2013, pp. 301–308.

[29] Leissa, A. W., and Kang, J. -H., "Three-Dimensional Vibration Analysis of Thick Shells of Revolution," *Journal of Engineering Mechanics*, vol. 125, no. 12, December 1999, pp. 1365–1371.

[30] Kapania, K. R.., and Liu, Y., "Static and Vibration Analysis of General Wing Structures Using Equivalent-Plate Models," *AIAA Journal*, vol. 38, no. 7, July 2000, pp. 1269–1277.

[31] Myfiu, E., "Modal Analysis of a Beam with Closely Spaced Mode Shapes," www.engfac.cooper.edu, Spring 2011, accessed December 2014.

[32] Caresta, M., "Vibrations of a Free-Free Beam," www.unsw.edu, accessed December 2014.

[33] Arndt, M., Machado, R. D., and, Scremin A, "An Adaptive Generalized Finite Element Method Applied to Free Vibration Analysis of Straight Bars And Trusses," *Journal of Sound and Vibration*, vol. 329, 2010, pp. 659–672.

[34] Sakshat Virtual Labs, Free Vibration of a Cantilever Beam (Continuous System), www.iitg.vlab.co.in, accessed December 2014.

[35] Malatkar, P., "Nonlinear Vibrations of Cantilever Beams and Plates," Doctor of Philosophy Dissertation,Virginia Polytechnic Institute and State University, Blacksburg, VA, 2003.

[36] Labonnote, N., and Malo, K. A., "Damping Measurements in Timber Beams Using Impact Testing," 8th International Conference on Structural Dynamics, EURODYN 2011, Leuven, Belgium, 2011.

[37] De Haro Silva, L., Paupitz Goncalves P. J., Santade, F., and Capello Sousa, E. A., "Dynamic Analysis for Different Finite Element Models of Beams with Viscoelastic Damping Layer," 9th International Conference on Structural Dynamics, EURODYN 2014, Porto, Portugal, 2014.

[38] Chaudhari, P. K., Patel, D., and Patel, V., "Theoretical and Software Based Comparison of Cantilever Beam: MODAL ANALYSIS," *International Journal of Innovative Research in Advanced Engineering*, vol. 1, iss. 5, June 2014, pp. 75–79.

[39] Azoury C., Kallassy, A., Combes, B., Moukarzel, I., and Boudet, R., "Experimental and Analytical Modal Analysis of a Crankshaft," *International Organizaiton of Scientific Research Journal of Engineering*, vol. 2, no. 4, April 2012, pp. 674–684.

[40] Emory, B. H., and Zhu, W. D., "Experimental Modal Analysis of Rectangular and Circular Beams," *Journal of STEM Education*, vol. 7, no. 3, 2006, pp. 80–100.

[41] Sawant, S. H., "Experimental Verification of Transverse Vibration of Free-Free Beam," *International Journal of Advanced Research in Electrical, Electronics and Instrumentation Engineering*, vol. 2, iss. 9, September 2013, pp. 4536–4541.

[42] Vaziri, M., Vaziri, A., and Kadam, S. S., "Vibration Analysis of a Cantilever Beam Using F.F.T Analyzer," *International Journal of Advanced Engineering Technology*, vol. IV, iss. II, April–June 2013, pp. 112–115.

[43] Malekjafarian, A., Ashory, R. M., Khatibi, M. M., and Latibari, M. S., "A New Method for Estimation of Rigid Body Properties from Output-Only Modal Data," 4th International Operational Modal Analysis Conference, Istanbul, Turkey, May 9–11, 2011.

[44] Klopper, R., Akita, H., Okuma, M., and Terada, S., "An Experimental Identification Method for Rigid Body Properties Enabled by Gravity-Dependent Suspension Modelling," 1st Joint International Conference on Multibody System Dynamics, Lappeenranta, Finland, May 25–27, 2010.

[45] Masoumi, M., Shahbazmohamadi, S., and Ashory, M.R "Sensitivity Analysis of Rigid body property estimation from modal method," *IMAC XXV111*, 28th International Modal Analysis Conference, Jacksonville, FL, Feburary 2010.

[46] Schedlinski, C., and Link, M., "On the identification of rigid body properties of an elastic system," 15th International Modal Analysis Conference, Orlando, FL, February 1997.

[47] Craig, R. R., and Kurdila, A. J., *Fundamentals of Structural Dynamics*, Wiley, 2006

[48] Meirovitch, L., *Fundamentals of Vibrations*, Waveland Printing, Inc., 2010.

[49] Logan, D. L., *A First Course in the Finite Element Method*, Thomson Brooks/Cole, 2002.

[50] Reddy, N. J., *An Introduction to Finite Element Method*, McGraw-Hill Science, 2005.

[51] LinkwitzLab, Sensible Recording and Rendering of Acoustic Scenes, www.linkwitzlab.com, accessed December 2014.

[52] Civil Engineering, Herff College of Engineering, The University of Memphis, "Development of Truss Equations," ww.ce.memphis.edu, accessed December 2014.

[53] FEM for Frames, What-When-How: In Depth Tutorials and Information, www.what-when-how.com, accessed December 2014.

[54] MSC Software, *MSC Nastran 2013.1.1 Quick Reference Guide*, 2014.

[55] University of Texas, "The Ground Vibration Test of a Star-Lite Aircraft," http://courses.ae.utexas.edu/ase363q/past_projects/StarLiteGVT, accessed May 1997.

APPENDIXES

APPENDIX A

CALCULATIONS OF VERTICAL BENDING AND TORSION FREQUENCIES OF FREE-FREE BEAM

NATURAL FREQUENCIES OF A FREE-FREE BEAM

L-Length of the beam
b1-Outer width of the beam
h1-Outer height of the beam
t-Thickness of the beam
b2-Inner width of the beam
h2-Inner height of the beam
A-Area of cross section
ω-angular natural frequency
f-ordinary frequency,Hz
I1-section modulus(vertical)
I2-section modulus(for & aft)
ρ-density
ν-poisson's ratio
E-Young's modulus
KL1-frequency parameter for bending1
KL2-frequency parameter for bending2
KL3-frequency parameter for bending3

VERTICAL BENDING FREQUENCIES:

$L := 54 \qquad b1 := 5 \qquad h1 := 3$

$t := 0.24$

$b2 := b1 - 2 \cdot t$

$h2 := h1 - 2 \cdot t$

$A := b1 \cdot h1 - b2 \cdot h2$

$$I1 := \left(\frac{b1 \cdot h1^2}{6}\right) - \left(\frac{b2 \cdot h2^3}{6 \cdot h1}\right)$$

$b2 = 4.52 \qquad h2 = 2.52 \qquad A = 3.61 \qquad I1 = 3.481$

$\rho := 0.1 \qquad E := 10^7 \qquad \nu := 0.3$

$KL1 := 4.73 \qquad KL2 := 7.85 \qquad KL3 := 11.00$

$$K1 := \frac{KL1}{L} \qquad K2 := \frac{KL2}{L} \qquad K3 := \frac{KL3}{L}$$

$K1 = 0.088 \qquad K2 = 0.145 \qquad K3 = 0.204$

$$\omega 1 := K1^2 \cdot \left(\sqrt{\frac{E \cdot I1 \cdot 386}{\rho \cdot A}}\right) \qquad \omega 2 := K2^2 \cdot \left(\sqrt{\frac{E \cdot I1 \cdot 386}{\rho \cdot A}}\right) \qquad \omega 3 := K3^2 \cdot \left(\sqrt{\frac{E \cdot I1 \cdot 386}{\rho \cdot A}}\right)$$

$\omega 1 = 1.48 \times 10^3 \qquad \omega 2 = 4.078 \times 10^3 \qquad \omega 3 = 8.007 \times 10^3$

$$f1 := \frac{\omega 1}{2 \cdot (3.14)} \qquad f2 := \frac{\omega 2}{2 \cdot (3.14)} \qquad f3 := \frac{\omega 3}{2 \cdot (3.14)}$$

$f1 = 235.733 \qquad f2 = 649.288 \qquad f3 = 1.275 \times 10^3$

TORSION FREQUENCY:

$L := 54$ $b1 := 5$ $h1 := 3$

$t := 0.24$

$b2 := b1 - 2 \cdot t$

$h2 := h1 - 2 \cdot t$

$b2 = 4.52$ $h2 = 2.52$ $A = 3.61$ $I1 = 3.481$

$\rho := 0.1$ $G := \left(4 \cdot 10^6\right)$ $\nu := 0.3$

$J := 8.33$ ...from load deflection

$$Jp := \frac{\left[(b1 \cdot h1) \cdot \left(b1^2 + h1^2\right)\right] - \left[(b2 \cdot h2) \cdot \left(b2^2 + h2^2\right)\right]}{12}$$

$$Ct := \sqrt{\frac{G \cdot J \cdot 386}{\rho \cdot Jp}}$$

$Ct = 8.678 \times 10^4$

$$\omega := Ct \cdot \frac{3.14}{L}$$

$\omega = 5.046 \times 10^3$

$$f := \frac{\omega}{2 \cdot 3.14}$$

$f = 803.494$

APPENDIX B

CALCULATIONS OF BENDING AND TORSION FREQUENCIES
OF CANTILEVER PLATE

NATURAL FREQUENCIES OF CANTILEVERED PLATE

$\lambda 1 := 3.486 \qquad \lambda 2 := 9.831 \qquad \lambda 3 := 21.79$

$E := 7.23 \cdot 10^{10}$ .....in Pascal

$h := 2.92 \cdot 10^{-3}$ .....in meters

$\upsilon := 0.3$ .....(Poissons)ratio

$a := 0.44$ .....in meters

$b := 0.36$ .....in meters

$\frac{a}{b} = 1.222$

$\rho := 2821$ .....in $\frac{kg}{m^3}$

$D := \frac{E \cdot h^3}{12 \cdot (1 - \upsilon^2)}$

$D = 164.841$

$\omega 1 := \frac{\lambda 1}{\sqrt{\frac{\rho \cdot h}{D}} \cdot a^2} \qquad \omega 2 := \frac{\lambda 2}{\sqrt{\frac{\rho \cdot h}{D}} \cdot a^2} \qquad \omega 3 := \frac{\lambda 3}{\sqrt{\frac{\rho \cdot h}{D}} \cdot a^2}$

$\omega 1 = 80.549$

$\omega 2 = 227.16$

$\omega 3 = 503.49$

$f1 := \frac{\omega 1}{2 \cdot (3.14)} \qquad f2 := \frac{\omega 2}{2 \cdot (3.14)} \qquad f3 := \frac{\omega 3}{2 \cdot (3.14)}$

$f1 = 12.826 \qquad f2 = 36.172 \qquad f3 = 80.174$